AN ABSTRACT OF THE THESIS OF

Dongjun Yuk for the degree of Master of Science in Civil Engineering presented on February 16, 2001. Title: Stochastic Analysis of the Nonlinear Response Transition Behavior of an Ocean System.

Abstract approved: Redacted for Privacy

Solomon C.S. Yim

The nonlinear response of an ocean system subjected to random excitations can exhibit very complex dynamic behaviors including jump phenomena and coexistence of attractors. In this study, the stochastic system response behavior of a simple (Duffing) oscillator under narrow-band random excitations is first examined in the subharmonic resonance region. A semi-analytical procedure based on the nonlinear response characteristics of the corresponding deterministic system is developed to derive the response transition probabilities within individual attraction domains and among finite attraction domains under the assumptions of stationarity and Markov process. Overall response amplitude probability distributions are obtained by applying the Bayes formula to the two different types of response transition probability distributions.

To validate the prediction capability of the semi-analytical method, numerical simulation of the responses of the Duffing system are generated and statistical characteristics of the response behavior are compared with prediction results. It is

shown that the semi-analytical procedure provides more accurate predictions than other approximate methods available in the literature. A parametric study on the effects of variations in excitation intensity and degree of narrow-bandedness is conducted. Results confirmed that the nonlinear response characteristics including jump phenomenon and co-existence of attraction domains are preserved under narrow-band random excitations.

The semi-analytical prediction method developed above is then applied to analyze the stochastic response behavior of a nonlinear mooring system subjected to random ocean waves. For modeling of the structural system, a nonlinear-structure, nonlinearly-damped (NSND) model is employed and a reverse multiple-input/single-output technique is applied to identify the system coefficients. To verify the accuracy and capability of the semi-analytical method in predicting the complex behaviors of the nonlinear mooring system, analytical predictions are compared with experimental results and numerical simulations. System response amplitude probability distributions predicted by the semi-analytical procedure are shown to be in good agreement with experimental and simulation results.

STOCHASTIC ANALYSIS OF THE NONLINEAR RESPONSE TRANSITION BEHAVIOR OF AN OCEAN SYSTEM

by
Dongjun Yuk

A THESIS

submitted to

Oregon State University

in partial fulfillment of
the requirements for the
degree of

Master of Science

Presented February 16, 2001
Commencement June 2001

Master of Science thesis of Dongjun Yuk presented on February 16, 2001

APPROVED:

Redacted for Privacy

Major Professor, representing Civil Engineering

Redacted for Privacy

Head of Department of Civil, Construction and Environmental Engineering

Redacted for Privacy

Dean of Graduate School

I understand that my thesis will become part of the permanent collection of Oregon State University libraries. My signature below authorizes release of my thesis to any reader upon request.

Redacted for Privacy

Dongjun Yuk, Author

ACKNOWLEDGEMENT

I would like to express my sincere gratitude to my major advisor, Prof. Solomon C.S. Yim, for his guidance and advice on my graduate study at Oregon State University. I also thank all the other members of my committee: Prof. Thomas H. Miller, Prof. John Sessions, Prof. Ted S. Vinson for their interest and comments. I also thank all the staff, faculty and fellow students of the Structure and Ocean Engineering program at Oregon State University.

This work was supported by United States Office of Naval Research under Grant No. N00014-92-J-1221. I am grateful for the support.

I also would like to express my deepest gratitude to my father and mother for their continuous support and encouragement, my wife for her patience and love.

TABLE OF CONTENTS

1. INTRODUCTION 1

1.1 Literature Review 2

1.2 Objectives and Scope 4

2. MODEL FORMULATION OF SEMI-ANALYTICAL METHOD 6

2.1 Deterministic Excitation Model and System Response Behaviors 6

2.1.1 Excitation model 6
2.1.2 System response behaviors 7
2.1.2.1 Co-existing attraction domains and initial condition dependency 7
2.1.2.2 Response amplitude domain overlap 10
2.1.2.3 Response amplitude jump phenomena 11

2.2 Stochastic Excitation Model and Assumptions 14

2.3 Stochastic Descriptions of Excitation Parameters 16

2.4 Response Inter-domain Transitions 18

2.5 Evaluation of Probability Transition Matrix K 19

2.6 Response Intra-domain Transition Probabilities 27

2.7 Evaluation of Response Intra-domain Transition Probabilities 29

3. ANALYSIS, PREDICTIONS, AND COMPARISONS OF STOCHASTIC RESPONSES 32

3.1 Analysis of Stochastic Response Behavior 32

3.1.1 Jump Phenomena Among Various Harmonic/Subharmonic Responses 32
3.1.2 Frequency of Occurrence and Transition Among Attraction Domains 35
3.1.3 Effects of Varying Excitation Bandwidth 35

TABLE OF CONTENTS (continued)

3.1.4 Effects of Varying Excitation Intensity 38

3.2 Predictions of Stochastic Response Behavior and Comparisons with Simulations 41

3.2.1 Effects of varying excitation randomness on inter-domain transitions 42
3.2.2 Effects of varying excitation randomness on intra-domain transitions 44
3.2.3 Effects of varying excitation intensity on intra-domain transitions 45
3.2.4 Effects of varying excitation randomness on response amplitude probability distribution 47
3.2.5 Effects of varying excitation intensity on response amplitude probability distribution 50

3.3 Comparisons with Existing Analytical Methods 51

3.3.1 Stochastic averaging method 51
3.3.2 Quasi-harmonic method 51
3.3.3 Comparisons of analytical predictions and simulation results 52

4. STOCHASTIC ANALYSIS OF A MOORED OCEAN SYSTEM 55

4.1 Description of Moored Ocean System 55

4.2 Analytical Model 57

4.3 Amplitude Jump Phenomena 58

4.4 Stochastic Excitation Parameters 64

4.5 Inter-domain Transition 67

4.5.1 System total energy 68
4.5.2 System energy level 73

4.6 Intra-domain Transitions 75

TABLE OF CONTENTS (continued)

4.7 Prediction, Experimental Results, and Simulation.....77

5. SUMMARY AND CONCLUDING REMARKS.....84

5.1 Summary.....84

5.2 Concluding Remarks.....86

5.3 Recommended Future Study.....89

BIBLIOGRAPHY.....90

APPENDICES.....93

LIST OF FIGURES

Figure Page

2.1 Time series of large amplitude harmonic response, small amplitude harmonic response, 1/2 subharmonic response, and 1/3 subharmonic response. {Cs=0.05, a_1=1, a_3=0.3, ω=3.6, ϕ=0, A=9, ($x(0)$, $dx/dt(0)$)= (4.6, 0), (4.2, 0.6), (4.1, 0), (4.3, 0)} 8

2.2 Attraction domain of : (a) small amplitude harmonic response, D_2, (b) 1/3 subharmonic response, D_4, (c) 1/2 subharmonic response, D_3, and (d) large amplitude harmonic response, D_1. {Cs=0.05, a_1=1, a_3=0.3, ω=3.6, ϕ=0, A=9} 9

2.3 Amplitude response curves of the system in the subharmonic resonance region. {ω_f=3.6, Cs=0.05, a_1=1, a_3=0.3, ϕ=0, A=9, ($x(0)$, $dx/dt(0)$)= (4.6, 0), (4.2, 0.6), (4.1, 0), (4.3, 0)} 11

2.4. System response in the small amplitude harmonic domain. (top) relationship between transient-state system total energy and mean energy over one excitation cycle. (bottom) relationship between response displacement and mean energy. {C_S = 0.05, a_1 =1, a_3=0.3, ω = 3.6, ϕ = 0, A = 12 ($x(0)$, $dx/dt(0)$) = (-1.8, 0)} 21

2.5 Mean energy level of the system response in the small amplitude harmonic domain and the 1/2 and 1/3 subharmonic domains. {C_S = 0.05, a_1 =1, a_3 = 0.3, ω = 3.6, ϕ = 0, A = 7}, ($x(0)$, $dx/dt(0)$) = {(-1, 0.5) (small amplitude harmonic response), (-3.75, 4.75) (1/2 subharmonic response), (-1.4, 0.75) (1/3 subharmonic response)} 22

3.1 System response in the subharmonic resonance region. Time series of narrowband excitation amplitude (top) and corresponding response amplitude (bottom). {Cs = 0.05, a_1 = 1, a_3 = 0.3, ω_f = 3.6, σ_f^2 = 157, γ = 0.005} 33

3.2 Amplitude response maps corresponding to the time series shown in Fig.3.1 34

3.3 (a), (b), (c), and (d): System response under varying excitation bandwidth in the subharmonic resonance region. Time series of narrowband excitation amplitude (top) and corresponding response amplitude (bottom). {Cs = 0.05, a_1 = 1, a_3 = 0.3, ω_f =3.6, σ_f^2 = 157, γ = (a) 0.001, (b) 0.005, (c) 0.01, (d) 0.05} 37

LIST OF FIGURES (continued)

Figure Page

3.4 (a), (b), (c), and (d): Amplitude response maps corresponding to the times series shown in Fig.3.3 (a) – (d), respectively.....38

3.5 (a) and (b): system response under varying excitation variance in the subharmonic resonance region. Time series of narrowband excitation (top) and corresponding response amplitude (bottom). {Cs = 0.05, a_1 = 1, a_3 = 0.3, ω_f =3.6, γ= 0.01, σ_f^2 = (a) 157, (b) 125}.....40

3.6 (a), and (b): Amplitude response maps corresponding to the times series shown in Fig.3.3 (a) and (b), respectively.....41

3.7 Variations in the response amplitude probability distribution under varying excitation bandwidth in the subharmonic resonance region. (a) simulation, (b) prediction 48

3.8 Variations in the response amplitude probability distribution under varying excitation bandwidth in the subharmonic resonance region. (a) case(i), (b) case(ii), (c) case(iii), (d) case(iv).....49

3.9 Variations in the response amplitude probability distribution under varying excitation variance in the subharmonic resonance region. (a) simulation, (b) prediction.....50

3.10 Response amplitude histogram and probability distributions predicted by the semi-analytical (SE-AN), quasi-harmonic (Q-H) and stochastic averaging (ST-AV) methods, respectively. {Cs = 0.16, a_1 = 1, a_3 = 0.3, ω_f =2, γ= 0.01, σ_f^2 = 3.05}. (a) γ= 0.02, and (b) γ= 0.08.....54

4.1 Experimental model of submerged, hydrodynamically damped and excited structural system.....55

4.2 Frequency response diagram (experimental results); ---- estimated stability boundaries 56

4.3 Coexisting attraction domain (a) 1/2subharmonic attraction domain, (b) large harmonic attraction domain { A=1.0 } 60

LIST OF FIGURES (continued)

Figure Page

4.4. Time series of the system response under deterministic excitation { A=2.0 for t≤600 sec, A=2.5 for t>600 sec } 60

4.5 Response amplitude curve {m=3.428, C_a=0.25, ξ=0.06, C_d'=0.02, C_m=1.25, C_d=0.1, a_1=9.3, a_2=4.0, a_3=4.0} 61

4.6 Schematic diagram of system response transitions among D_1, D_2, D_3 62

4.7 Transitions and variations of system response amplitude along the response amplitude curves 63

4.8 Schematic diagram of system response transitions under infinitesimal (⟶) and finite (--▶) excitation amplitude variations among D_1, D_2 and D_3 64

4.9 Experimental excitation: (a) wave profile (b) wave spectra 66

4.10 Time series and total energy of large amplitude harmonic response {m=3.428, Ca=0.25, ξ=0.06, C_d'=0.02, C_m=1.25, C_d=0.1, a_1=9.3, a_2=4.0, a_3=4.0, (x(0),dx/dt(0))=(4.0, 1.0), A=0.95} 70

4.11 Time series and total energy of small amplitude harmonic response {m=3.428, Ca=0.25, ξ=0.06, C_d'=0.02, C_m=1.25, C_d=0.1, a_1=9.3, a_2=4.0, a_3=4.0, (x(0),dx/dt(0))=(0.0, 0.0), A=0.5} 71

4.12 Time series and total energy of 1/2 subharmonic response {m=3.428, Ca=0.25, ξ=0.06, C_d'=0.02, C_m=1.25, C_d=0.1, a_1=9.3, a_2=4.0, a_3=4.0, (x(0),dx/dt(0))=(0.0, 0.0), A=0.95} 72

4.13 Mean energy level of the system response. (a) small amplitude harmonic and 1/2 subharmonic domains. (b) small and large amplitude harmonic domains. {m=3.428, Ca=0.25, ξ=0.06, C_d'=0.02, C_m=1.25, C_d=0.1, a_1=9.3, a_2=4.0, a_3=4.0, (x(0),dx/dt(0))=(0.0, 0.0) (small amplitude harmonic, and 1/2 subharmonic responses), (4.0, 1.0) (large amplitude harmonic response)}, {a=0.95 (large amplitude harmonic, and 1/2 subharmonic responses), 0.5 (small amplitude harmonic response)} 74

LIST OF FIGURES (continued)

Figure Page

4.14 Overall response amplitude distribution : (a) Test D15 (b) Test D16....81

4.14 Overall response amplitude distribution (continued) : (c) Test D17 (d) Test D18 82

4.14 Overall response amplitude distribution (continued): (e) Test D19.....83

LIST OF TABLES

Table Page

3.1 Excitation parameters of the system varied in the subharmonic resonance region. Excitation frequency ω_f = 3.6, and system parameters Cs = 0.05, a_1 = 1, a_3 = 0.3 are held constant. 42

3.2 Effects of varying excitation bandwidth on response inter-domain probability transition in the subharmonic resonance region 44

3.3 Effects of varying excitation bandwidth on the variance of the response amplitude within the co-existing attraction domains D_d^R (d=1,2,3,4), respectively, in the subharmonic resonance region.....45

3.4 Effects of varying excitation variance on response inter-domain transition probability in the subharmonic resonance region 46

4.1 Parameters of narrowband excitation on SDOF, 90° configuration 78

4.2 Inter-domain transition probability in the subharmonic resonance.....79

STOCHASTIC ANALYSIS OF THE NONLINEAR RESPONSE TRANSITION BEHAVIOR OF AN OCEAN SYSTEM

1. INTRODUCTION

In ocean and structural engineering, the dynamic loads from environment, which includes earthquake, wind, and waves, are often modeled as narrowband stochastic processes. Due to the random nature of the environmental loads and complex behavior of nonlinear systems, accurate analysis and prediction of nonlinear dynamic system response behaviors is highly challenging. The complex behaviors of nonlinear systems have been demonstrated in many previous studies (Rice, 1954; Lyon, et al, 1961; Dimentberg, 1971; Richard and Anand, 1983; Davies and Liu, 1990; Gottlieb and Yim, 1992; Koliopulos and Bishop, 1993; Lin and Yim, 1995). These complex behaviors include co-existence of attractors, instability, initial condition dependency, amplitude jump phenomenon, and chaos (Nayfeh and Mook, 1979; Guckenheimer and Holmes, 1986; Thompson and Stewart, 1986; Jordan and Smith, 1987).

A mooring system subjected to wave forces is an example of highly nonlinear offshore structures and has been investigated in depth to demonstrate the characteristics of the system behaviors (Yim, *et al.*, 1993). Shih (1998) and Yim investigated the stochastic behavior of the mooring system under narrowband excitations and developed a semi-analytical method to predict the probability distribution of the responses using a simple (Duffing oscillator) model with

nonlinear restoring force terms up to third order and hydrodynamic damping terms. They showed that the semi-analytical procedure is capable of predicting the system response behavior accurately and can potentially be used to analyze more complicated models.

1.1 Literature Review

Recently a significant amount of research has been devoted to nonlinear system response having single- and multi-degrees-of-freedom (Krylov and Bogoliubov, 1947; Hayashi, 1953; Bogoliubov and Mitropolsky, 1961; Davis, 1962; Davies and Liu, 1990; Koliopulos and Bishop, 1993). Several analytical methods to study the nonlinear system response under deterministic excitation including multiple scales, harmonic balance, averaging, and Lindstedt-Poincaré have been developed.

However, the stochastic behaviors of nonlinear system response subjected to narrowband excitations are not well understood due to the complex characteristics of the system responses. Gradual variations of excitation parameters can make the system response undergo transient states continuously. Development of analytical methods to describe nonlinear system behaviors accurately is difficult due to these complex transitions among co-existing attractors.

Yim and Lin (1991) and Gottlieb and Yim (1992) showed that the multi-point mooring system with geometric nonlinearity can exhibit highly nonlinear response behaviors including chaos and semi-analytical methods, and numerical techniques are required in general to investigate these complex responses.

Recently, several stochastic analysis methods have been developed to describe the stochastic behaviors of nonlinear system response under narrowband excitation. Roberts and Spanos (1986) and Davies and Liu (1990) assumed both the excitation and response to be Markov processes and applied the stochastic averaging method to analyze the stochastic response under narrowband excitations. The probability density function of the response envelope process was obtained by solving the Fokker-Planck equation associated with the excitation and the response envelope.

Alternatively, Koliopulos and Bishop (1993) proposed a quasi-harmonic method. In their formulation of the probability density function of the response envelope, both the excitation and the response processes are assumed to be narrowband. However, the effects of variation of randomness in the excitation on response behaviors are not taken into account by this method, even though an extra parameter is employed to indicate the occurrence and persistence of the response amplitude jump phenomenon.

Another method is a semi-analytical method developed by Shih and Yim (Shih, 1998). The excitation and the response processes are assumed to be Markov processes. The system response under stochastic narrowband excitation is considered a transient state as excitation parameters vary continuously. Transitions of the response are divided into inter-domain and intra-domain. The stochastic behaviors of the excitation are used to determine the probability density function of

the system response. In developing the semi-analytical method, the well-known Duffing oscillator is used for simplicity.

In this study, a nonlinear-structure, nonlinearly-damped (NSND) model is used to describe the mooring system. The quadratic hydrodynamic damping force and nonlinear restoring force terms up to third order are considered. The semi-analytical method is applied to analyze the responses of the NSND model under narrowband excitations in the subharmonic resonance region. Predicted probability density distributions obtained from the semi-analytical method are compared with experimental results and numerical simulations.

1.2 Objectives and Scope

The long-term objective of the research described herein is to obtain a better understanding of the nonlinear system response behaviors from a stochastic perspective for structural design and control applications. The specific objective of this study is to validate the capability and accuracy of the semi-analytical method in predicting the response amplitude probability density function of the multi-point mooring system under narrowband excitation using NSND model. To demonstrate the capability of the semi-analytical method, predicted probability distributions of the response amplitude are compared with experimental results and numerical simulations.

A brief summary of the scope of work of this thesis is presented in this section. In Chapter 1, literature related to this study is reviewed and objectives and

scope are provided. Configuration of the structural system considered and description of the semi-analytical method are presented in Chapter 2. Formulation and procedures of the semi-analytical method developed by Shih and Yim are summarized to provide the background of the analysis method employed in this study. In the development of the semi-analytical method, the Duffing oscillator is employed for its simplicity and well-known nonlinear characteristic behavior. In Chapter 3, the capability and accuracy of the semi-analytical method in analyzing the Duffing oscillator are demonstrated. Comparisons of analytically predicted response amplitude probability distribution with numerical simulations are made to validate the proposed method. In Chapter 4, the NSND model is employed to describe the structural system. Applying the semi-analytical method to the NSND model in the subharmonic resonance region, analytical predictions are obtained and compared with experimental results and numerical simulations. Finally, a summary of the results, concluding remarks and recommended future studies are provided in Chapter 5.

2. MODEL FORMULATION AND SEMI-ANALYTICAL METHOD

2.1 Deterministic Excitation Model and System Response Behaviors

2.1.1 Excitation model

The governing equation of a general deterministic Duffing oscillator is expressed as

$$\ddot{x} + C_S\dot{x} + a_1 x + a_3 x^3 = f(t) \tag{2.1}$$

where, C_s is the damping coefficient, and a_1 and a_3 are the linear and nonlinear stiffness coefficients, respectively. The system is subjected to an external excitation $f(t)$. The elastic restoring force represented by the cubic polynomial is the only source of nonlinearity in the system. Even though the mooring lines have linear elastic properties, it is observed that restoring force provided by multi-point mooring lines is nonlinear due to geometry (Yim, *et al*, 1993). For the excitation, both deterministic and stochastic model are used.

When the excitation is deterministic, the excitation parameters are all time independent and $f(t)$ can be expressed as

$$f(t) = A\cos(\omega t + \phi) \tag{2.2}$$

where $(A,\ \omega,\ \phi)$ are constants.

2.1.2 System response behaviors

2.1.2.1 Co-existing attraction domains and initial condition dependency

A major difference in the response characteristics between a linear and nonlinear system is the dependency of the steady-state response on system initial conditions. To demonstrate the system response initial condition dependency in the subharmonic resonance region, four co-existing attraction domains corresponding to an excitation amplitude A=9 and their corresponding response time series are shown in Fig. 2.1 and Fig. 2.2.

Fig. 2.1 shows that under identical excitation parameters, i.e., excitation amplitude, frequency, and phase angle, system responses can exhibit completely different behaviors. Notice that the system response behavior with certain set of parameters is sensitive to initial conditions around the boundaries of co-existing attraction domains. Small variations in initial condition near the boundaries of attraction domains may cause period doubling of response or large amplitude response. As shown in Fig. 2.2, co-existing attraction domains have such complex patterns that a probabilistic description is needed to describe sensitive system response behaviors. For convenience of notations, the large harmonic, small harmonic, 1/2 subharmonic and 1/3 subharmonic attraction domains are denoted as D_1, D_2, D_3 and D_4, respectively.

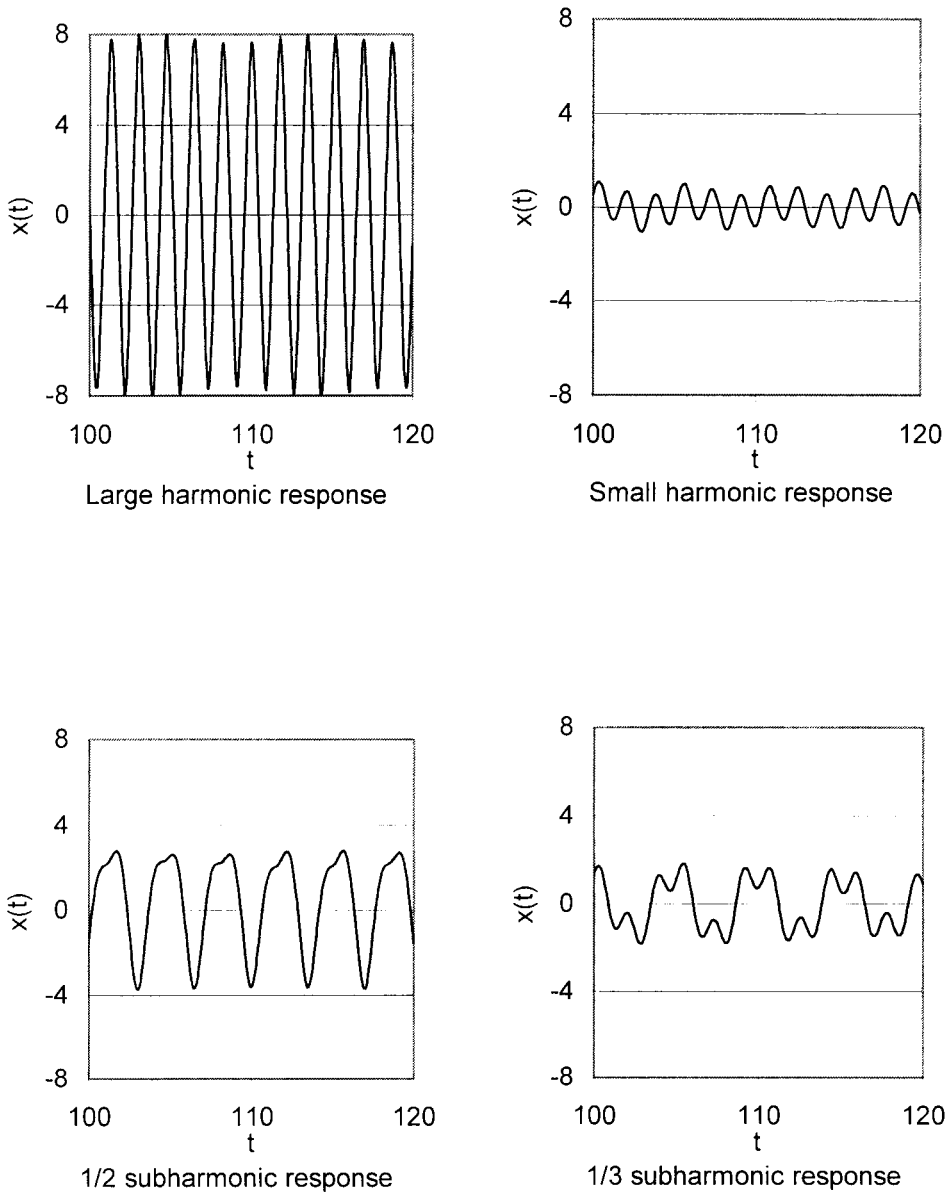

Fig. 2.1 Time series of large amplitude harmonic response, small amplitude harmonic response, 1/2 subharmonic response, and 1/3 subharmonic response. $\{Cs=0.05, a_1=1, a_3=0.3, \omega=3.6, \phi=0, A=9, (x(0), dx/dt(0))= (4.6, 0), (4.2, 0.6), (4.1, 0), (4.3, 0)\}$.

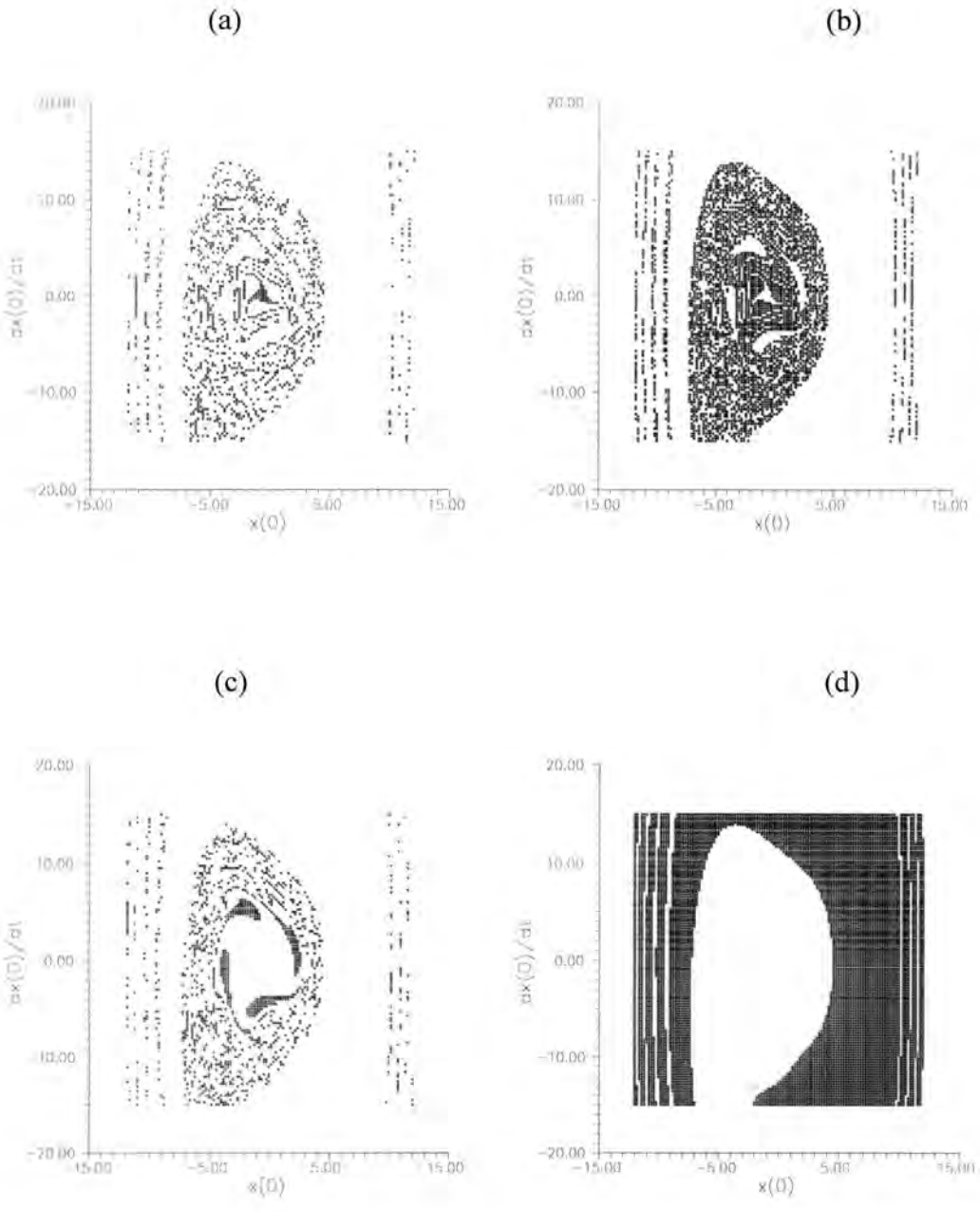

Fig. 2.2 Attraction domain of (a) small amplitude harmonic response, D_2, (b) 1/3 subharmonic response, D_4, (c) 1/2 subharmonic response, D_3, and (d) large amplitude harmonic response, D_1. {Cs=0.05, a_1=1, a_3=0.3, ω=3.6, ϕ=0, A=9}.

2.1.2.2 Response amplitude domain overlap

Previous investigations showed that, when the excitation frequency ω is close to three times the system linear natural frequency, five attraction domains co-exist (Thompson and Stewart, 1986). These attraction domains include two harmonic (large and small amplitude), two 1/2 subharmonic, and one 1/3 subharmonic responses. It is found that the two co-existing 1/2 subharmonic response attractors are of the same steady-state amplitude but with different biases in the time series. Thus, they are considered as being parts of the same attraction domain (i.e., they belong to the same attractor) henceforth in this study.

Amplitude response curves of the system in the subharmonic resonance region are shown in Fig. 2.3. Due to the complexity of solving approximate steady-state response amplitudes in these attraction domains, these curves are obtained by direct integration of Eq.(2.1), and the parameters are the same as in Fig. 2.1. In the figure, the vertical dashed lines indicate intervals of excitation amplitudes where different types of system response, or attraction domain D_d, exist and those excitation amplitude domains are denoted as D_d^A (d=1,2,3,4). Note that, in each domain D_d, the steady-state response amplitudes also form a response amplitude domain D_d^R (d=1,2,3,4), as shown in Fig. 2.3. In addition, unlike the case of the large amplitude resonance region, response amplitude domain overlaps are observed among D_d^R. That is, single response amplitude may belong to more than one attraction domain and thus, may correspond to different excitation amplitudes.

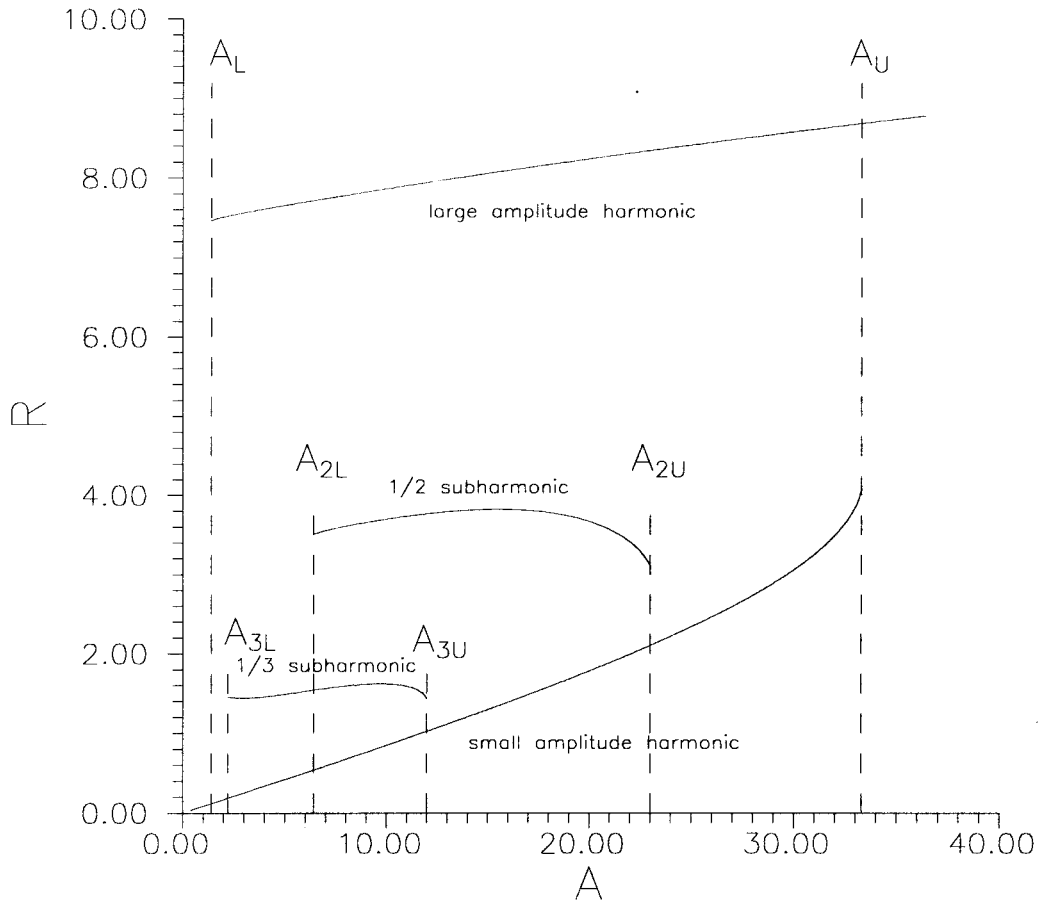

Fig. 2.3 Amplitude response curves of the system in the subharmonic resonance region. {ω=3.6, Cs=0.05, a_1=1, a_3=0.3, ϕ=0, A=9, ($x(0)$, $dx/dt(0)$)= (4.6, 0), (4.2, 0.6), (4.1, 0), (4.3, 0)}.

2.1.2.3 Response amplitude jump phenomena

When the excitation amplitude exits from the small amplitude domain by crossing A_{2U} (see Fig. 2.3), the system response goes to the large amplitude harmonic domain because it is the only existing domain for $A > A_{2U}$. Similarly, an exit of the system response from the large amplitude harmonic domain by varying the excitation amplitude across A_{1L} will induce the response amplitude to jump to

the small amplitude harmonic domain. This is because the small amplitude harmonic domain is the only existing one for $A < A_{1L}$.

(1) 1/2 subharmonic domain upper bound A_{3U} At the 1/2 subharmonic domain upper bound A_{3U}, the possible destination domains are the large and the small amplitude harmonic domains (see Fig. 3.3). When the excitation amplitude increases from $A < A_{3U}$ to $A > A_{3U}$, the 1/2 subharmonic domain evolves into either the small or the large amplitude harmonic domains. When the transient-state system mean energy is greater than the steady-state 1/2 subharmonic response mean energy at $A = A_{3U}$, the large amplitude harmonic domain may likely be the destination of the inter-domain transition. Conversely, if the transient-state system mean energy is lower than the steady-state 1/2 subharmonic response mean energy at $A = A_{3U}$, the system response will likely go to the small amplitude harmonic domain.

(2) 1/2 subharmonic domain lower bound A_{3L} At the 1/2 subharmonic domain lower bound A_{3L}, the possible destination domains are the large and the small amplitude harmonic domains, and the 1/3 subharmonic domain (see Fig.2.3). However, a jump from a 1/2 subharmonic response domain to the large amplitude resonance response domain is highly unlikely due to the decreasing excitation amplitude (hence input energy). Thus, during the inter-domain transition, the system response may transition to either the small amplitude harmonic or the 1/3 subharmonic domain (see Fig.2.3) when the excitation amplitude varies from $A > A_{3L}$ to $A < A_{3L}$. It is assumed that, after the response exits from the 1/2

subharmonic domain, it will first visit the 1/3 subharmonic domain before it can visit the small amplitude harmonic domain.

(3) 1/3 subharmonic domain upper bound A_{4U} At 1/3 subharmonic domain upper bound A_{3U}, the possible destination domains are the large and the small amplitude harmonic domains and the 1/2 subharmonic domain (see Fig.2.3). Although the excitation amplitude is increasing (hence higher energy input), a jump from a 1/3 subharmonic response to a large amplitude resonance response is highly unlikely due to the large gap between the two energy levels and the presence of the 1/2 subharmonic domain in between. Thus, during the inter-domain transition, the system response may transition to either the small amplitude harmonic or the 1/2 subharmonic domain (see Fig. 2.3) when the excitation amplitude varies from $A < A_{4U}$ to $A > A_{4U}$. The system response will more likely go to the 1/2 subharmonic domain during the inter-domain transition at $A = A_{4U}$ if the transient-state system mean energy is greater than the steady-state 1/3 subharmonic response mean energy at $A = A_{4U}$. Otherwise, the small amplitude harmonic domain will become the destination of the inter-domain transition.

(4) 1/3 subharmonic domain lower bound A_{4L} At the 1/3 subharmonic domain lower bound A_{4L}, the possible destination domains are the large and the small amplitude harmonic domains (see Fig. 2.3). However, as explained in (2), a jump from a 1/3 subharmonic response domain to the large amplitude resonance response domain is highly unlikely due to the decreasing excitation amplitude (hence input energy). Thus, during the inter-domain transition, the system response will likely

transition to the small amplitude harmonic domain (see Fig. 2.3) when the excitation amplitude varies from $A > A_{4L}$ to $A < A_{4L}$.

2.2 Stochastic Excitation Model and Assumptions

If the excitation is random, *f(t)* may be interpreted as a stochastic process, the parameters *(A, ω, ϕ)* then become time dependent random variables and their behaviors may vary significantly depending on the spectral bandwidth of the process. The narrowband process can be modeled as the output process of a lightly damped linear system with a white noise process as the excitation (Stratonovich, 1963). This linear system in frequency domain can be expressed in the form of a stochastic differential equation as

$$\ddot{f} + \gamma \dot{f} + \omega_f{}^2 f = \gamma^{1/2} \omega_f W_0 \tag{2.3}$$

where γ serves as a bandwidth parameter, ω_f is the peak frequency of the output process *f(t)* and W_0 is a stationary Gaussian white noise process with zero mean and spectral intensity S_0. In the time domain, a stationary narrowband random process is defined as a process that is close to sinusoidal oscillations of a fixed peak frequency with the time interval equal to a large number of oscillation cycles (Stratonovich, 1963). The amplitude and phase of the process vary slowly and randomly while the frequency retains a constant value (Ochi, 1990).

The envelope and phase processes associated with a given random process are useful concept in the theory of random vibrations. A narrowband stochastic

process $f(t)$ can be represented as a cosine function having time varying amplitude governed by the envelope process, and time varying frequency governed by the phase process (Langley, 1986), that is,

$$f(t) = A(t)\cos\left[\omega_f t + \phi\ (t)\right] \tag{2.4}$$

where, $A(t)$ and $\phi(t)$ are the envelope and the phase processes, respectively.

By assuming the narrowband process $f(t)$ to be Guassian with zero-mean and variance σ_f^2, the joint probability density function of the envelope $A(t)$ and the phase $\phi(t)$ processes is obtained as (Ochi, 1990)

$$p(A(t),\phi(t)) = \frac{A(t)}{2\pi\,\sigma_f{}^2}\exp\left[-\frac{A^2(t)}{2\pi\,\sigma_f{}^2}\right] \quad 0 \le A(t) < \infty,\ \ 0 \le \phi(t) \le 2\pi \tag{2.5}$$

For the narrowband excitation process, $f(t)$, the frequency is assumed to be constant and equal to the peak frequency ω_f of the spectrum of the system input in Eq.(2.3). Effects of excitation frequency variations on the response behavior are taken into account through excitation phase angle variations (Rice, 1954; Stratonovich, 1963; Langley, 1986). For the response process, it is assumed that the prominent deterministic system response behavior described earlier, including co-existing attraction domains, and the domain-dependent characteristics, are preserved in the narrowband random excitation environment.

From a stochastic point of view, the probability transitions of the excitation amplitude and phase angle processes and the corresponding response amplitude process are assumed to be ergodic Markov processes.

2.3 Stochastic Descriptions of Excitation Parameters

To investigate the stochastic behaviors of the amplitude and the phase processes, a four dimensional joint probability density function (PDF) of the random variables representing the excitation amplitudes and phase angles corresponding to consecutive excitation cycles, i.e., $A^{(1)}$, $A^{(2)}$, $\phi^{(1)}$ and $\phi^{(2)}$, can be obtained as (Ochi, 1990)

$$p(A^{(1)},\phi^{(1)},A^{(2)},\phi^{(2)})$$
$$= \frac{A^{(1)}A^{(2)}}{4\pi^2\sqrt{|\Sigma|}} \exp\left\{\frac{-1}{2\sqrt{|\Sigma|}}\left\{\sigma_f{}^2\left[\left(A^{(1)}\right)^2+\left(A^{(2)}\right)^2\right]-2A^{(1)}A^{(2)}\left[\begin{matrix}\rho\cos\left(\phi^{(2)}-\phi^{(1)}\right)\\+\lambda\sin\left(\phi^{(2)}-\phi^{(1)}\right)\end{matrix}\right]\right\}\right\}$$

$$0 \le A^{(1)}, A^{(2)} < \infty, \quad 0 \le \phi^{(1)}, \phi^{(2)} \le 2\pi \tag{2.6}$$

where,

$$\rho = \int_0^\infty S_{ff}(\omega)\cos\left[(\omega-\omega_f)T\right]d\omega$$
$$\lambda = \int_0^\infty S_{ff}(\omega)\sin\left[(\omega-\omega_f)T\right]d\omega \tag{2.7}$$
$$\sqrt{|\Sigma|} = \sigma_f{}^4 - \rho^2 - \lambda^2$$

and superscripts (1) and (2) indicate that the quantities are in the current and the next excitation cycles, respectively; $S_{ff}(\omega)$ is the one-sided spectral density function of $f(t)$, and T is the excitation period equal to $2\pi/\omega_f$. If a random variable Φ is introduced to represent the phase angle difference $\phi^{(2)} - \phi^{(1)}$, the joint PDF of $A^{(1)}$, $A^{(2)}$ and Φ can be obtained from Eq.(2.6) by the transformation of the random variables (Ochi, 1990)

$$p(A^{(1)}, A^{(2)}, \Phi)$$

$$= \frac{A^{(1)}A^{(2)}}{2\pi\sqrt{|\Sigma|}} \exp\left\{\frac{-1}{2\sqrt{|\Sigma|}}\left\{\sigma_f{}^2\left[\left(A^{(1)}\right)^2 + \left(A^{(2)}\right)^2\right] - 2A^{(1)}A^{(2)}\left[\rho\cos(\Phi) + \lambda\sin(\Phi)\right]\right\}\right\} \quad (2.8)$$

$$-2\pi \le \Phi \le 2\pi$$

In addition, the joint PDF of $A^{(1)}$ and $A^{(2)}$ can be obtained by integrating Eq.(2.6) with respect to $\phi^{(1)}$ and $\phi^{(2)}$.

$$p(A^{(1)}, A^{(2)}) = \frac{A^{(1)}A^{(2)}}{\sqrt{|\Sigma|}} \exp\left\{\frac{-1}{2\sqrt{|\Sigma|}}\sigma_f{}^2\left[\left(A^{(1)}\right)^2 + \left(A^{(2)}\right)^2\right]\right\} I_0\left(\frac{A^{(1)}A^{(2)}}{\sqrt{|\Sigma|}}\sqrt{\rho^2 + \lambda^2}\right) \quad (2.9)$$

where, I_0 is the modified Bessel function of order zero. The excitation bandwidth dependency of Eq.(2.6) is transferred to Eq.(2.8)-(2.9).

Under the assumption of Markov process, the probability propagation density function of the excitation amplitude process represented by the Markov state density function (Gillespie, 1992) can be expressed as

$$p(A^{(2)} \mid A^{(1)}) = \frac{p(A^{(1)}, A^{(2)})}{p(A^{(1)})} \quad (2.10)$$

where, $p(A^{(1)})$ is a Rayleigh-distributed marginal density function of $p(A^{(1)},A^{(2)})$. Since Eq.(2.10) is a conditional probability density function, the probability density function of $A^{(2)}$ can be obtained as

$$p(A^{(2)}) = \int_0^\infty p(A^{(2)} \mid A^{(1)})p(A^{(1)})dA^{(1)} \quad (2.11)$$

2.4 Response Inter-domain Transitions

When the excitation amplitude drifts out of the attraction domain boundaries defined in the response amplitude curves, the system response may be attracted to a competing attraction domain and this transition is defined as an inter-domain transition. For a stationary Markov response process, the response inter-domain transition (or the amplitude jump phenomenon) among finite number of domains, D_d^R can be modeled as a stationary Markov process with discrete states (Gillespie, 1992) or a stationary Markov chain (Ochi, 1990; Bouleau and Lepingle, 1994).

Stochastic behaviors of the inter-domain transition are characterized by an inter-domain transition probability matrix K. Thus, the governing equation of the probability inter-domain transition can be expressed as

$$\hat{p}(D^{(2)}) = K\hat{p}(D^{(1)}) \tag{2.12}$$

where, $\hat{p}(D^{(1)})$ and $\hat{p}(D^{(2)})$ are probability vectors of the system response being in each individual attraction domain in the current and the next excitation cycles, respectively.

The dimensions of $\hat{p}$ and K are *(n x 1)* and *(n x n)*, respectively, where n is the number of coexisting attraction domains. Thus, Eq.(2.12) can also be written as

$$\left\{p_i\left(D_i^{(2)}\right)\right\} = \left[p_{ij}(i \mid j)\right]\left\{p_j\left(D_j^{(1)}\right)\right\}, \quad i, j = 1, \ldots, n \tag{2.13}$$

where, $p_{ij}(i|j)$, an element of the inter-domain transition probability matrix K, is a conditional probability that the system response is going to the i^{th} attraction domain given that it is currently in the j^{th} attraction domain. $p_i(Di^{(2)})$ and $p_j(Dj^{(1)})$ are the i^{th}

and j^{th} elements of the probability vectors $\hat{p}(D^{(2)})$ and $\hat{p}(D^{(1)})$, respectively, stand for the probabilities of the system response being in the i^{th} and j^{th} attraction domains in the next and the current excitation cycles, respectively. The conditional probabilities $p_{ij}(i|j)$ in Eq.(2.13) depend on the domain exit probabilities, $p(E_{dL})$ and $p(E_{dU})$, and the probability that an attraction domain becomes the destination domain.

Note that under stationary condition $\hat{p}(D^{(2)})$ is equal to $\hat{p}(D^{(1)})$. Thus, obtaining a stationary probability vector $\hat{p}(D) = \{p_i(D_i)\}$ from Eq.(2.10) or Eq.(2.13) is equivalent to obtaining the eigenvector of the transition matrix K corresponding to the unit eigenvalue. Normalization of the eigenvector is required to meet the probability rule.

2.5 Evaluation of Probability Transition Matrix *K*

Conditional probabilities, $p_{ij}(i|j)$, can be evaluated by considering the mechanism of the system response inter-domain transition behavior depicted previously and the stochastic behavior of the excitation amplitude characterized by Eq.(2.9). For the system response to stay in the same attraction domain, D_d, in the next excitation cycle, the excitation amplitude must remain within the same domain, D_d^A, in the next cycle. The probability, $p(A|D_d^A)$, of the excitation amplitude being in the domain D_d^A can be expressed as

$$p(A \mid D_d^{\,A}) = \frac{p(A)}{\int_{D_d^{\,A}} p(A)dA}, \qquad A \in D_d^{\,A} \tag{2.14}$$

where, $p(A)$ is a Rayleigh distribution. From Eq.(2.9), the probability distribution, $p(A^{(2)}|A^{(1)} \in D_d^A)$, of the excitation amplitude in the next cycle given that the excitation amplitude belongs to D_d^A in the current cycle can be obtained by

$$p(A^{(2)} \mid A^{(1)} \in D_d^{\,A}) = \int_{D_d^{\,A}} p(A^{(2)} \mid A^{(1)}) p(A^{(1)} \mid D_d^{\,A}) dA^{(1)} \tag{2.15}$$

Thus, the probability that the system response remains in the same attraction domain, D_d, in the next excitation cycle reads

$$p(R^{(2)} \in D_d^{\,R} \mid R^{(1)} \in D_d^{\,R}) = \int_{D_d^{\,A}} p(A^{(2)} \mid A^{(1)} \in D_d^{\,A}) dA^{(2)} \tag{2.16}$$

Note that $p(R^{(2)} \in D_d^R \mid R^{(1)} \in D_d^R)$ is equal to the diagonal elements of K, $p_{ii}(i|i)$, in Eqs.(2.12-2.13). The probability, $p(E_{dU})$, that the system response exits from the attraction domain D_d at the domain upper limit A_{dU} is equivalent to the probability that the excitation amplitude $A^{(2)}$ is greater than A_{dU}. Thus, from Eq.(2.15), $p(E_{dU})$ can be obtained by

$$p(E_{dU}) = 1 - \int_0^{A_{dU}} p(A^{(2)} \mid A^{(1)} \in D_d^{\,A}) dA^{(2)} \tag{2.17}$$

Accordingly, the probability, $p(E_{dL})$, that the system response exits from the attraction domain D_d at the domain lower limit A_{dL} can be obtained by

$$p(E_{dL}) = 1 - \int_{A_{dL}}^{\infty} p(A^{(2)} \mid A^{(1)} \in D_d^{\,A}) dA^{(2)} \tag{2.18}$$

Note that, after the system response exits from an attraction domain, there may exist multiple possible destination domains of the inter-domain transition. In this

case, the transient-state system mean energy, or equivalently, the transient-state system response amplitude is employed to determine the attraction domain that the system will settle to during the inter-domain transition. The system energy level can be represented by the system mean energy which is defined as the averaged system total energy over one excitation cycle. Fig. 2.4 shows the relationship between the system total energy and the system mean energy. When the system response has a higher total energy local maximum, the system mean energy is also higher. In addition, when the system response has a higher mean energy, the response also has a larger amplitude as shown in Fig. 2.4.

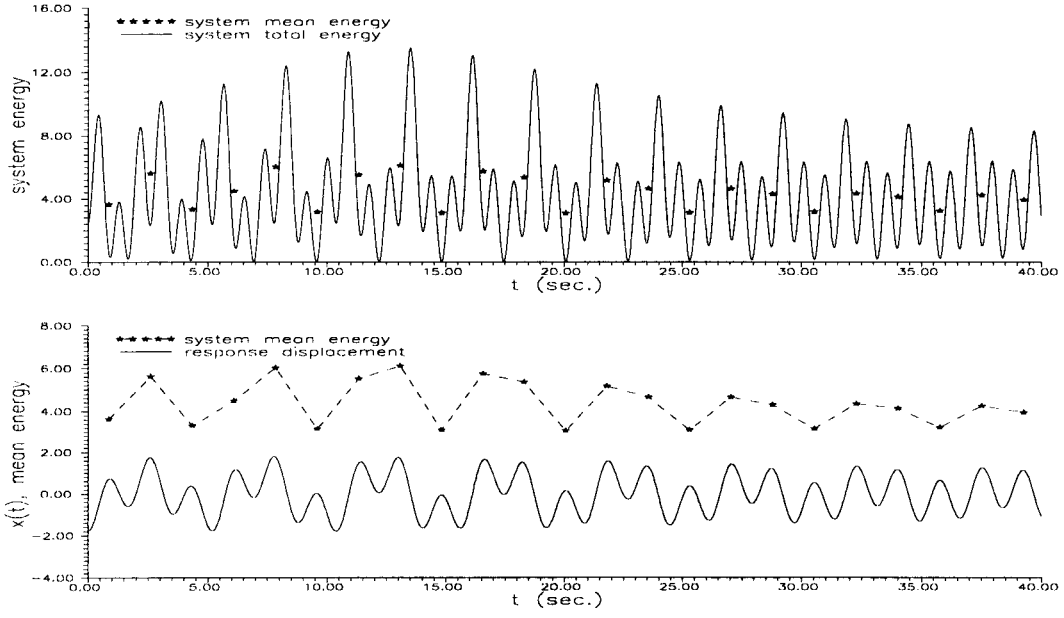

Fig. 2.4 System response in the small amplitude harmonic domain. (Top) relationship between transient-state system total energy and mean energy over one excitation cycle. (Bottom) relationship between response displacement and mean energy. $\{C_S = 0.05, a_1 = 1, a_3 = 0.3, \omega = 3.6, \phi = 0, A = 12$ $(x(0), dx/dt(0)) = (-1.8, 0)\}$.

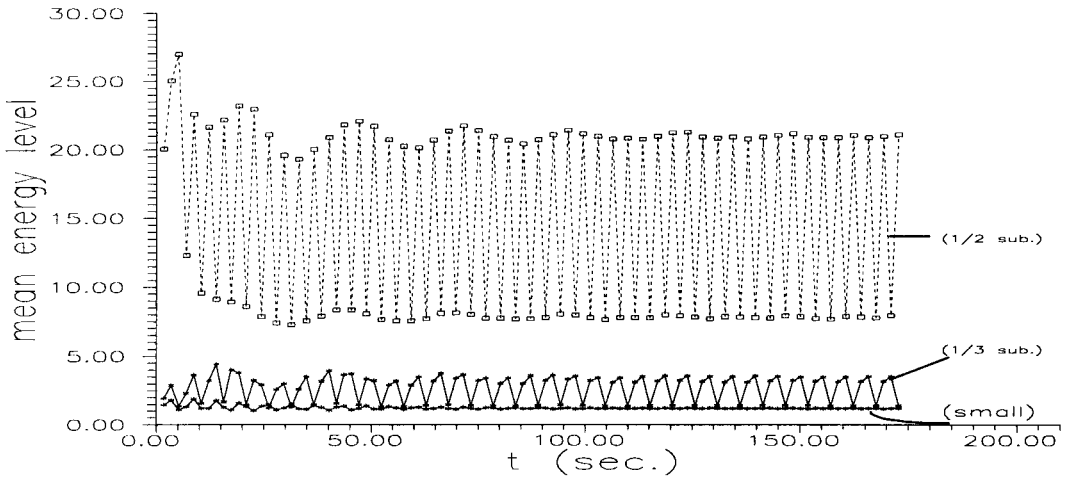

Fig. 2.5 Mean energy level of the system response in the small amplitude harmonic domain and the 1/2 and 1/3 subharmonic domains. $\{C_S = 0.05, a_1 = 1, a_3 = 0.3, \omega = 3.6, \phi = 0, A = 7\}$, $(x(0), dx/dt(0)) = \{(-1, 0.5)$ (small amplitude harmonic response), (-3.75, 4.75) (1/2 subharmonic response), (-1.4, 0.75) (1/3 subharmonic response)$\}$.

For example, consider the 1/2 subharmonic domain lower boundary A_{2L}. At this lower bound, the possible destination domains are the large and the small amplitude harmonic domains, and the 1/3 subharmonic domain (see Fig. 2.3). However, a jump from a 1/2 subharmonic response domain to the large amplitude resonance response domain is highly unlikely due to the decreasing excitation amplitude (hence input energy). Thus, during the inter-domain transition, the system response may transition to either the small amplitude harmonic or the 1/3 subharmonic domain (see Fig. 2.3) when the excitation amplitude varies from $A > A_{2L}$ ($A = 7$ in this case) to $A < A_{2L}$ ($A = 6$). Fig. 2.5 shows that the system mean energy of a typical response in the 1/2 subharmonic domain is higher than those corresponding to the 1/3 subharmonic domain, which in turn is higher than those in

the small amplitude harmonic domain. Therefore, it can be assumed that, after the response exits from the 1/2 subharmonic domain, it will first visit the 1/3 subharmonic domain before it can visit the small amplitude harmonic domain.

The four diagonal elements of matrix K, $p(L|L) = p_{11}(1|1)$, $p(S|S) = p_{22}(2|2)$, $p(1/2|1/2) = p_{33}(3|3)$, and $p(1/3|1/3) = p_{44}(4|4)$, can also be obtained by Eq.(2.16). Evaluation of the rest elements of K can be performed with following steps:

1. $p(L|1/3)$, $p(1/2|S)$, $p(1/3|S)$ According to the response inter-domain transition behavior, these three conditional probabilities are equal to zeros.

$$p_{14}(1|4) = p_{32}(3|2) = p_{42}(4|2) = 0 \tag{2.19}$$

2. $p(L|S)$ This probability is equal to the complement of $p(S|S)$. Thus,

$$p_{12}(1|2) = 1 - p_{22}(2|2) \tag{2.20}$$

3. $p(1/3|1/2)$ When the system is in the 1/2 subharmonic domain, D_3, an exit from the domain at the lower boundary A_{3L} leads the system to the 1/3 subharmonic domain, D_4. Therefore, from Eq.(2.18), $p(1/3|1/2) = p_{43}(4|3)$ can be calculated as

$$p_{43}(4|3) = 1 - \int_{A_{3L}}^{\infty} p(A^{(2)} \mid A^{(1)} \in D_3^A) dA^{(2)} \tag{2.21}$$

4. $p(L|1/2)$ and $p(S|1/2)$ An exit of the system response from the 1/2 subharmonic domain, D_3, at the upper boundary A_{3U} may lead the system to the large (D_1) or the small (D_2) amplitude harmonic domain. The probability of the exit $p(E_{3U})$ can be calculated from Eq.(2.17). The probability that the system response goes to the large amplitude harmonic domain after the exit, $p(L|E_{3U})$, can be approximated by the probability that the system transient-state mean energy

corresponding to A_{3U} is greater than the 1/2 subharmonic steady-state system mean energy at A_{3U}. In addition, because the system mean energy is directly related to the response amplitude, $p(L|E_{3U})$ may also be approximated by the probability that the transient-state response amplitude R corresponding to A_{3U} is greater than the steady-state 1/2 subharmonic response amplitude $R_{3U}^{(S)}$ at A_{3U}. The response amplitude probability distribution $\tilde{p}(R|(D_3^R)_{3U})$ at the domain upper boundary A_{3U} can be obtained from intra-domain transition probability distribution. Therefore,

$$p_{13}(1|3) = p(E_{3U})p(\mathrm{R} > \mathrm{R}_{3\mathrm{U}}^{(\mathrm{S})} | \mathrm{A}_{3\mathrm{U}}) = p(E_{3U}) \sum_{\mathrm{R}>\mathrm{R}_{3\mathrm{U}}^{(\mathrm{S})}} \tilde{\mathrm{p}}(\mathrm{R} | (\mathrm{D}_3^{\mathrm{R}})_{3U}) \tag{2.22}$$

$$p_{23}(2|3) = p(E_{3U})p(\mathrm{R} \le \mathrm{R}_{3\mathrm{U}}^{(\mathrm{S})} | \mathrm{A}_{3\mathrm{U}}) = p(E_{3U}) \sum_{\mathrm{R}\le\mathrm{R}_{3\mathrm{U}}^{(\mathrm{S})}} \tilde{\mathrm{p}}(\mathrm{R} | (\mathrm{D}_3^{\mathrm{R}})_{3U}) \tag{2.23}$$

5. <u>$p(1/2|1/3)$ and $p(S|1/3)$</u> Based on the response inter-domain transition behavior described in Section 2.1.2 and the arguments presented step 4, the probability of the system response going to the 1/2 subharmonic (D_3) and the small amplitude harmonic (D_2) domains after an exit from the 1/3 subharmonic domain (D_4) can be calculated as,

$$p_{24}(2|4) = p(E_{4U})p(\mathrm{R} > \mathrm{R}_{4\mathrm{U}}^{(\mathrm{S})} | \mathrm{A}_{4\mathrm{U}}) = p(E_{4U}) \sum_{\mathrm{R}>\mathrm{R}_{4\mathrm{U}}^{(\mathrm{S})}} \tilde{\mathrm{p}}(\mathrm{R} | (\mathrm{D}_4^{\mathrm{R}})_{4U}) \tag{2.24}$$

$$p_{24}(2|4) = 1 - p_{44}(4|4) - p_{34}(3|4) \tag{2.25}$$

respectively, where, $R_{4U}^{(S)}$ is the steady-state 1/3 subharmonic response amplitude at A_{4U}. The probabilities $p(E_{4U})$ and $\tilde{\mathrm{p}}(\mathrm{R}|(\mathrm{D}_4^{\mathrm{R}})_{4\mathrm{U}})$ are obtained from Eqs.(2.17) and intra-domain transition probability distribution, respectively.

6. <u>$p(1/2|L)$, $p(1/3|L)$ and $p(S|L)$</u> During the inter-domain transition following the exit of the system response from the large amplitude harmonic domain, D_1, the

response amplitude keeps decreasing while the excitation amplitude varies randomly. Depending on the excitation amplitude variation, the possible destination domains of the transition include the 1/2 subharmonic, D_3, the 1/3 subharmonic, D_4, and the small amplitude harmonic, D_2, attraction domains.

For the system response transition to the 1/2 subharmonic domain, D_3, it is assumed that the excitation amplitude A must be within the domain D_{3A} when the response amplitude R decreases to the mean steady-state 1/2 subharmonic response amplitude, $R_3^{(S)}$. Similarly, for the system transition to the 1/3 subharmonic domain, D_4, the excitation amplitude must be within the domain D_4^A when the response amplitude decreases to the mean steady-state 1/3 subharmonic response amplitude, $R_4^{(S)}$.

To estimate the number of excitation cycles required for the harmonic response amplitude decreasing from attraction domain D_1 to D_3 and D_4, the response amplitude decay rate of an unforced linear system is employed (Clough and Penzien, 1993). The damping and stiffness coefficients of the linear system are identical to those of the nonlinear system considered. Thus, the required excitation cycles may be estimated by

$$m(i,j) = \frac{R_i^{(s)} - R_j^{(s)}}{C_S \pi \, R_j^{(s)}} \sqrt{\mathrm{a}_1} \tag{2.26}$$

where, $m(i, j)$ is the excitation cycles of the transition from the attraction domain D_i to the attraction domain D_j. Note that $R_1^{(S)}$ is the steady-state response amplitude corresponding to the excitation amplitude $A = A_{1L}$, in the attraction domain D_1. Let $m1 = m(1, 3)+1$ and $m2 = m(3, 4)$. Thus, when the response amplitude decreases

from $R_1^{(S)}$ to $R_3^{(S)}$, the probability distribution of the excitation amplitude is obtained as

$$p_3(A^{(m1)} \mid A^{(1)} \in \mathrm{D}_1^{\mathrm{A}}) = \int_{A^{(m1-1)}} p(A^{(m1)} \mid A^{(m1-1)}) \cdots \int_{\mathrm{D}_1^{\mathrm{A}}} p(A^{(3)} \mid A^{(2)}) \int_{A^{(1)} \in \mathrm{D}_1^{\mathrm{A}}} p(A^{(2)} \mid A^{(1)}) p(A^{(1)} \mid D_1^A) dA^{(1)} dA^{(2)} \cdots dA^{(m1-1)} \tag{2.27}$$

$$p(A^{(m1)} \in \mathrm{D}_3^{\mathrm{A}}) = \int_{\mathrm{D}_3^{\mathrm{A}}} p_3(A^{(m1)} \mid A^{(1)} \in \mathrm{D}_1^{\mathrm{A}}) dA^{(m1)} \tag{2.28}$$

where $\bar{D}_1^A$ is the complement domain of D_1^A. A part of the excitation amplitudes $A^{(m1)}$ not within D_3^A will propagate toward D_4^A and the rest are going to D_2^A. Thus,

$$p_4(A^{(m1+m2)} \mid A^{(1)} \in \mathrm{D}_1^{\mathrm{A}}) = \int_{A^{(m1+m2-1)}} p(A^{(m1+m2)} \mid A^{(m1+m2-1)}) \cdots \int_{A^{(m1-1)}} p(A^{(m1+2)} \mid A^{(m1+1)}) \int_{\bar{\mathrm{D}}_3^{\mathrm{A}}} p(A^{(m1+1)} \mid A^{(m1)}) p_3(A^{(m1)} \mid A^{(1)} \in D_1^A) dA^{(m1)} dA^{(m1+1)} \cdots dA^{(m1+m2-1)} \tag{2.29}$$

$$p(A^{(m1+m2)} \in \mathrm{D}_4^{\mathrm{A}}) = \int_{D_4^A} p_4(A^{(m1+m2)} \mid A^{(1)} \in D_1^A) dA^{(m1+m2)} \tag{2.30}$$

where, $\bar{D}_3^A$ is the complement domain of D_3^A. The probabilities $p_{31}(3|1)$, $p_{41}(4|1)$ and $p_{21}(2|1)$ can be obtained as

$$p_{31}(3 \mid 1) = [1 - p_{11}(1 \mid 1)] p(A^{(m1)} \in \mathrm{D}_3^{\mathrm{A}}) \tag{2.31}$$

$$p_{41}(4 \mid 1) = [1 - p_{11}(1 \mid 1)][1 - p(A^{(m1)} \in \mathrm{D}_3^{\mathrm{A}})] p(A^{(m1+m2)} \in \mathrm{D}_4^{\mathrm{A}}) \tag{2.32}$$

$$p_{21}(2 \mid 1) = [1 - p_{11}(1 \mid 1)][1 - p(A^{(m1)} \in \mathrm{D}_3^{\mathrm{A}})][1 - p(A^{(m1+m2)} \in \mathrm{D}_4^{\mathrm{A}})] \tag{2.32}$$

2.6 Response Intra-domain Transition Probabilities

The intra-domain transition is defined as the cycle-to-cycle response amplitude transition behavior that takes place within the same attraction domain. Due to variations in the excitation amplitude, transitions of the response amplitude probability will occur among response amplitude domains, $(D_d^R)_A$, corresponding to different excitation amplitude within D_d^A. The governing equation of the intra-domain probability transition from $(D_d^R)_A^{(1)}$ at the current excitation cycle to $(D_d^R)_A^{(2)}$ at the next excitation cycle reads

$$p\left(R^{(2)} \mid A^{(1)}, A^{(2)}, D_d{}^R\right) = \int_{\left(D_d{}^R\right)_A^{(1)}} p\left(R^{(2)} \mid R^{(1)}, A^{(1)}, A^{(2)}, D_d{}^R\right) p\left(R^{(1)} \mid \left(D_d{}^R\right)_A^{(1)}\right) dR^{(1)} \quad (2.33)$$

where, $p(R^{(2)} \mid R^{(1)}, A^{(1)}, A^{(2)}, D_d^R)$ is a domain dependent response amplitude probability transition density function.

Note that the probability distribution of the response amplitude $p(R^{(2)}|(D_d^R)_A^{(2)})$ may be transitioned from all $p(R^{(1)}|(D_d^R)_A^{(1)}, A^{(1)} \in D_d^R)$ and is the union of all the possible transitions. These events are mutually exclusive and thus, according to the Bayes formula (Ochi, 1990), $p(R^{(2)}|(D_d^R)_A^{(2)})$ can be expressed as

$$p\left(R^{(2)} \mid \left(D_d{}^R\right)_A^{(2)}\right) = \int_{D_d{}^R} p\left(R^{(2)} \mid A^{(1)}, A^{(2)}, D_d{}^R\right) p\left(A^{(1)} \mid D_d{}^A\right) dA^{(1)} \quad (2.34)$$

On the other hand, occurrence of a response amplitude R being in the domains, D_d^R, corresponding to different attraction domains, D_d, are mutually exclusive events. Therefore, the response amplitude PDF can be expressed as (Ochi, 1990)

$$p\left(R^{(z)}\right)=\sum_{d=1}^{n} p\left(R^{(z)} \mid D_d{}^R\right)p\left(D_d{}^R\right) \qquad z=1,\ 2 \tag{2.35}$$

In addition, within an attraction domain, the response amplitude PDF can also be expressed as

$$p\left(R^{(z)} \mid D_d{}^R\right)=\int p\left(R^{(z)} \mid \left(D_d{}^R\right)_A\right)p\left(\left(D_d{}^R\right)_A\right)d\left(D_d{}^R\right)_A, \qquad z=1,\ 2 \tag{2.36}$$

Note that $\{p(\,(D_d^R)_A\,)\,d((D_d^R)_A\,)\}$ is equivalent to $\{p(\,A|\,D_d^R\,)\,dA\}$ which stands for the probability of the excitation amplitude being equal to A given that A belongs to D_d^A. The integration of Eq.(2.36) is carried out over the entire domain D_d^A. Thus, Eq.(2.36) can be rewritten as

$$p\left(R^{(z)} \mid D_d{}^R\right)=\int_{D_d{}^A} p\left(R^{(z)} \mid \left(D_d{}^R\right)_A\right)p\left(A \mid D_d{}^A\right)dA, \qquad z=1,\ 2 \tag{2.37}$$

By substituting Eq.(2.33) and (2.34) into Eq.(2.36), the governing equation of the response amplitude intra-domain probability transition yields

$$\begin{aligned} &p\left(R^{(2)} \mid D_d{}^R\right) \\ &=\int\left\{\int\left[\int p\left(R^{(2)} \mid R^{(1)}, A^{(1)}, A^{(2)}, D_d{}^R\right)p\left(R^{(1)} \mid \left(D_d{}^R\right)_A^{(1)}\right)dR^{(1)}\right]p\left(A^{(1)} \mid D_d{}^A\right)dA^{(1)}\right\}p\left(A^{(2)} \mid D_d{}^A\right)dA^{(2)} \end{aligned} \tag{2.38}$$

Finally, the overall stationary response amplitude PDF can be approximated as

$$\tilde{p}(R^{(1)})=\tilde{p}(R^{(2)})=\sum_{d=1}^{n}\tilde{p}(R^{(1)} \mid D_d{}^R)p(D_d) \tag{2.39}$$

2.7 Evaluation of Response Intra-domain Transition Probabilities

From a deterministic point of view, the variation in the response amplitude is a function of: (1) the excitation amplitude and the response amplitude in the current excitation cycle, (2) variation in the excitation parameters (amplitude and phase angle), and (3) the system phase status *(x, dx/dt)* at the time when the excitation parameter variation takes place, which is also considered as the initial condition of the following transient-state response. That is,

$$R^{(2)} = g(R^{(1)}, A^{(1)}, A^{(2)}, \Phi = \phi^{(2)} - \phi^{(1)}, X^0) \tag{2.40}$$

where, $R^{(1)}$ and $R^{(2)}$ are response amplitudes in the domains $(D_d^R)_A^{(1)}$ and $(D_d^R)_A^{(2)}$, respectively; Φ is the variation in the excitation phase angle; and X^0 stands for the system initial condition. Note that the function g is domain dependent. If the response amplitude $R^{(1)}$, the excitation amplitude $A^{(1)}$ and $A^{(2)}$ are fixed, then $R^{(2)}$ can be considered as a function of Φ and X^0 only, i.e., $R^{(2)} = \breve{g}(\Phi, X^0)$ where $\breve{g}$ is a domain dependent function. As a result, the probability distribution of $R^{(2)}$ can be derived from the joint probability distribution of Φ and X^0 through the functional relationship $R^{(2)} = \breve{g}(\Phi, X^0)$, given that $R^{(1)}$, $A_j^{(1)}$ and $A_i^{(2)}$ are fixed. However, to date, an explicit expression of the function $\breve{g}$ (or g) is not available and, thus, a direct derivation of $p(R^{(2)} \mid R^{(1)}, A^{(1)}, A^{(2)}, D_d^R)$ from $p(\Phi, X^0 \mid R^{(1)}, A^{(1)}, A^{(2)}, D_d^R)$ is not feasible. Thus, to obtain $p(R^{(2)} \mid R^{(1)}, A^{(1)}, A^{(2)}, D_d^R)$, the use of a numerical technique is required.

To facilitate a numerical evaluation of $p(R^{(2)} \mid R^{(1)}, A^{(1)}, A^{(2)}, D_d^R)$, the response amplitude domains $\{(D_d^R)_A^{(z)}, z=1,2\}$, the system initial condition X^0 domain, the excitation phase angle difference Φ domain, and the excitation amplitude domain D_d^A are discretized. The value of $\breve{g}(\Phi_{up}, X_{uo}^0) = R_{ur2}^{(2)}$, given $R_{ur1}^{(1)}$, $A_j^{(1)}$ and $A_i^{(2)}$ can be obtained by direct numerical integration of Eq.(2.1), where the subscripts indicate sample points of their corresponding discretized random variables, Φ, X^0, $R^{(1)}$, $R^{(2)}$, and D_d^A, respectively. Thus, $p(\Phi_{up}, X_{uo}^0 \mid R_{ur1}^{(1)}, A_j^{(1)}, A_i^{(2)}, D_d^R) = p(R_{ur2}^{(2)} \mid R_{ur1}^{(1)}, A_j^{(1)}, A_i^{(2)}, D_d^R)$.

The probability distribution of the phase difference Φ is characterized by Eq.(2.8) and depends on $A_j^{(1)}$ and $A_i^{(2)}$ only. The initial condition, X^0, is assumed to be uniformly distributed over the domain which is the phase trajectory of the current response cycle. In addition, Φ and X^0 can be assumed as statistically independent because the excitation properties Φ is not affected by the system response and the uniformly distributed system initial condition is affected by neither the variation in the excitation parameters nor the system response. Thus,

$$\begin{aligned} & p(R_{ur2}^{(2)} \mid R_{ur1}^{(1)}, A_j^{(1)}, A_i^{(2)}, D_d^R) \\ & = p(\Phi_{up}, X_{uo}^0 \mid R_{ur1}^{(1)}, A_j^{(1)}, A_i^{(2)}, D_d^R) = \frac{1}{m_x} \int_{\Phi_{up}-\Delta\Phi/2}^{\Phi_{up}+\Delta\Phi/2} \frac{p(A_j^{(1)}, A_i^{(2)}, \Phi)}{p(A_j^{(1)}, A_i^{(2)})} d\Phi \end{aligned} \tag{2.41}$$

where, m_x is the total number of intervals in discretized X^0 domain; $p(A_j^{(1)}, A_i^{(2)}, \Phi)$ and $p(A_j^{(1)}, A_i^{(2)})$ can be obtained by Eqs.(2.8)-(2.9). By varying Φ_{up} and X_{uo}^0 over their entire respective domains and lumping all computed $p(R_{ur2}^{(2)} \mid R_{ur1}^{(1)}, A_j^{(1)},$

$A_i^{(2)}$, D_d^R), a probability vector of the response amplitude $p(R^{(2)} \mid R_{url}^{(1)}, A_j^{(1)}, A_i^{(2)}, D_d^R)$ can be obtained.

3. ANALYSIS AND PREDICTIONS AND COMPARISONS OF STOCHASTIC RESPONSES

3.1 Analysis of Stochastic Response Behavior

3.1.1 Jump phenomena among various harmonic/subharmonic responses

The system response under a narrowband excitation exhibits amplitude jumps between several levels as shown in Fig. 3.1. To depict the mechanism of the jump phenomenon, an amplitude response map, Fig. 3.2, which is obtained by plotting the excitation amplitudes versus the corresponding measured response amplitudes, is employed. In the figure, the corresponding amplitude response curves of the system are presented as solid lines. Note that the characteristics of the response inter-domain transition behavior depicted in Chapter 2 are preserved under the narrowband excitation environment. Namely, the system response goes from the large amplitude domain to the small amplitude domain when the excitation amplitude varies from greater than to less than the large amplitude domain lower boundary.

Under close examination of the details of response time histories (e.g., Fig. 3.1), 1/2 and 1/3 subharmonic responses are observed to occur repeatedly under narrowband excitations. These subharmonic responses are often difficult to identify due to overlapping of the different response amplitude (i.e., small amplitude harmonic, 1/2 and 1/3 subharmonic) domains (e.g., clustered 4.0 length units in Fig. 3.1). However, the existence of these responses can be identified

relatively clearly in the associated amplitude response maps (e.g., Fig. 3.2) by observing the points located along to the corresponding subharmonic amplitude response curves.

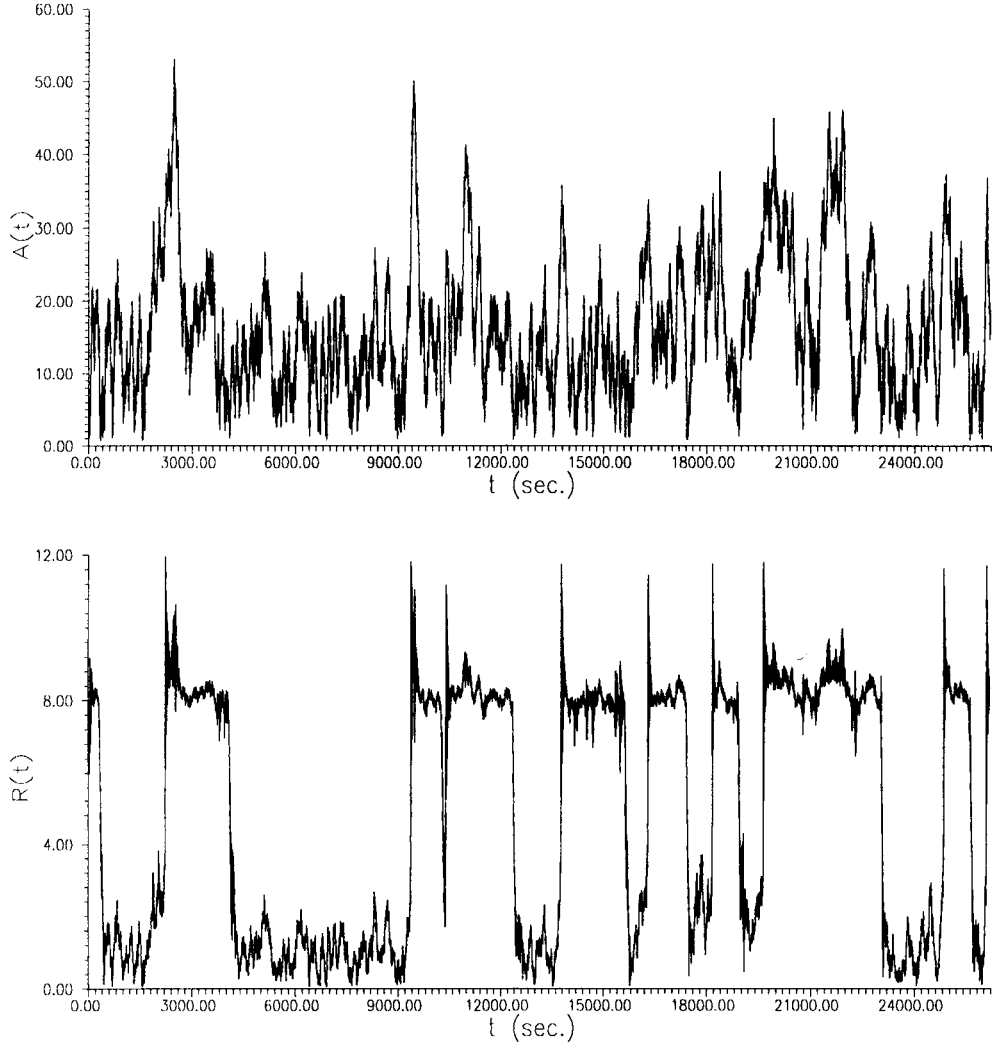

Fig. 3.1 System response in the subharmonic resonance region. Time series of narrowband excitation amplitude (top) and corresponding response amplitude (bottom). $\{Cs = 0.05, a_1 = 1, a_3 = 0.3, \omega_f = 3.6, \sigma_f^2 = 157, \gamma = 0.005\}$.

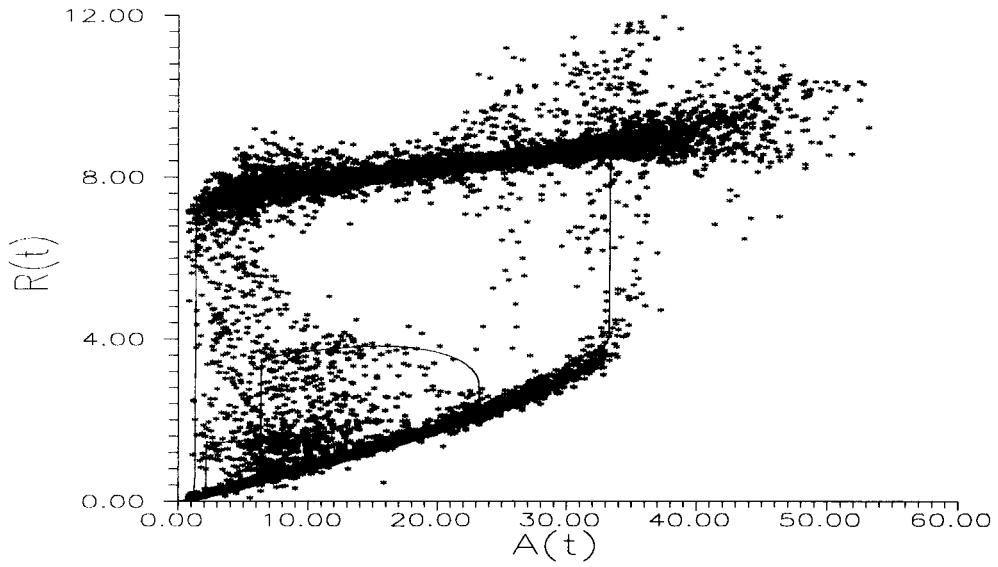

Fig. 3.2 Amplitude response maps corresponding to the time series shown in Fig. 3.1.

Existence of the 1/3 subharmonic response under narrowband excitation was also observed in simulations conducted in previous studies (Davies and Rajan, 1988; Francescutto, 1991) when an extremely small excitation bandwidth and special system initial conditions are employed. However, it was concluded that the 1/3 subharmonic response only exists in the beginning of a response realization, and once it disappears, it will not be observed. This contradiction in the observation of repeated occurrence of the subharmonic response may be due to different simulation durations employed. In this study, the simulation duration is on the order of 12,000 excitation cycles, significantly longer than the approximately 600 cycles employed in previous studies.

3.1.2 Frequency of occurrence and transition among attraction domains

Stochastic system response characteristics, including frequency of occurrence and transition among various attraction domains can be observed in the time histories and amplitude response maps. As indicated in Figs.3.1-2, the frequencies of occurrence are relatively high for large and small amplitude harmonic responses, and low for 1/2 and 1/3 subharmonic responses. As mentioned in previous sections, when the excitation gradually exceeds the region of small amplitude harmonic response, a jump to the large amplitude response is almost certain, while decrease in excitation amplitude induces possible jumps from large amplitude harmonic response to either 1/2 or 1/3 subharmonic or small amplitude responses. Trends for jumps among 1/2 and 1/3 subharmonic and small amplitude responses are less clear. Numerical values governing these probabilities of occurrence and transition will be presented and discussed in a later section. Dependency of the probabilities of occurrence and transition among various domains will also be examined.

3.1.3 Effects of varying excitation bandwidth

Effects of varying the degree of randomness of the excitation (i.e., excitation bandwidth) on the response behavior are demonstrated in Fig. 3.3(a-d). Observe that as the degree of randomness in the excitation increases (increasing excitation bandwidth parameter γ), the response time series exhibits more frequent amplitude jumps between distinct levels. In addition, the total time of the response in higher

amplitude level also increases. As a result, the probability of the system response staying in the higher amplitude level increases as the excitation bandwidth increases. Consequently, the response inter-domain probability transition and the response amplitude PDF are related to the excitation bandwidth. As shown in the corresponding amplitude response maps (Fig. 3.4), increasing excitation randomness also results in spreading of the amplitude distribution around the deterministic response amplitude curves. For a low degree of excitation randomness (Fig. 3.4(a)), amplitude spreading is concentrated at the jump transitions among large and small amplitude and 1/3 subharmonic responses. (Note that 1/2 subharmonic does not appear to occur.) The interior regions of the large and small amplitude responses resemble those of their corresponding deterministic system. However, as the degree of excitation randomness increases (Fig. 3.4(b-c)), amplitude spreading moves towards the overlapping region involving all responses (large and small amplitude as well as 1/2 and 1/3 subharmonics). For a large degree of excitation randomness (Fig. 3.4(d)), spreading of the amplitude distribution among various attraction domains becomes even more significant, resulting in the increase in variance of the response amplitude in each response attraction domain. Therefore, the response intra-domain probability transition and, thus, the response amplitude PDFs are clearly affected by variations in the excitation bandwidth.

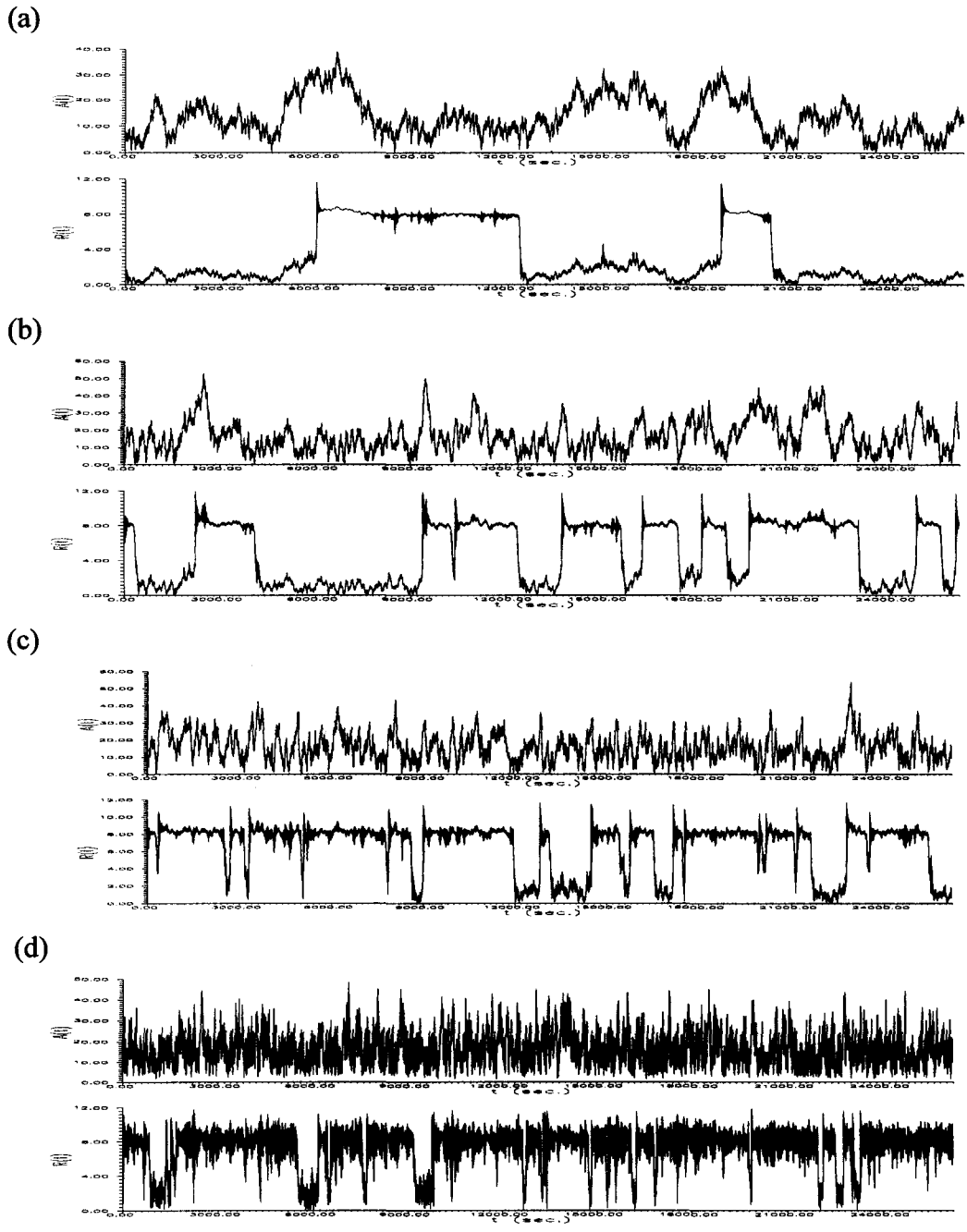

Fig. 3.3 (a), (b), (c), and (d): System response under varying excitation bandwidth in the subharmonic resonance region. Time series of narrowband excitation amplitude (top) and corresponding response amplitude (bottom). {Cs=0.05, a_1=1, a_3=0.3, ω_f=3.6, σ_f^2 = 57, γ= (a) 0.001, (b) 0.005, (c) 0.01, (d) 0.05}.

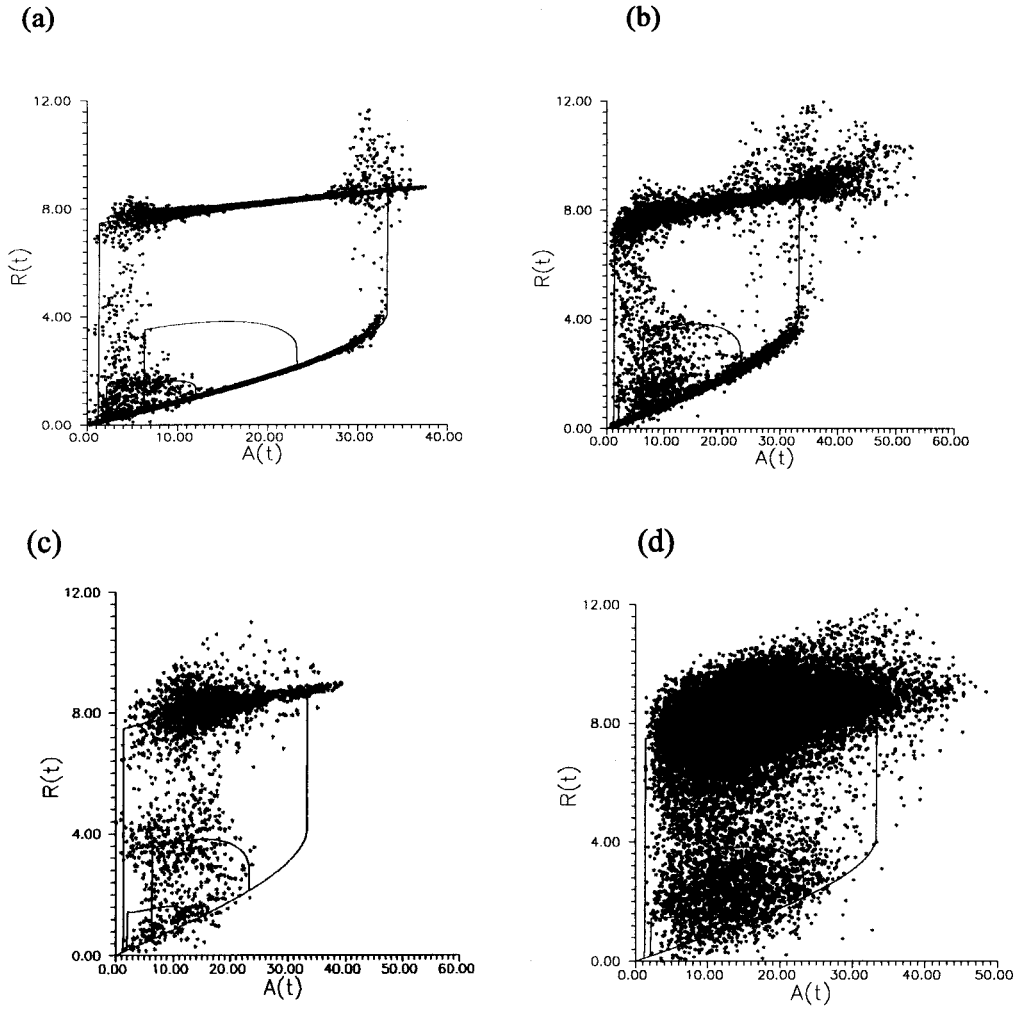

Fig. 3.4 (a), (b), (c), and (d): Amplitude response maps corresponding to the times series shown in Fig. 3.3 (a) – (d), respectively.

3.1.4 Effects of varying excitation intensity

The responses of the nonlinear Duffing system subjected to two levels of excitation intensity are shown in Fig. 3.5. Note that for smaller value of excitation intensity, the relative time of the system response spends in the lower amplitude

level is longer. Because the excitation bandwidth employed is fixed in these cases, the degree of randomness in the excitation is not changed. Consequently, as observed, the frequency of the response amplitude jumps is approximately unchanged. However, with lower excitation intensity, it appears that on the average, the system response stays longer in the lower amplitude level during each visit. In other words, the probability of the system response in the lower amplitude level increases as the excitation intensity decreases. Consequently, the response inter-domain probability transition is also affected by the excitation intensity.

Note that, in the amplitude response maps shown in Fig. 3.6, the density of the points in the small amplitude as well as the 1/2 and 1/3 subharmonic response region increases as the excitation intensity decreases. Thus variations in the density of the amplitude response maps also reflect the influence of variations in excitation intensity on the system response.

(a)

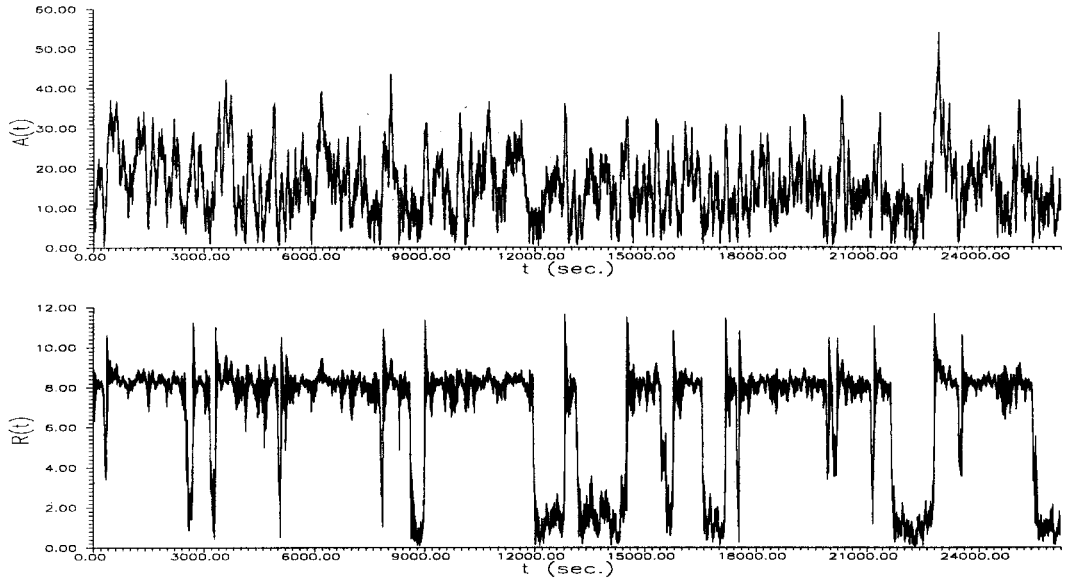

(b)

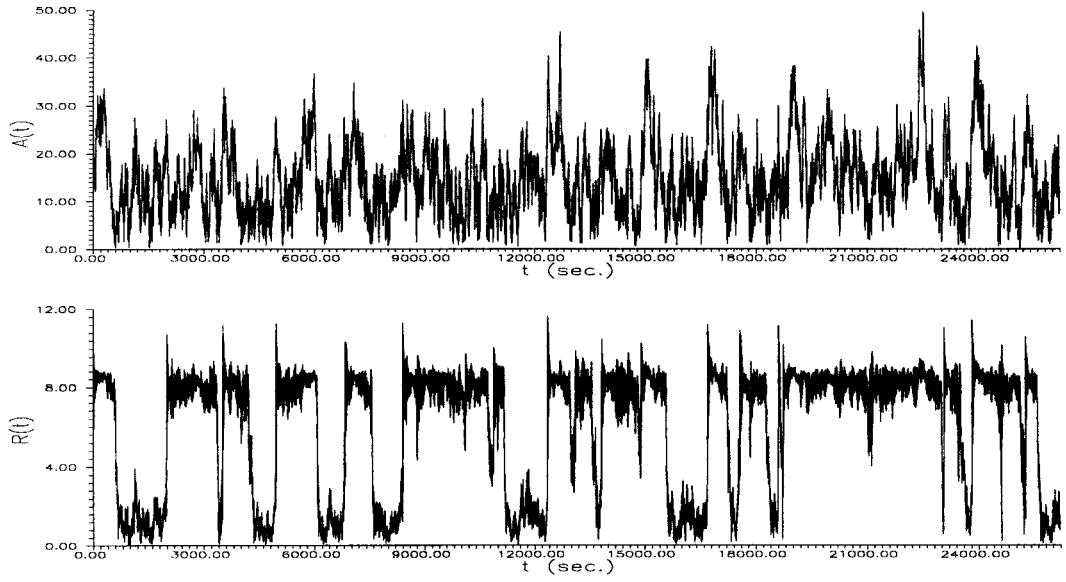

Fig. 3.5 (a) and (b): system response under varying excitation variance in the subharmonic resonance region. Time series of narrowband excitation (top) and corresponding response amplitude (bottom). {$Cs = 0.05$, $a_1 = 1$, $a_3 = 0.3$, $\omega_f = 3.6$, $\gamma = 0.01$, σ_f^2 = (a) 157, (b) 125}.

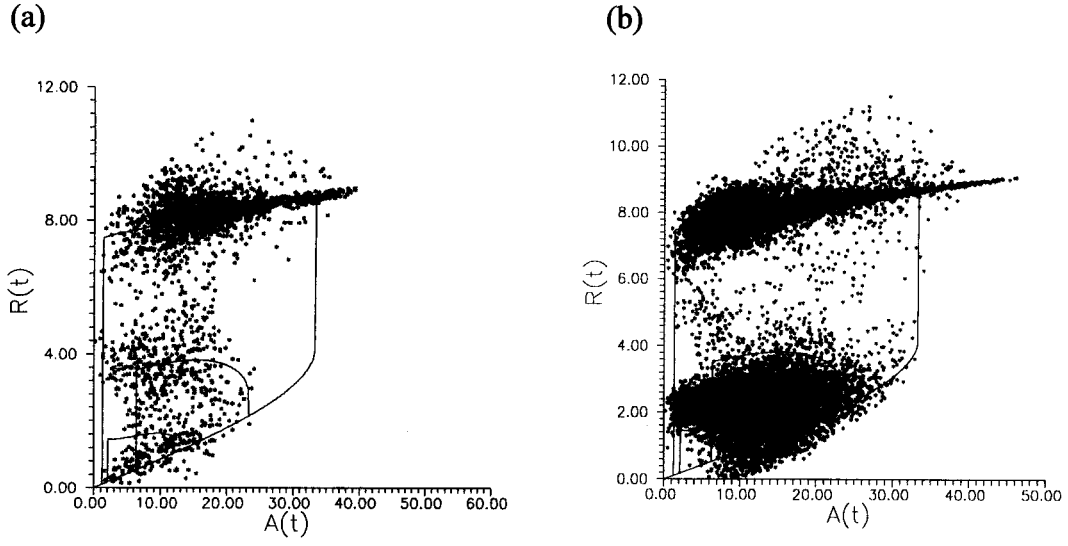

Fig. 3.6 (a), and (b): Amplitude response maps corresponding to the times series shown in Fig. 3.3 (a) and (b), respectively.

3.2 Predictions of Stochastic Response Behavior and Comparisons with Simulations

To verify the capability of the proposed semi-analytical method in characterizing the stochastic system response behavior in the subharmonic resonance region described above, analytical predictions of the system response in five cases with various excitation parameter sets (see Table 3.1 below) are presented and compared to simulation results.

Case	(i)	(ii)	(iii)	(iv)	(v)
γ	0.001	0.005	0.01	0.05	0.01
σ_f^2	157				125

Table 3.1 Excitation parameters of the system varied in the subharmonic resonance region. Excitation frequency ω_f = 3.6, and system parameters Cs = 0.05, a_1 = 1, a_3 = 0.3 are held constant.

The system damping, linear and nonlinear restoring force parameters, Cs, a_1 and a_3, respectively, as well as the excitation frequency ω_f are held constant for all five cases. For completeness, the domain boundaries of each response attractor are listed here: lower boundary of large harmonic domain, A_{1L} = 1.4, upper boundary of small harmonic domain, A_{2U} = 33.3, upper boundary of 1/2 subharmonic domain, A_{3U} = 23, lower boundary of 1/2 subharmonic domain, A_{3L} = 6.4, upper boundary of 1/3 subharmonic domain, A_{4U} = 12, and lower boundary of 1/3 subharmonic domain, A_{4L} = 2.2.

3.2.1 Effect of varying excitation randomness on inter-domain transitions

The system response behavior under varying degree of excitation randomness, γ, with constant excitation intensity, σ_f^2, is investigated in this section. The normalized auto-correlation, $\rho' = |\rho|/\sigma_f^2$, and the cross-correlation coefficients of the cosine and sine components $\lambda' = |\lambda|/\sigma_f^2$, of the excitation envelop process with time lag equal to the central excitation period (Ochi, 1990), the inter-domain

probability transition matrices K, and the normalized eigenvectors corresponding to the unit eigenvalues for four values of γ are listed in Table 3.2.

Observe that ρ' decreases and λ' increases as the excitation bandwidth parameter γ increases. Thus, the randomness in the excitation amplitude cosine and sine component processes increases with bandwidth as expected. As a result, the randomness in the excitation amplitude and phase angle processes increases with excitation bandwidth.

In the transition matrix K, decreasing values of diagonal elements with increasing excitation randomness indicate increasing probability of the response exiting from the current attraction domain. The off-diagonal elements, except the zero entries and $p_{41}(4|1)$, increase at different rates with increasing degree of excitation randomness, indicating that the probability of a given attraction domain becomes the destination domain of a transition from another domain increases as the degree of excitation randomness increases. In the last column of Table 3.2, the probability of the response being in the large amplitude harmonic domain $p_1(D_1)$, increases with increasing γ, confirming the observation that the time spend in the region of large amplitude response increase with increasing randomness. Although the values of the probability are of an order of magnitude smaller, the same trend can be said of the 1/2 subharmonic response. Contrarily, the probability the response staying in the small amplitude domain decreases as γ increases. The probability of the response staying in the 1/3 subharmonic domain varies little with changing γ. Thus, the trends of variation in the $p_d(D_d)$ observed in Table 3.2 agree

with the stochastic response behavior observed earlier, hence, validating the inter-domain transition assumption of the proposed semi-analytical procedure.

Case	γ	ρ'	λ'	Transition Matrix, K	Normalized Eigenvector
(i)	0.001	0.999	0.00011	$\begin{bmatrix} 0.9977 & 0.0014 & 0.0014 & 0 \\ 0.0005 & 0.9986 & 0.0116 & 0.0385 \\ 0.0001 & 0 & 0.9802 & 0.0008 \\ 0.0015 & 0 & 0.0068 & 0.9607 \end{bmatrix}$	$\begin{Bmatrix} p_1(D_1) \\ p_2(D_2) \\ p_3(D_3) \\ p_4(D_4) \end{Bmatrix} = \begin{Bmatrix} 0.399 \\ 0.586 \\ 0.001 \\ 0.014 \end{Bmatrix}$
(ii)	0.005	0.996	0.00056	$\begin{bmatrix} 0.9959 & 0.0031 & 0.0039 & 0 \\ 0.0006 & 0.9969 & 0.0143 & 0.0742 \\ 0.0004 & 0 & 0.9566 & 0.0098 \\ 0.0031 & 0 & 0.0252 & 0.961 \end{bmatrix}$	$\begin{Bmatrix} p_1(D_1) \\ p_2(D_2) \\ p_3(D_3) \\ p_4(D_4) \end{Bmatrix} = \begin{Bmatrix} 0.426 \\ 0.547 \\ 0.009 \\ 0.018 \end{Bmatrix}$
(iii)	0.010	0.992	0.00112	$\begin{bmatrix} 0.9949 & 0.0031 & 0.0063 & 0 \\ 0.0008 & 0.9956 & 0.0195 & 0.0949 \\ 0.0017 & 0 & 0.939 & 0.0216 \\ 0.0026 & 0 & 0.0352 & 0.8835 \end{bmatrix}$	$\begin{Bmatrix} p_1(D_1) \\ p_2(D_2) \\ p_3(D_3) \\ p_4(D_4) \end{Bmatrix} = \begin{Bmatrix} 0.462 \\ 0.504 \\ 0.018 \\ 0.016 \end{Bmatrix}$
(iv)	0.050	0.958	0.00549	$\begin{bmatrix} 0.9935 & 0.0097 & 0.0183 & 0 \\ 0.001 & 0.9903 & 0.0389 & 0.1532 \\ 0.0047 & 0 & 0.8679 & 0.0846 \\ 0.0008 & 0 & 0.0749 & 0.7622 \end{bmatrix}$	$\begin{Bmatrix} p_1(D_1) \\ p_2(D_2) \\ p_3(D_3) \\ p_4(D_4) \end{Bmatrix} = \begin{Bmatrix} 0.608 \\ 0.352 \\ 0.029 \\ 0.011 \end{Bmatrix}$

Table 3.2 Effects of varying excitation bandwidth on response inter-domain probability transition in the subharmonic resonance region.

3.2.2 Effect of varying excitation randomness on intra-domain transition

To investigate the influence of varying excitation randomness on the response intra-domain transition behavior, the corresponding variance σ_d^2 of the response amplitude PDF within each attraction domain D_d^R (d=1,2,3,4) is calculated from $\tilde{p}(R \mid D_d^R)$. The results obtained for cases (i) to (iv) are tabulated in Table 3.3. The predicted σ_{Di}^2 increases with increasing excitation bandwidth in all the four co-existing attraction domains, which is in accordance with the

response behavior observed earlier in Fig 3.3. In addition, σ_{Di}^2 (i=1,2,3,4) varies with attraction domains, reflecting the domain dependency of the system response characteristics, validating the proposed semi-analytical method in characterizing the stochastic response behavior under varying excitation bandwidth.

Variance σ_{Di}^2 of Response Amplitude within Attraction Domain				
Case	(i)	(ii)	(iii)	(iv)
γ	0.001	0.005	0.010	0.050
σ_{D1}^2	0.0883	0.1623	0.2370	1.8192
σ_{D2}^2	0.4738	0.5364	0.9796	2.1156
σ_{D3}^2	0.4489	0.6716	0.8203	1.6155
σ_{D4}^2	0.0397	0.1100	0.1885	0.8431

Table 3.3 Effects of varying excitation bandwidth on the variance of the response amplitude within the co-existing attraction domains D_{Di}^R (i=1,2,3,4), respectively, in the subharmonic resonance region.

3.2.3 Effect of varying excitation intensity on inter-domain transition

The effects of varying excitation intensity (i.e., variance σ_f^2) on the system response behavior are investigated in cases (iii) and (v). For these two cases, the values of the normalized parameters ρ' and λ', inter-domain probability transition matrix K, and the normalized eigenvectors corresponding to the unit eigenvalues are listed in Table 3.4.

Case	σ_f^2	ρ'	λ'	Transition Matrix, K	Normalized Eigenvector
(iii)	157	0.992	0.00112	$\begin{bmatrix} 0.9949 & 0.0031 & 0.0063 & 0 \\ 0.0008 & 0.9956 & 0.0195 & 0.0949 \\ 0.0017 & 0 & 0.939 & 0.0216 \\ 0.0026 & 0 & 0.0352 & 0.8835 \end{bmatrix}$	$\begin{Bmatrix} p_1(D_1) \\ p_2(D_2) \\ p_3(D_3) \\ p_4(D_4) \end{Bmatrix} = \begin{Bmatrix} 0.462 \\ 0.504 \\ 0.018 \\ 0.016 \end{Bmatrix}$
(v)	125	0.997	0.00113	$\begin{bmatrix} 0.9936 & 0.0021 & 0.0040 & 0 \\ 0.0010 & 0.9979 & 0.0138 & 0.0894 \\ 0.0015 & 0 & 0.946 & 0.0155 \\ 0.0039 & 0 & 0.0362 & 0.8951 \end{bmatrix}$	$\begin{Bmatrix} p_1(D_1) \\ p_2(D_2) \\ p_3(D_3) \\ p_4(D_4) \end{Bmatrix} = \begin{Bmatrix} 0.243 \\ 0.733 \\ 0.011 \\ 0.013 \end{Bmatrix}$

Table 3.4 Effects of varying excitation variance on response inter-domain transition probability in the subharmonic resonance region.

As shown in the table, the normalized excitation parameters ρ' and λ' (with respect to variance σ_f^2) remain practically constant when the excitation variance σ_f^2 decreases from 157 to 125, confirming that randomness in the excitation is not affected by variations in the excitation intensity. In the transition matrix, K, the complexity of the transition behavior is reflected by variations in the off-diagonal elements. Under response inter-domain transitions, trends of variation in the probabilities that the response in the higher and lower amplitude levels are accurately predicted as shown in the last column of Table 4. That is, $p_1(D_1)$ decreases but $\Sigma p_i(D_i)$ (i=2,3,4) increases with decreasing excitation variance σ_f^2. This result agrees with the response characteristics observed in a previous section.

3.2.4 Effect of varying excitation randomness on response amplitude probability density function

As the degree of excitation randomness (i.e., bandwidth parameter γ) increases (cases (i) through (iv)), Fig. 3.7 shows that the response amplitude probability mass in the high level region increases in accordance with the response behavior observed earlier. In case (iv), although the simulation appear to show only a single mode located in the high amplitude level region in the probability distribution, the long tail of the distribution in the lower amplitude level indicates the existence of a less obvious mode in that region. The less consistent match in the results of case (iv) in the lower amplitude level is probably due to insufficient samples in that region. The comparisons of predictions with simulations for four cases are shown in Fig. 3.8. Note that the semi-analytical method clearly predicts the decreasing probability mass in the small amplitude region and the increasing probability at, and spreading of, the large amplitude response region. The predicted quantitative values match quite well with simulation results also.

(a)

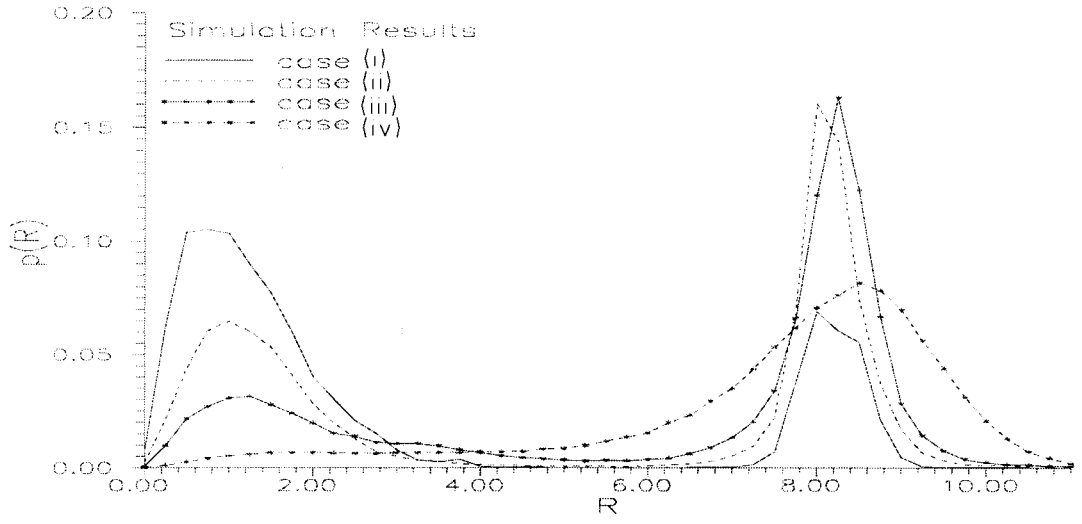

(b)

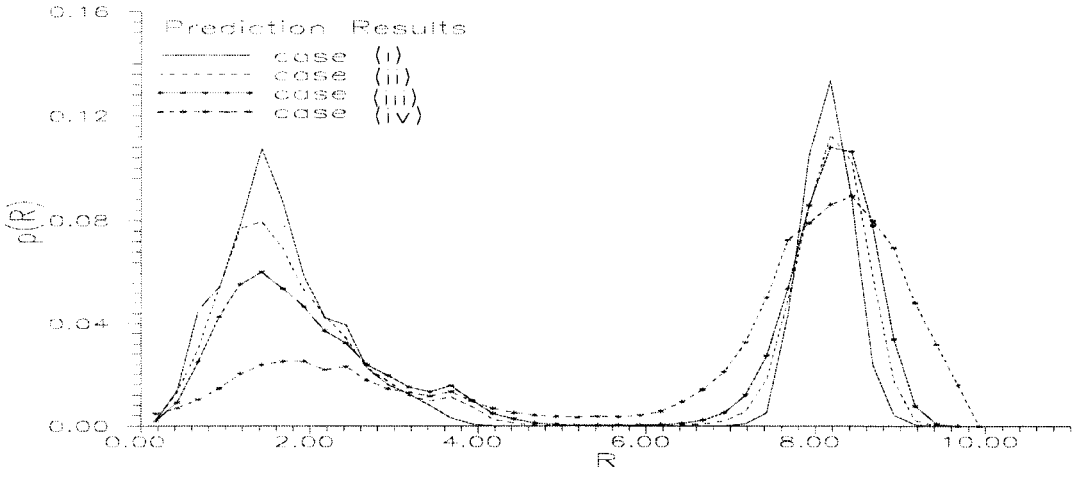

Fig 3.7 Variations in the response amplitude probability distribution under varying excitation bandwidth in the subharmonic resonance region, (a) simulation, (b) prediction.

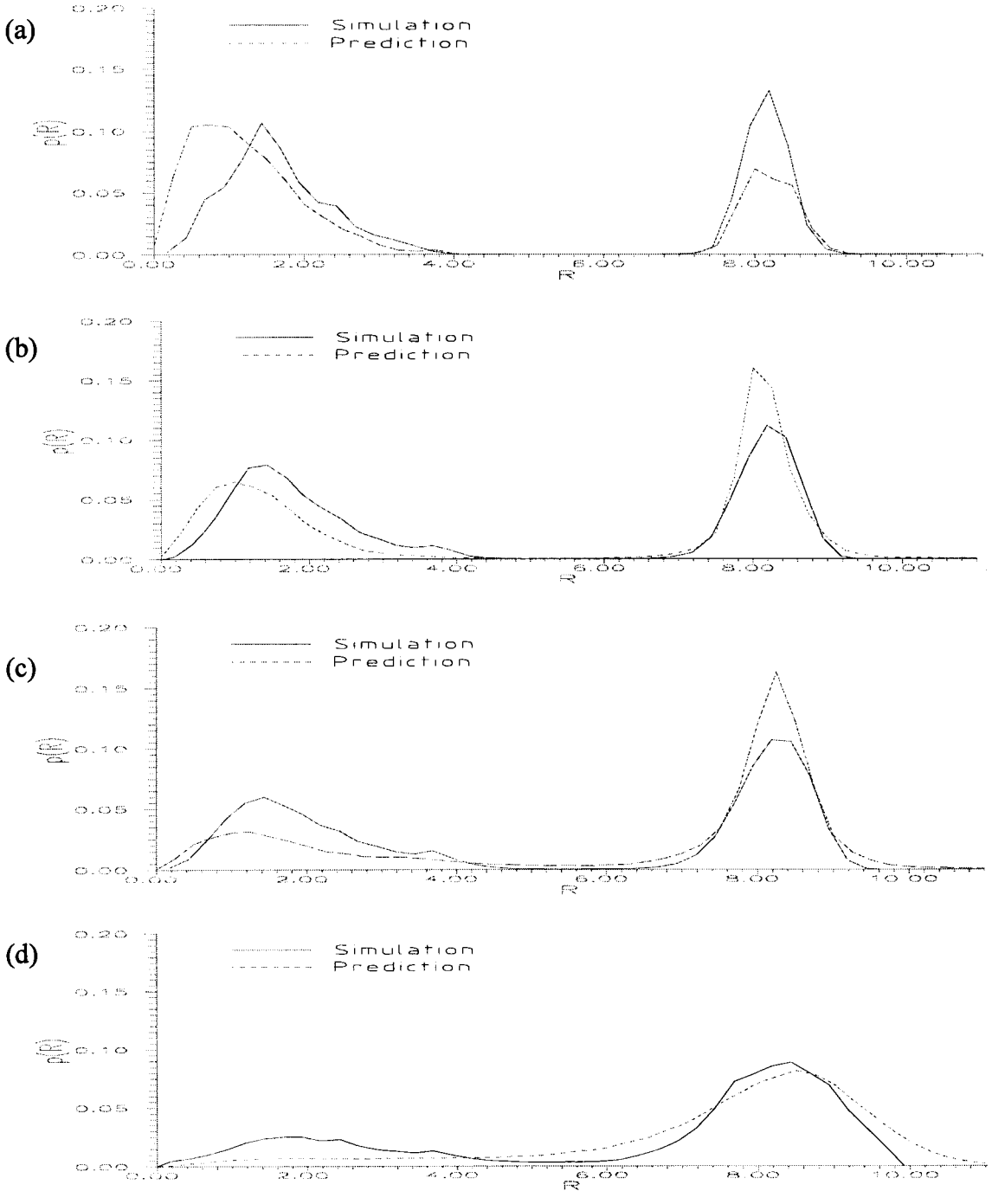

Fig 3.8 Variations in the response amplitude probability distribution under varying excitation bandwidth in the subharmonic resonance region, (a) case(i), (b) case(ii), (c) case(iii), (d) case(iv).

3.2.5 Effects of varying excitation intensity on response amplitude probability distribution

Fig. 3.9 shows that as the excitation variance decreases from 157 (case (iii)) to 125 (case (v)), the probability mass in the large amplitude response region decreases in accordance with the response behavior described earlier. This trend is captured by the proposed semi-analytical procedure.

(a)

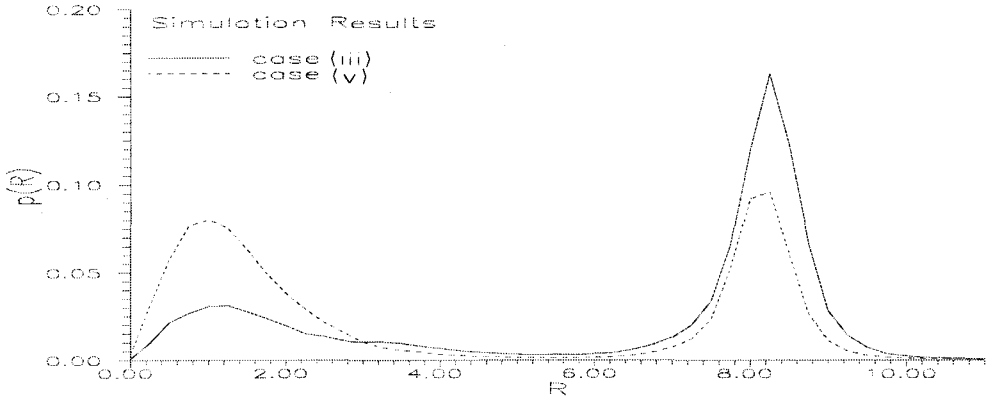

(b)

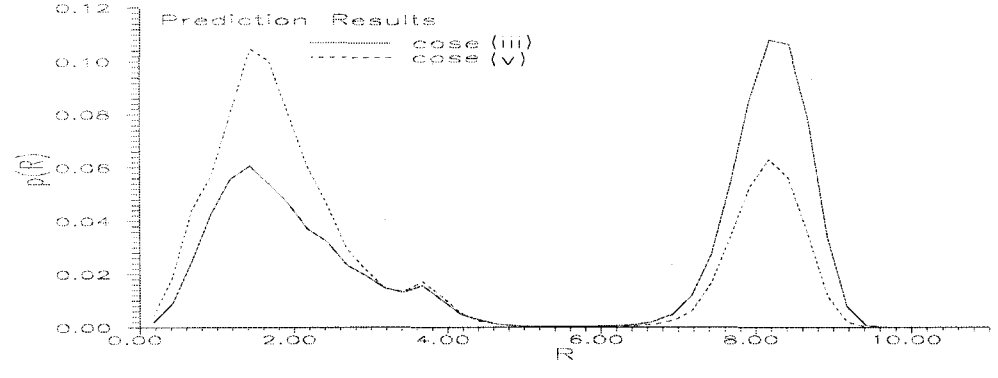

Fig 3.9 Variations in the response amplitude probability distribution under varying excitation variance in the subharmonic resonance region, (a) simulation, (b) prediction.

3.3 Comparisons With Existing Analytical Methods

3.3.1 Stochastic averaging method

Using the method of stochastic averaging, Davis and Liu (1990) and Koliopulos and Bishop (1993) derived the form of the response amplitude PDF

$$p(y) = C \exp\left\{ \frac{-2v^2\delta}{(\varepsilon+\delta)\eta} y \left[(\varepsilon+\delta)^2 + \frac{(v^2-1)^2}{4v^2} - \frac{3(v^2-1)y}{16v^2} + \frac{9y^2}{192v^2} \right] \right\} \tag{3.1}$$

where, $y = \frac{a_3}{a_1} R^2$, $\delta = \frac{s_C}{2\sqrt{a_1}}$, $\eta = \frac{a_3}{a_1^3}\sigma_f^2$, $\varepsilon = \frac{\gamma}{2\sqrt{a_1}}$, $v = \frac{\omega_f}{\sqrt{a_1}}$ (3.2)

R is the response amplitude; s_C, a_1, and a_3 are structural damping, linear stiffness and nonlinear stiffness coefficients, respectively; γ, ω_f, and σ_f^2 are excitation bandwidth parameter, central frequency and variance, respectively

3.3.2 Quasi-harmonic method

Using the quasi-harmonic method, Koliopulos and Bishop (1993) obtained a relationship between the narrowband excitation amplitude A and its corresponding response amplitude R

$$y^3 + \frac{8}{3}(1-v^2)y^2 + \frac{16}{9}\left[(1-v^2)^2 + 4\delta^2 v^2 y\right] = \frac{32}{9}\theta, \quad \theta = \frac{A^2 a_3}{2a_1^3} \tag{3.3}$$

where, scaled parameters y, δ and v are defined in Eq.(3.2). The response amplitude PDF can be obtained by a probability transformation rule between the random variable θ and y through the functional relationship defined in Eq.(3.3)

(Ochi, 1990). The probability density function of θ is obtained as (Koliopulos and Bishop, 1993):

$$p(\theta) = \frac{1}{\eta} e^{-\frac{\theta}{\eta}}, \qquad \eta = \frac{a_3 \sigma_f^{\,2}}{a_1^{\,3}} \tag{3.4}$$

Since Eq.(3.3) is a third-degree polynomial equation, for a given θ, there may exist three real solutions. The real solutions with the smallest and the largest magnitudes correspond to the co-existing stable (physically observable) small and large amplitude steady-state responses. The real intermediate magnitude solution, associated with the unstable steady-state response, is physically unobservable. In this case, the probability mass associated with θ will be transferred and distributed to the smallest and the largest values of y, respectively, by a ratio κ determined by the following equation (Dimentberg, 1988; Koliopulos and Bishop, 1993):

$$\kappa = \frac{Ei\left(\frac{\theta_{\max}}{\eta}\right) - Ei\left(\frac{\theta_{\min}}{\eta}\right)}{\ln\left(\frac{\theta_{\max}}{\theta_{\min}}\right)} - 1, \qquad Ei(x) = \int_{-\infty}^{x} \frac{e^{v}}{v} dv \tag{3.5}$$

where θ_{max} and θ_{min} are the respective upper and lower bounds of θ which corresponds to multiple solutions of Eq.(3.1)

3.3.3 Comparisons of analytical predictions and simulation results

The prediction capability of the proposed semi-analytical method and the stochastic averaging method presented by Davies and Liu (1990) and the quasi-harmonic method presented by Koliopulos and Bishop (1993) is examined in this

section. In particular, the response amplitude PDF predicted by these methods for two specific excitation bandwidths selected by Koliopulos and Bishop (1993) are compared. In both cases, (a) and (b), the system and excitation parameters are: {Cs = 0.16, a_1 = 1, a_3 = 0.3, ω_f =2, γ = 0.01, σ_f^2 = 3.05}, whereas, the excitation bandwidth parameter are γ = 0.02 and γ = 0.08, respectively. Note that corresponding to these system and excitation parameters, the scaled parameters employed in the stochastic averaging and the quasi-harmonic methods are {v=2, δ=0.08, $\varepsilon=\gamma/(2\sqrt{a1})$=0.01, η=0.91} and {v=2, δ=0.08, ε=0.04, η=0.91}, respectively.

Prediction results of the semi-analytical, stochastic averaging and quasi-harmonic methods are shown in Fig. 3.10(a and b). Comparisons are also made with the response amplitude histogram obtained from simulations. Note that in each case, while all three methods predict the trends, the semi-analytical method developed in this study match simulation results significantly better, especially in the small amplitude response region.

(a)

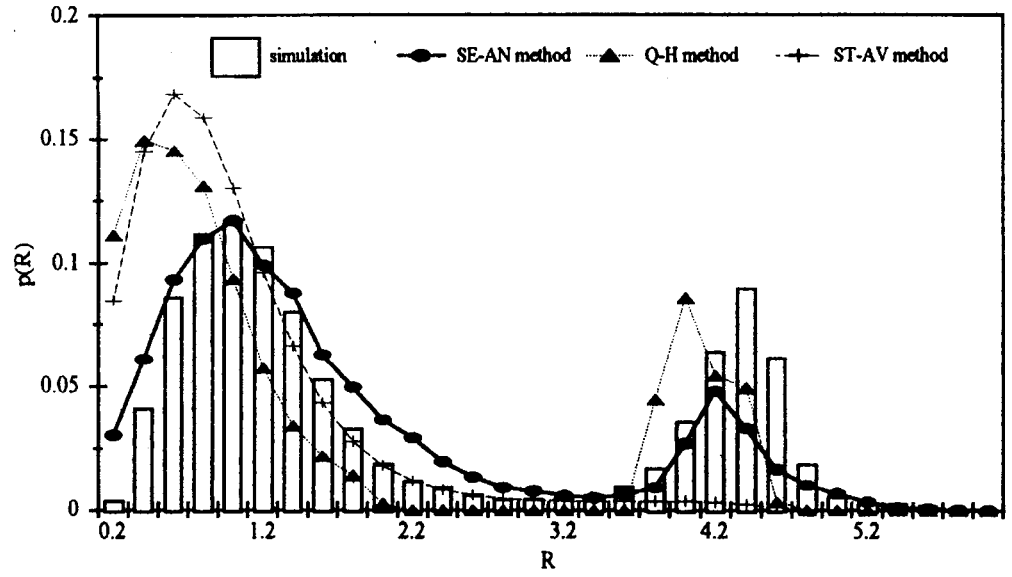

(b)

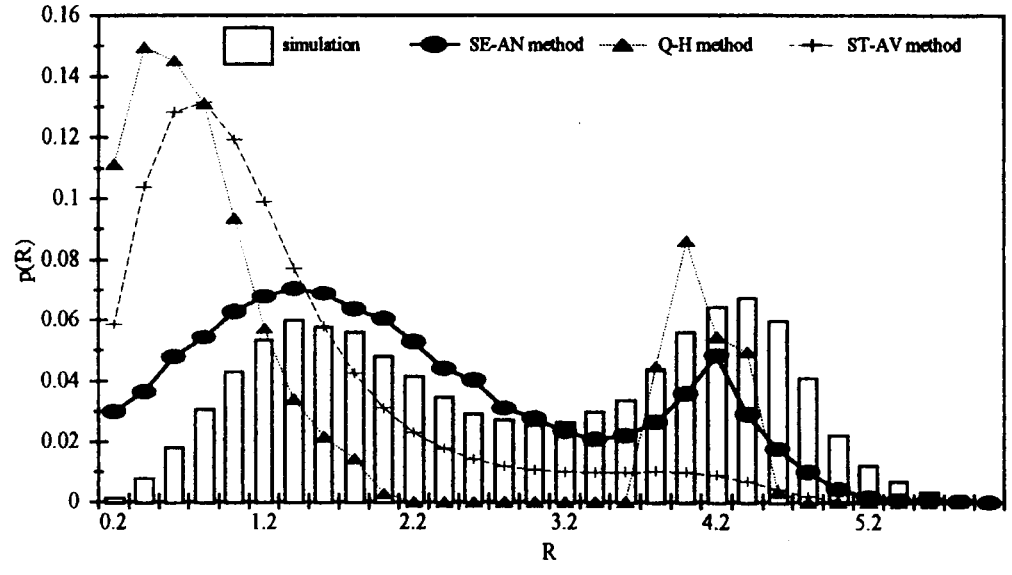

Fig. 3.10 Response amplitude histogram and probability distributions predicted by the semi-analytical (SE-AN), quasi-harmonic (Q-H) and stochastic averaging (ST-AV) methods, respectively. $\{Cs = 0.16, a_1 = 1, a_3 = 0.3, \omega_f = 2, \gamma = 0.01, \sigma_f^2 = 3.05\}$. (a) $\gamma = 0.02$, and (b) $\gamma = 0.08$.

4. STOCHASTIC ANALYSIS OF A MOORED OCEAN SYSTEM

4.1 Description of Moored Ocean System

An experiment has been performed at the O. H. Hinsdale Wave Research Laboratory at Oregon State University on a submerged multi-point moored ocean system under wave excitation. The experimental model consists of a 45.72 cm diameter PVC spherical rigid body with a 2.54 cm square rod through the center of the sphere, restricting its motion to surge (along the direction of the exciting waves) only. The rod is rigidly supported 1.83 m above the bottom of the wave channel by guyed masts. The sphere is neutrally buoyant when submerged. Linear springs are attached to the sphere, providing a nonlinear restoring force due to large geometry (see Fig. 4.1).

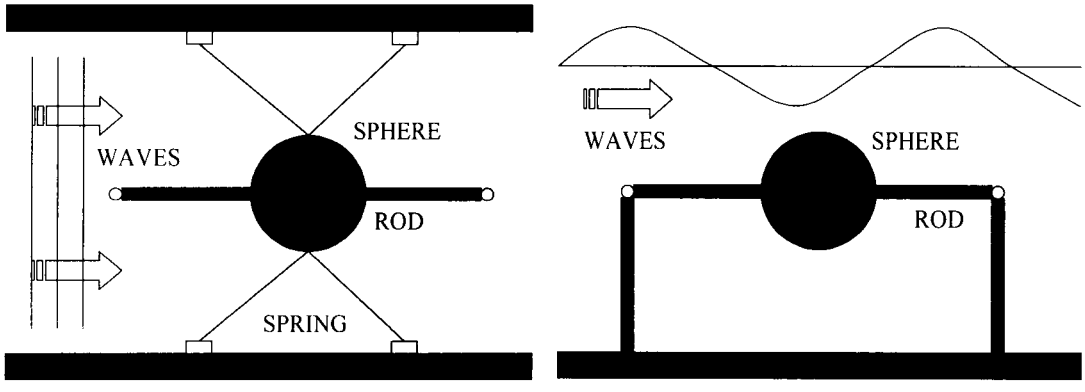

(a) Plan View (b) Profile View

Fig. 4.1 Experimental model of a submerged, hydrodynamically damped and excited structural system.

Steady-state system responses under deterministic wave excitations over a wide range of wave frequencies are examined first. Periodic wave excitations with sufficiently long duration are applied to the moored system to achieve steady-state responses. Superharmonic, primary and subharmonic resonance responses are observed around regions with wave frequency centralized at 0.14 Hz, 0.27 Hz and 0.50 Hz, respectively (Fig. 4.2). Notice that while the primary resonance is clearly demonstrated, the superharmonic and subharmonic resonance regions are indicated by relatively small humps. In the subharmonic resonance region, the sphere oscillates at a period near twice that of the excitation, indicating the responses are 1/2 subharmonics. Dashed lines in the figure show the estimated stability boundaries of the corresponding superharmonic, primary and subharmonic resonance regions (Yim and Lin, 2000).

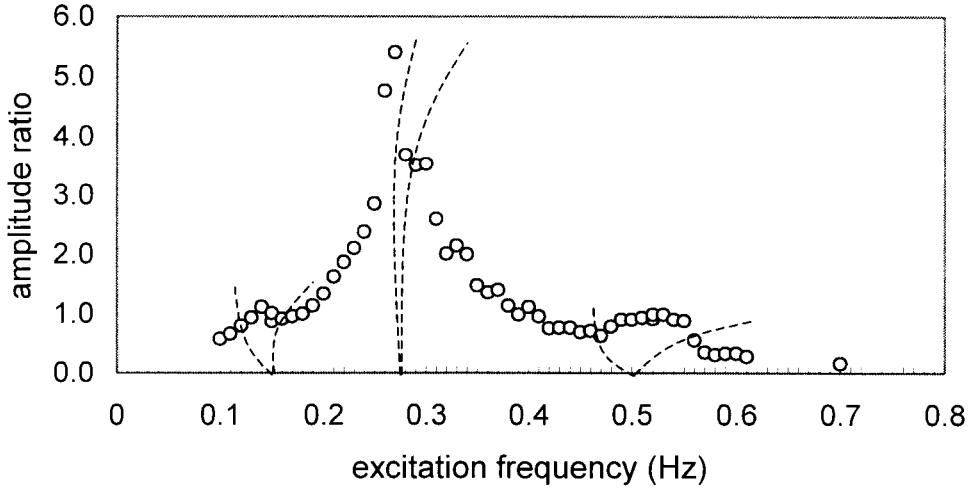

Fig. 4.2. Frequency response diagram (experimental results); ---- estimated stability boundaries.

In this study, we are interested in examining the transition behaviors between subharmonic and harmonic system responses. For this purpose, narrowband-random excitations with dominant frequencies centered around 0.5 Hz (the subharmonic resonance region) will be employed. Corresponding experimental tests of the moored ocean system will also be examined and used to calibrate analytical predictions and simulation results.

4.2 Analytical Model

The general form of equation of motion can be described mathematically as

$$m\ddot{x}(t) + C_S\dot{x}(t) + R(x(t)) = f(t) \tag{4.1}$$

where, m = mass, Cs = damping coefficient, $R(x(t))$ = restoring force, and $f(t)$ = external excitation forcing. For the moored sphere model, in addition to the hydrodynamic inertia and drag forces, nonlinear structural (restoring) force and nonlinear damping force (NSND) are also included. The nonlinear equation of motion for the NSND model is given by

$$(m+m_a)\ddot{x}(t) + C_S\dot{x}(t) + a_1x(t) + a_2x^2(t) + a_3x^3(t) + \rho C_d'\frac{\pi}{4}D^2\dot{x}(t)|\dot{x}(t)| = f(t) \tag{4.2}$$

where

$$\begin{aligned} f(t) &= \rho\frac{\pi}{6}D^3C_m\dot{u}(t) + \rho C_d\frac{\pi}{4}D^2u(t)|u(t)|, \\ u(t) &= a\omega\frac{\cosh(ks)}{\sinh(kh)}\cos(kx(t) - \omega t) \end{aligned} \tag{4.3}$$

m_a = added mass, C_d = hydrodynamic drag coefficient, C_m = hydrodynamic inertia coefficient, C_S = linear damping coefficient, C_d' = nonlinear structural damping coefficient, ρ = water density, and D = diameter of the sphere. Linear wave theory is used for the horizontal water particle velocity, $u(t)$.

For modeling of the structural system using the NSND model, the coefficients of the governing equation of motion should be determined accurately. System identification technique developed in a previous study by Narayanan (1999) is used to determine the coefficients. It is shown that the system response resulting from predictions using the coefficients determined by Narayanan's system identification technique match the experimental results accurately.

4.3 Amplitude Jump Phenomena

A typical nonlinear response behavior, the amplitude jump phenomenon, which is observed in both analytical analysis and experiment, can be explained by the response amplitude curve. The amplitude jumps occur when the excitation amplitude gradually drifts out of attraction domain boundaries. This (jump) phenomenon is defined as an inter-domain transition. For the specific set of system parameters, m = 3.428, C_a = 0.25, ξ = 0.06, C_d' = 0.02, C_m = 1.25, C_d = 0.1, a_1 = 9.3, a_2 = 4.0, a_3 = 4.0, three different attraction domains are found over the region of excitation amplitudes and frequencies considered. The nonlinear system response dependency on initial conditions is shown in Fig. 4.3. For trajectories with initial displacements and velocities high-lighted in Fig. 4.3(a), the steady-state responses

result in 1/2 subharmonics. On the other hand, if the initial conditions belong to the regions high-lighted in Fig. 4.3(b), the resulting steady-state responses are large amplitude harmonics. The time series shown in Fig. 4.4 demonstrate the amplitude jump phenomenon from the small amplitude harmonic attraction domain to the large amplitude harmonic domain when excitation amplitudes increased from 2.26 to 2.27. The system initially is subjected to deterministic excitation with amplitude A = 2.26 until the system response amplitude stabilizes at 1.8. The "steady-state" response shows the small amplitude harmonic response having the same frequency as the excitation. Then, the excitation amplitude is increased from A=2.26 to A=2.27 at time = 600 sec. For such a small increase in amplitude, it is observed that the steady-state response amplitude is increased about three times in magnitude. The response amplitude curves shown in Fig. 4.5 are the steady-state response amplitudes under deterministic excitation obtained by numerical integration of the equation of motion.

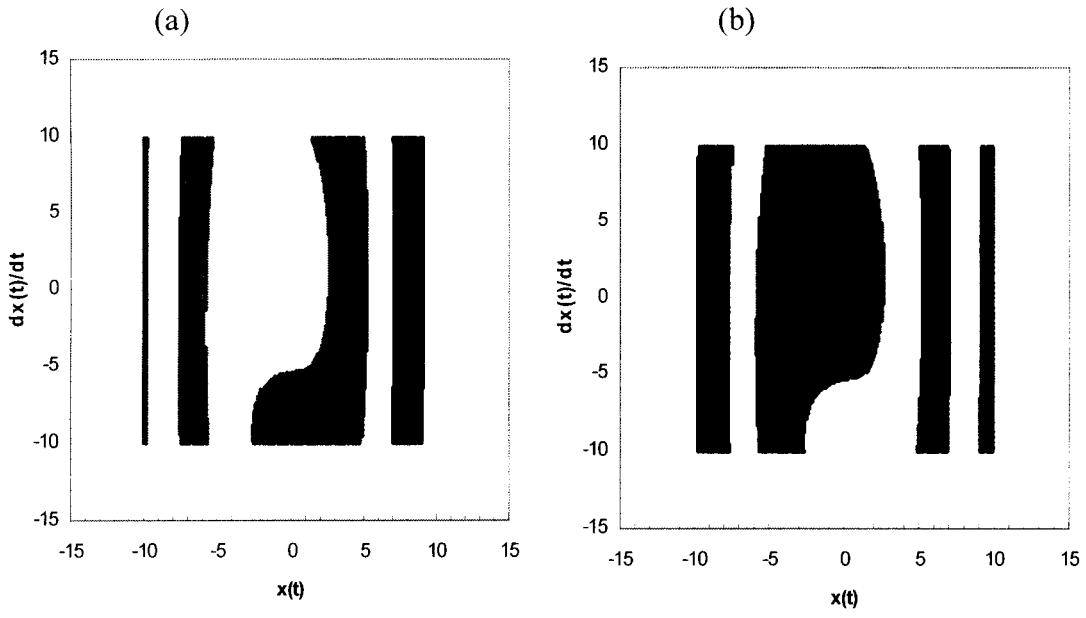

Fig. 4.3 Coexisting attraction domain (a) 1/2 subharmonic attraction domain, (b) large harmonic attraction domain {A=1.0}.

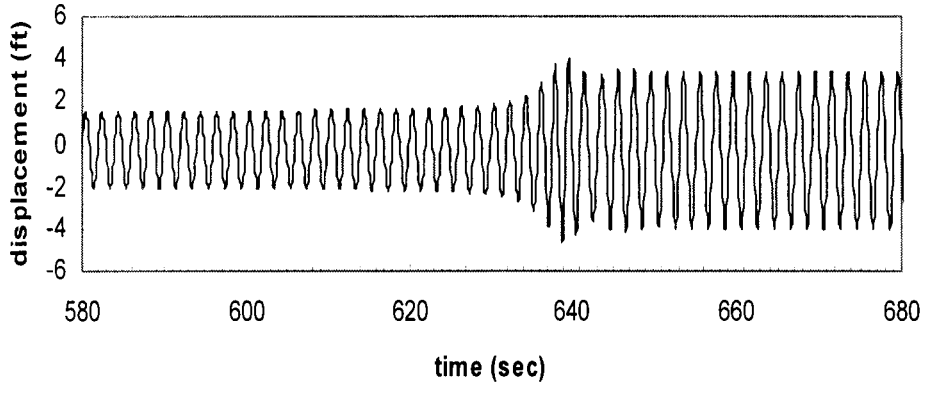

Fig 4.4 Time series of the system response under deterministic excitation { A=2.26 for t≤600 sec, A=2.27 for t>600 sec }.

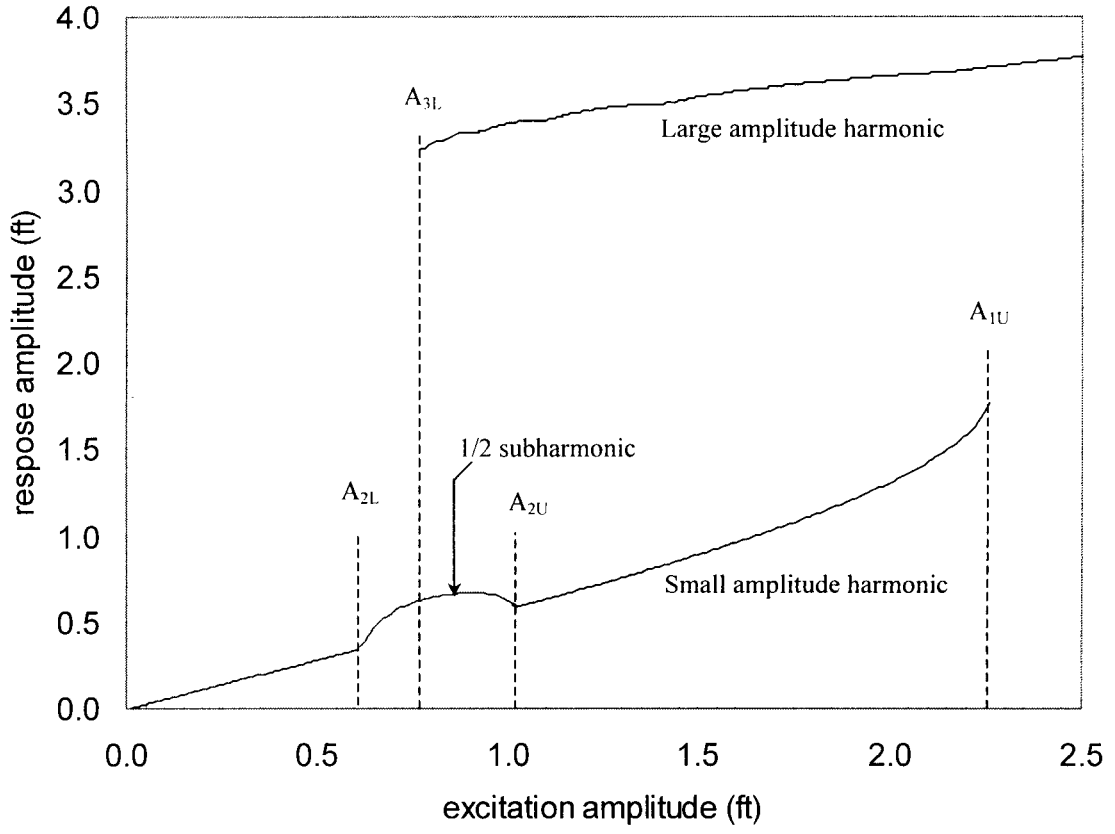

Fig. 4.5 Response amplitude curve {m=3.428, C_a=0.25, ξ=0.06, C_d'=0.02, C_m=1.25, C_d=0.1, a_1=9.3, a_2=4.0, a_3=4.0}.

Transitions among different domains depend on the attraction domains that the system response belongs to at the moment of excitation variation. For example, as the excitation amplitude slowly decreases from $A_{2U} < A < A_{1U}$ to $A_{2L} < A < A_{2U}$, the occurrence of jump phenomenon depends on the current attraction domain the response belongs to. If the system response belongs to the large amplitude domain (D_3), amplitude jump will not occur. When the small amplitude domain (D_1), is the current attraction domain, transition from D_1 to 1/2 subharmonic domain (D_2), will occur. With infinitesimal variations in excitation amplitude, jumps from D_3 to D_1,

and from D_3 to D_1 cannot occur. Schematic diagram of transitions that can occur among domains are shown in Fig. 4.6.

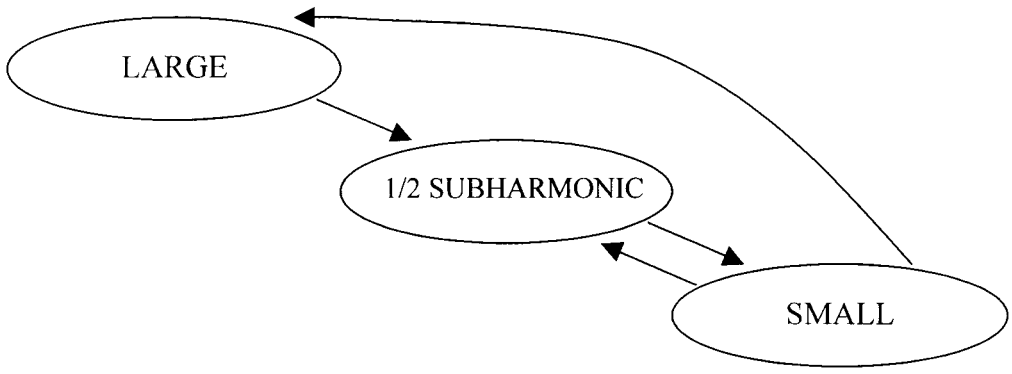

Fig. 4.6 Schematic diagram of system response transitions among D_1, D_2, D_3 .

For the gradual excitation amplitude variation within an attraction domain, response amplitude varies along the response amplitude curve. When the excitation amplitudes are increased from 0 to beyond the small amplitude harmonic domain upper boundary A_{1U}, transitions occur from D_1 to D_2 and D_2 to D_1 and D_1 to D_3. On the other hand, for the excitation amplitude decreasing from $A > A_{1U}$ to 0, responses undergo the transitions from D_3 to D_2 and D_2 to D_1. Transitions and variations of system response amplitudes with increasing and decreasing excitation amplitude are shown in Fig. 4.7.

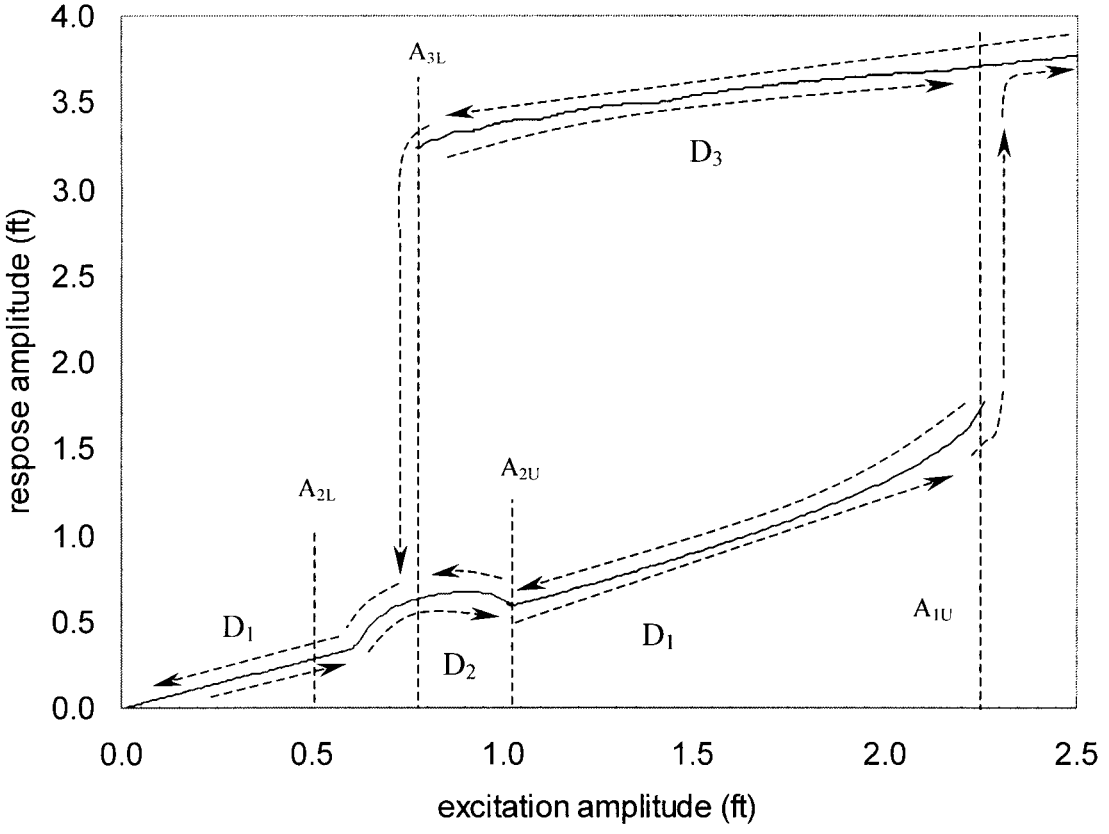

Fig. 4.7 Transitions and variations of system response amplitude along the response amplitude curves.

For stochastic excitation model with the finite variation in excitation amplitude, response amplitude curves become response amplitude map where groups of data points indicating existence of corresponding attraction domains. Schematic diagram of response amplitude transitions with finite excitation amplitude variation is shown in Fig. 4.8. Notice that transitions from D_3 to D_1 and D_2 to D_3 are assumed to occur even though the occurrences of those transitions are highly unlike. The dashed lines (Fig. 4.8) indicate the transitions considered to occur with finite excitation amplitude variations.

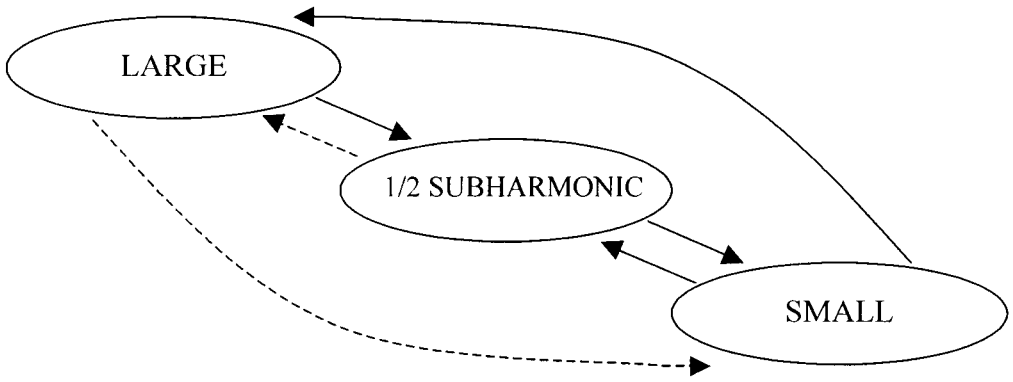

Fig. 4.8 Schematic diagram of system response transitions under infinitesmal (⟶) and finite (--▶) excitation amplitude variations among D_1, D_2 and D_3.

4.4 Stochastic Excitation Parameters

Excitation forces on ocean structures under random wave fields are often modeled as narrowband random processes. In addition, to study the transitions of system responses among competing attractors over a narrow range of excitation frequency, the narrowband random process is employed to model the wave excitation. As shown in an earlier section, a narrowband Gaussian random excitation process, $f(t)$, is written as

$$f(t) = A(t)\cos\{\omega_f t + \varepsilon(t)\} \tag{4.3}$$

The four dimensional joint probability density function of the random variables representing the excitation amplitudes and phase angles corresponding to consecutive excitation cycles, i.e., $A^{(1)}$, $A^{(2)}$, $\phi^{(1)}$ and $\phi^{(2)}$, is given by

$$p(A^{(1)},\phi^{(1)},A^{(2)},\phi^{(2)})$$
$$= \frac{A^{(1)}A^{(2)}}{4\pi^2\sqrt{|\Sigma|}}\exp\left\{\frac{-1}{2\sqrt{|\Sigma|}}\left\{\sigma_f{}^2\left[\left(A^{(1)}\right)^2+\left(A^{(2)}\right)^2\right]-2A^{(1)}A^{(2)}\left[\begin{matrix}\rho\cos\left(\phi^{(2)}-\phi^{(1)}\right)\\+\lambda\sin\left(\phi^{(2)}-\phi^{(1)}\right)\end{matrix}\right]\right\}\right\}$$

$$0 \le A^{(1)}, A^{(2)} < \infty, \quad 0 \le \phi^{(1)}, \phi^{(2)} \le 2\pi \tag{4.4}$$

where

$$\rho = \int_0^\infty S_{ff}(\omega)\cos\left[(\omega-\omega_f)T\right]d\omega$$
$$\lambda = \int_0^\infty S_{ff}(\omega)\sin\left[(\omega-\omega_f)T\right]d\omega$$
$$\sqrt{|\Sigma|} = \sigma_f{}^4 - \rho^2 - \lambda^2 \tag{4.5}$$

with superscripts (1) and (2) indicating that the quantities are in the current and the next excitation cycles, respectively; $S_{ff}(\omega)$ is the one-sided spectral density function of $f(t)$, and T is the excitation period equal to $2\pi/\omega_f$. The spectral density function of a time series are usually obtained numerically using a standard data analysis procedure. (A typical example of a time series and its spectral density are shown in Figs.4.9(a) and (b), respectively.) All stochastic parameters of the excitation random process can be obtained from the spectral density of the time series. By introducing a random variable Φ to represent the phase angle difference $\phi^{(2)} - \phi^{(1)}$, the joint PDF of $A^{(1)}$, $A^{(2)}$ and Φ can be obtained from Eq.(4) by the transformation of the random variables

$$p(A^{(1)}, A^{(2)}, \Phi)$$
$$= \frac{A^{(1)}A^{(2)}}{2\pi\sqrt{|\Sigma|}}\exp\left\{\frac{-1}{2\sqrt{|\Sigma|}}\left\{\sigma_f{}^2\left[\left(A^{(1)}\right)^2+\left(A^{(2)}\right)^2\right]-2A^{(1)}A^{(2)}\left[\rho\cos(\Phi)+\lambda\sin(\Phi)\right]\right\}\right\} \tag{4.6}$$
$$-2\pi \le \Phi \le 2\pi$$

In addition, the joint PDF of $A^{(1)}$ and $A^{(2)}$ can be obtained by integrating Eq.(4.4) with respect to $\phi^{(1)}$ and $\phi^{(2)}$.

$$p(A^{(1)}, A^{(2)}) = \frac{A^{(1)}A^{(2)}}{\sqrt{|\Sigma|}} \exp\left\{\frac{-1}{2\sqrt{|\Sigma|}}\sigma_f{}^2\left[\left(A^{(1)}\right)^2 + \left(A^{(2)}\right)^2\right]\right\} I_0\left(\frac{A^{(1)}A^{(2)}}{\sqrt{|\Sigma|}}\sqrt{\rho^2 + \lambda^2}\right) \quad (4.7)$$

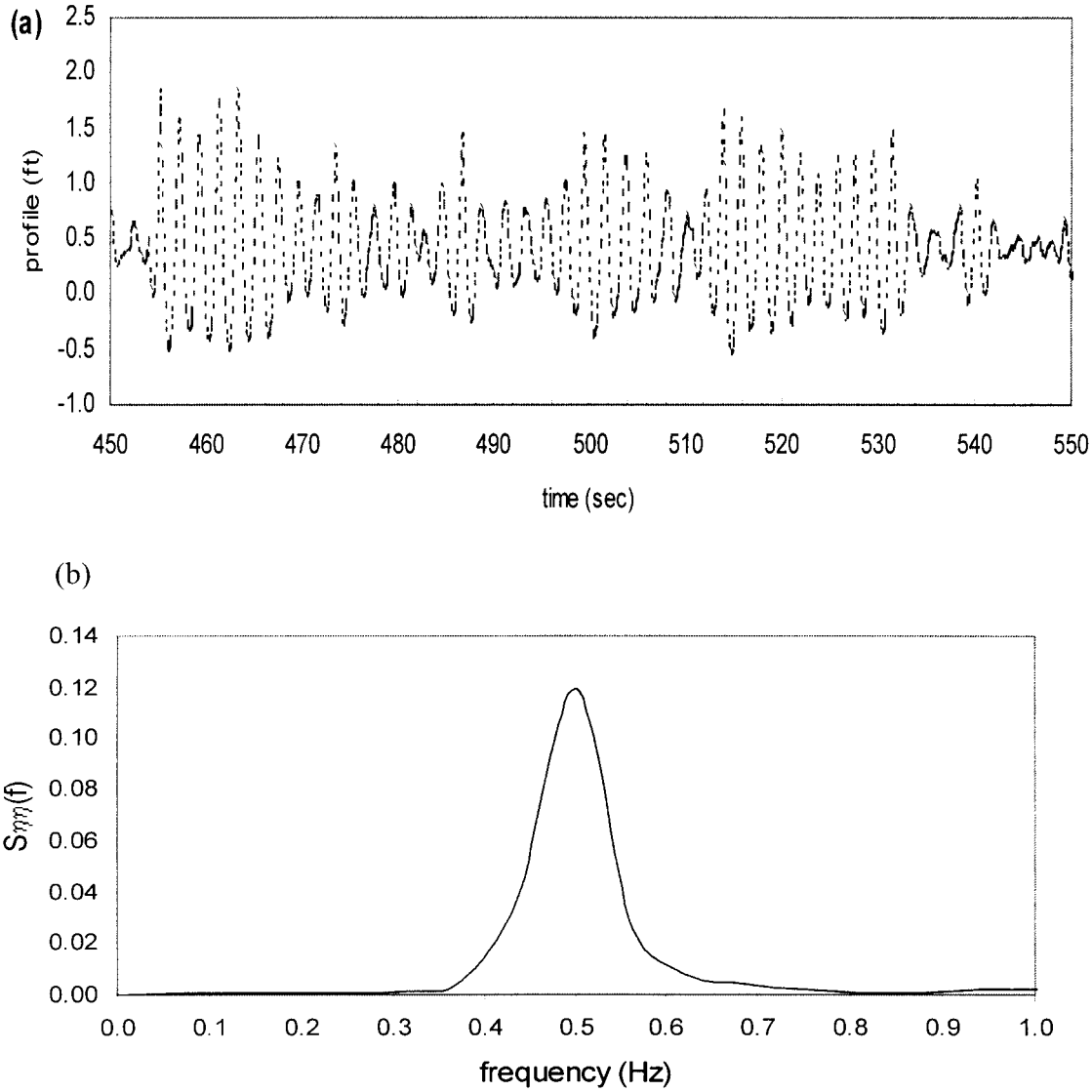

Fig. 4.9 Experimental excitation: (a) wave profile (b) wave spectra.

4.5 Inter-domain Transitions

When the stochastic excitation is applied to the system, excitation amplitude, frequency and phase keep varying slowly from cycle to cycle. Due to the gradual variations in the excitation parameters, the system response undergoes transition from one attraction domain to another attraction domain. To describe these transitions between different attraction domains a probability distribution is employed. The governing equation for inter-domain transition is given by

$$\hat{p}(D^{(2)}) = K\hat{p}(D^{(1)}) \tag{4.8}$$

where, K is the transition matrix whose dimension is $n \times n$ (n = the number of co-existing attraction domains = 3), and superscripts (1), (2) denote the current and next cycles respectively. The element of the transition matrix K in i^{th} row and j^{th} column is a conditional probability, $p_{ij}(i|j)$, where i is the attraction domain of the next cycle and j is the attraction domain of the current cycle. These conditional probabilities can be evaluated by considering the stochastic behavior of the excitation amplitude and system response inter-domain transition behavior. For the system response to stay in the same attraction domain, D_d in both current and next cycle, the excitation amplitude must remain within same domain, D_d^A, as in the current cycle. The probability of the excitation amplitude being in the domain, D_d^A, can be written as

$$p(A \mid D_d^{\,A}) = \frac{p(A)}{\int_{D_d^{\,A}} p(A)dA}, \qquad A \in D_d^{\,A} \tag{4.9}$$

where, $p(A)$ is a Rayleigh distribution. Then, the probability distribution of the excitation amplitude in the next cycle given that the excitation amplitude is in D_d^A in the current cycle can be expressed as

$$p(A^{(2)} \mid A^{(1)} \in D_d^{\ A}) = \int_{D_d^{\ A}} p(A^{(2)} \mid A^{(1)}) p(A^{(1)} \mid D_d^{\ A}) dA^{(1)} \tag{4.10}$$

Thus, the probability of the system response amplitude remaining in the same attraction, D_d, in the next cycle is

$$p(R^{(2)} \in D_d^{\ R} \mid R^{(1)} \in D_d^{\ R}) = \int_{D_d^{\ A}} p(A^{(2)} \mid A^{(1)} \in D_d^{\ A}) dA^{(2)} \tag{4.11}$$

The conditional probability given by Eq.(4.10) is equal to the diagonal elements of the inter-domain transition matrix, $p_{ii}(i|i)$. The off-diagonal elements of K can be determined by considering the transient-state system mean energy, or equivalently, the transient-state response amplitude.

4.5.1 System total energy

Transient system total energy is employed to determine the destination attraction domain for the case that there exist multiple possible destination domains after excitation amplitude exit through one of the domain boundaries. The system total energy (TE) is defined as the sum of the potential energy (PE) and the kinetic energy (KE). Potential energy and kinetic energy are expressed as a function of the response displacement, and a function of the response velocity, respectively. Therefore, the system total energy of the NSND moored ocean system model can be written (up to a constant) as

$$TE = PE + KE = \frac{1}{2}a_1 x^2 + \frac{1}{3}a_2 x^3 + \frac{1}{4}a_3 x^4 + \frac{1}{2}(m + m_a)\dot{x}^2 \qquad (4.12)$$

Three different types of response behavior are shown in Figs.4.10, 11, 12. For the large amplitude response and 1/2 subharmonic response in Fig. 4.10. and Fig 4.12., respectively, the system is subjected to excitation forces with identical frequencies and amplitudes. The difference in system response behavior is caused by the initial condition dependency of the nonlinear system. It is observed that the magnitudes of the total energy in those two responses are significantly different. On the other hand, as shown in Figs.4.11 and 12, it is observed that the total energy of the small amplitude harmonic and 1/2 subharmonic response overlaps for increasing excitation amplitude. These observations imply that when the excitation amplitude exit through the upper boundary of 1/2 subharmonic domain, it is impossible for the system response to jump up to the large amplitude harmonic domain because of the large gap in the system total energy even though the input energy increases as the excitation amplitude increases. In addition, when the excitation amplitude increased from 0.5 to 0.95, there exist two possible destination domains, i.e., large amplitude domain, and 1/2 subharmonic domain. However, the total energy of the small amplitude harmonic response overlaps that of 1/2 subharmonic response while there is a large difference between small and large amplitude harmonic response. Thus, in this case, the destination domain would be the 1/2 subharmonic domain.

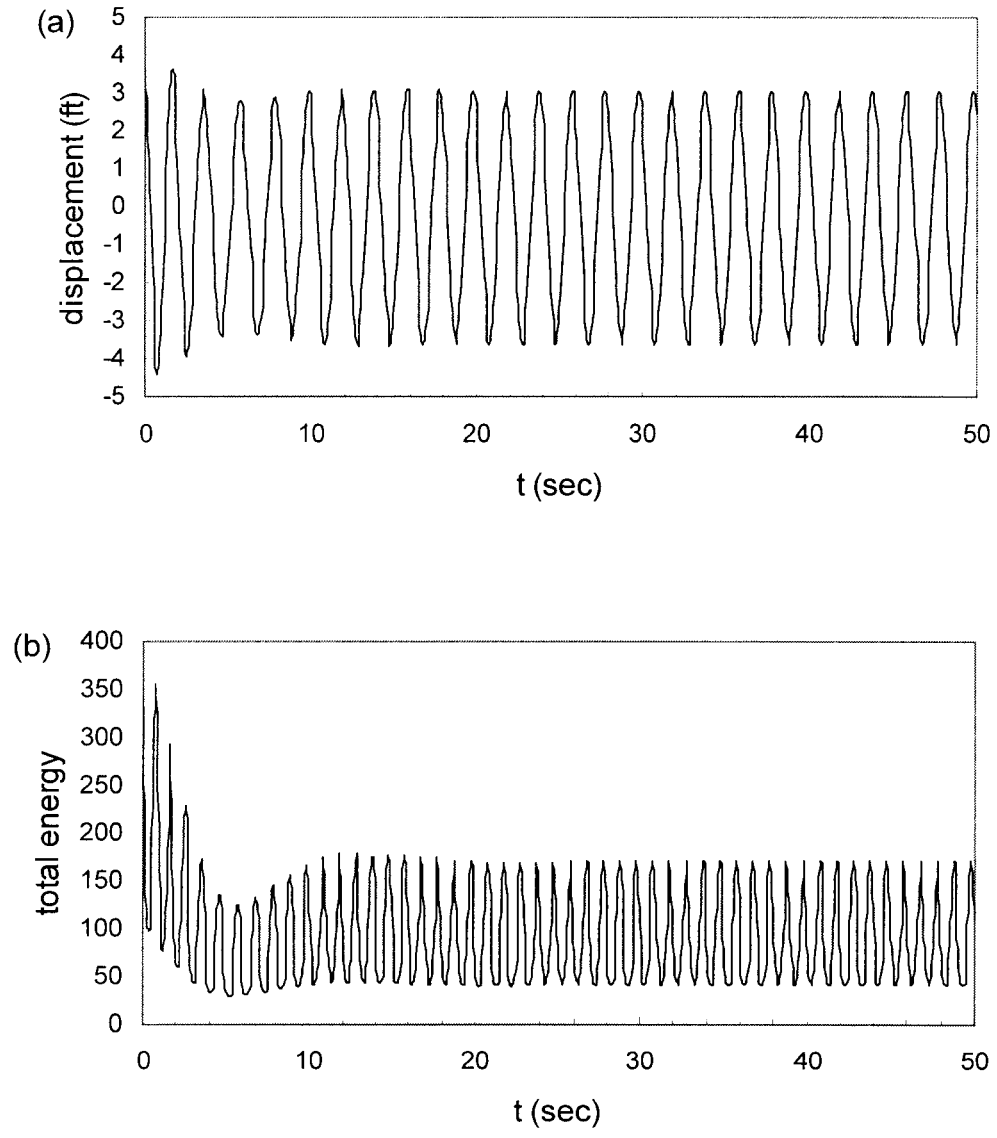

Fig. 4.10 Time series and total energy of large amplitude harmonic response. $\{m=3.428, C_a=0.25, \xi=0.06, C_d'=0.02, C_m=1.25, C_d=0.1, a_1=9.3, a_2=4.0, a_3=4.0, (x(0),dx/dt(0))=(4.0, 1.0), a=0.95\}$.

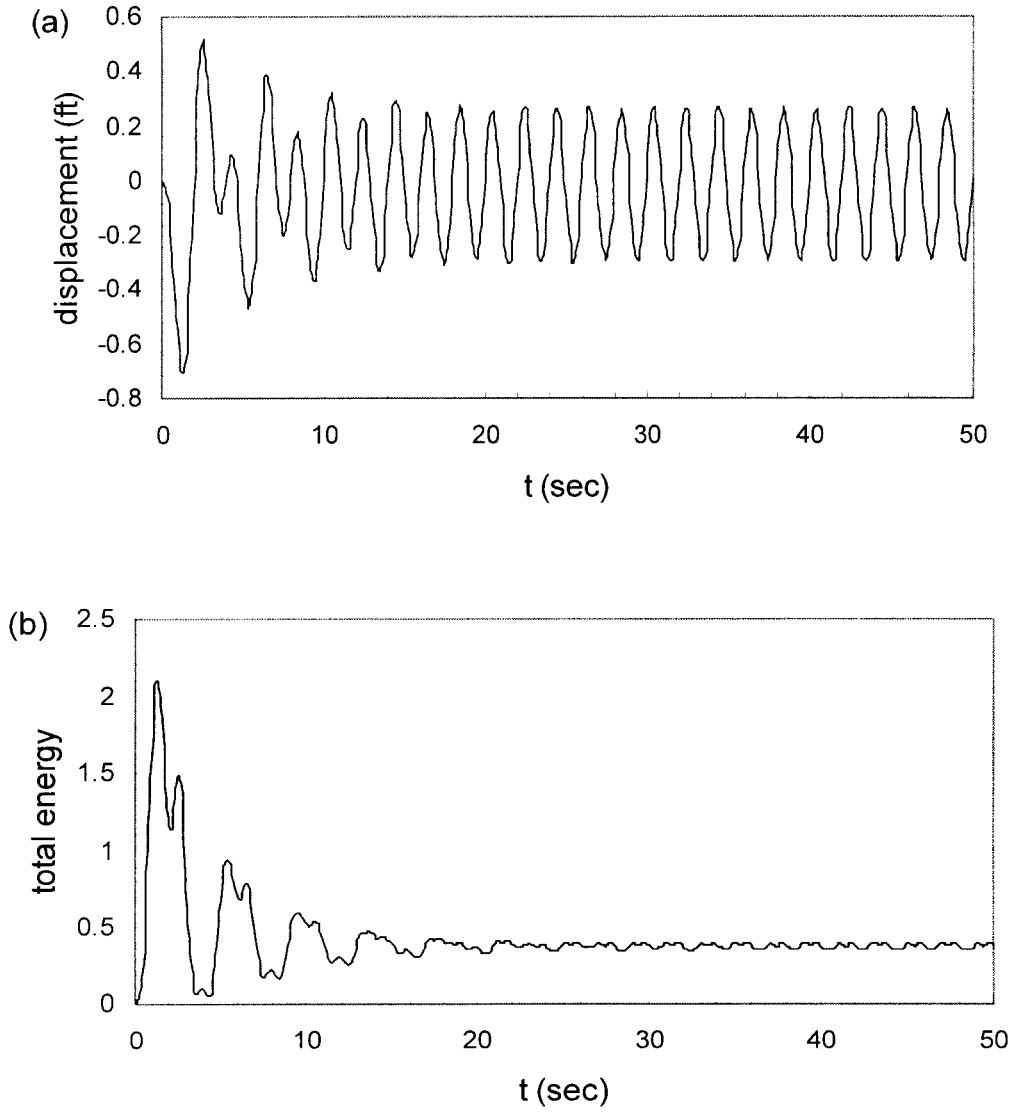

Fig. 4.11 Time series and total energy of small amplitude harmonic response. {m=3.428, C_a=0.25, ξ=0.06, C_d'=0.02, C_m=1.25, C_d=0.1, a_1=9.3, a_2=4.0, a_3=4.0, (x(0),dx/dt(0))=(0.0, 0.0), a=0.5}.

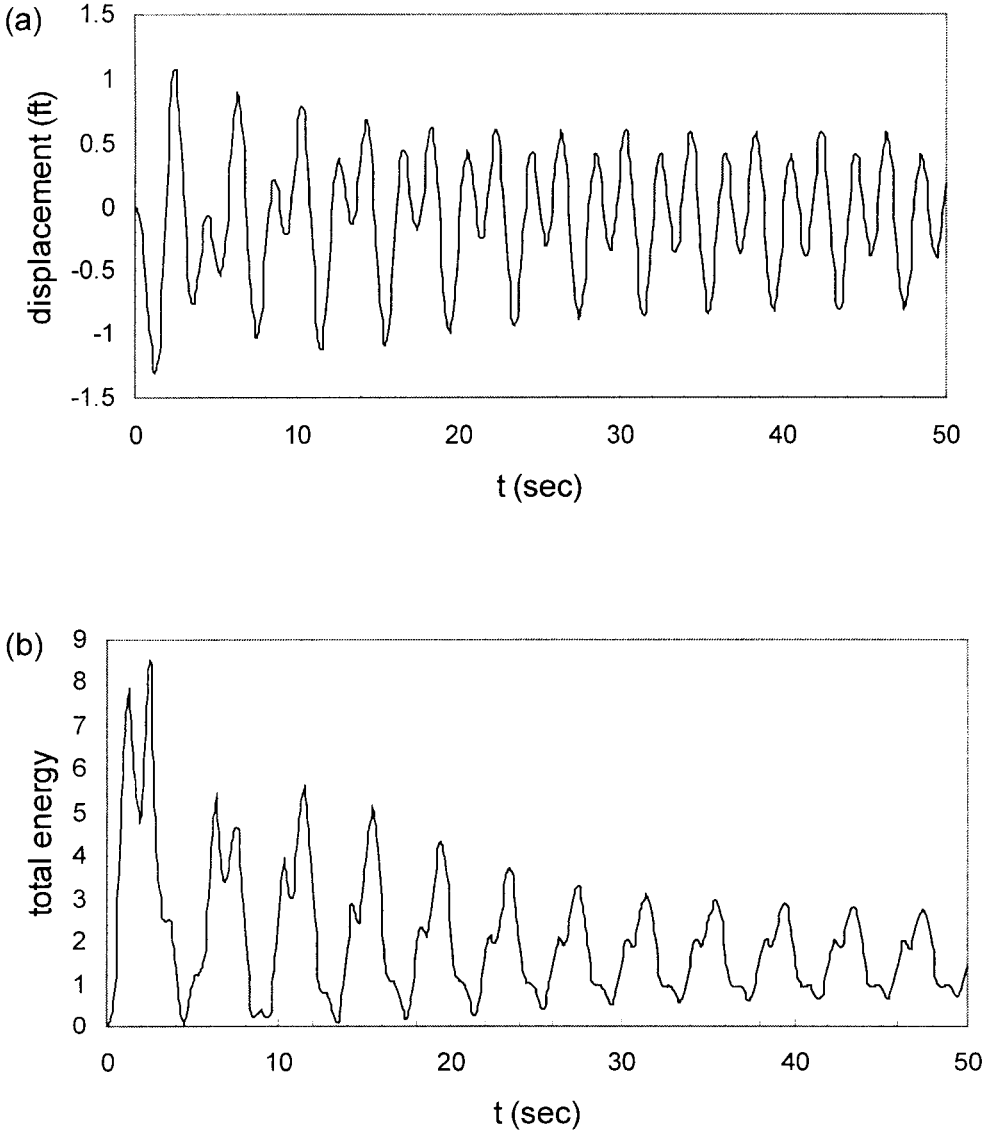

Fig. 4.12 Time series and total energy of 1/2 subharmonic response. { m=3.428, C_a=0.25, ξ=0.06, C_d'=0.02, C_m=1.25, C_d=0.1, a_1=9.3, a_2=4.0, a_3=4.0, ($x(0)$,$dx/dt(0)$)=(0.0, 0.0), a=0.95}.

4.5.2 System energy level

The system energy level in a transient state can be also used to determine the destination domain when the excitation amplitude varies out of the attraction domain boundaries. The system energy level can be represented by the system mean energy, which is defined as the averaged system total energy over one excitation cycle (Shi, 1998).

At the 1/2 subharmonic domain lower boundary (one of the boundaries of the small amplitude harmonic domain), the possible destination domains are the large amplitude harmonic domain and the 1/2 subharmonic domain. When the excitation amplitude increases from A=0.5 to 0.95, the small amplitude harmonic domain evolves into either the 1/2 subharmonic or large amplitude harmonic domains. The relationship among the system mean energies of a typical responses in the 1/2 subharmonic and large amplitude harmonic domains at A=0.95 shown in Fig. 4.13(a) and 4.13(b) are examined. For time t greater than 30 seconds, all three different types of system response are close to steady state. It is found that the system mean energy of a typical response in the small amplitude harmonic domain is less than that in the 1/2 subharmonic response (Fig. 4.13a). On the other hand, it is observed that the system mean energy in the large harmonic domain is much greater than that of the steady-state small amplitude harmonic response. The system mean energy level of the 1/2 subharmonic response is found to lie between those of the small and large amplitude harmonic responses.

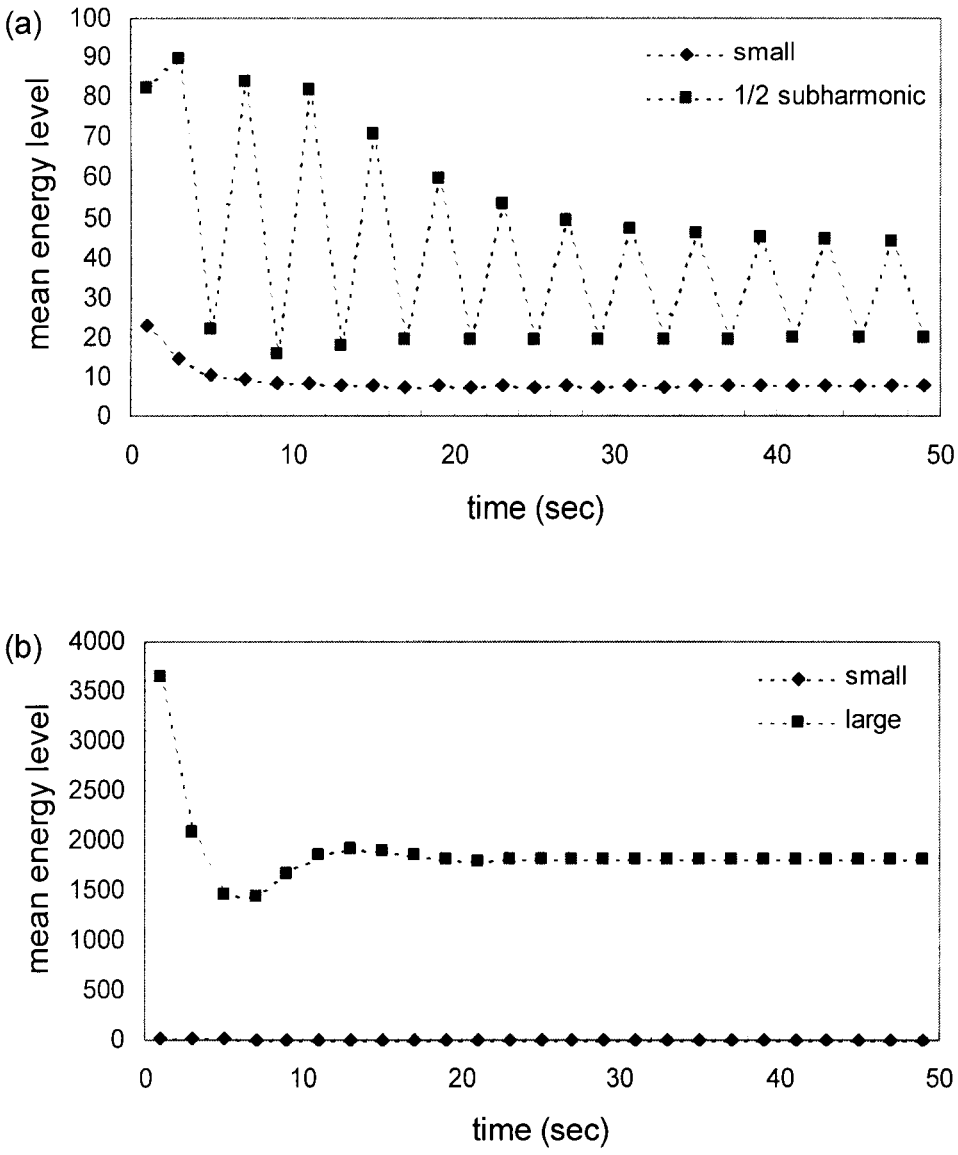

Fig. 4.13 Mean energy level of the system response. (a) small amplitude harmonic and 1/2 subharmonic domains. (b) small and large amplitude harmonic domains. {m=3.428, Ca=0.25, ξ=0.06, Cd'=0.02, Cm=1.25, Cd=0.1, a_1=9.3, a_2=4.0, a_3=4.0}, ($x(0)$,$dx/dt(0)$)={(0.0, 0.0) (small amplitude harmonic, and 1/2 subharmonic responses), (4.0, 1.0) (large amplitude harmonic response)}, {a=0.95 (large amplitude harmonic, and 1/2 subharmonic responses), 0.5 (small amplitude harmonic response)}.

Thus, with the excitation amplitude range of (0.5, 1.5) during the inter-domain transition, a jump from small amplitude harmonic response to large amplitude harmonic response is highly unlikely. This confirms that the characteristics of inter-domain transition at lower boundary of the 1/2 subharmonic domain described by using the system mean energy level is in good agreement with that obtained by employing the system total energy.

Considering the system mean energy level of typical responses in competing domains around domain boundaries, all the elements of inter-domain probability transition matrix K can be evaluated. The detailed description of evaluation of inter-domain probability matrix K is provided in Appendix B.

4.6 Intra-domain Transitions

In addition to the inter-domain transition of the system response, the system response also undergoes successive transient-state within the attraction domain as the excitation parameter varies within an excitation amplitude domain. These transitions within attraction domains are defined as intra-domain transitions. As shown in an earlier section, the governing equation of the response amplitude probability intra-domain transition can be written as

$$p(R^{(2)} \mid D_d{}^R) = \int \left\{ \int \left[\int p(R^{(2)} \mid R^{(1)}, A^{(1)}, A^{(2)}, D_d{}^R) p(R^{(1)} \mid (D_d{}^R)_A^{(1)}) dR^{(1)} \right] p(A^{(1)} \mid D_d{}^A) dA^{(1)} \right\} p(A^{(2)} \mid D_d{}^A) dA^{(2)} \tag{4.13}$$

where $p(R^{(2)} \mid (D_d{}^R)_A^{(2)}) = \int_{D_d{}^A} p(R^{(2)} \mid A^{(1)}, A^{(2)}, D_d{}^R) p(A^{(1)} \mid D_d{}^A) dA^{(1)}$ (4.14)

$$p(R^{(2)} \mid A^{(1)}, A^{(2)}, D_d{}^R) = \int_{D_{d'}} p(R^{(2)} \mid A^{(1)}, A^{(2)}, D_d{}^R) p(R^{(1)} \mid (D_d{}^R)_A^{(1)}) dR^{(1)} \quad (4.15)$$

To numerically evaluate the intra-domain transition probability, the response amplitude domains $\{(D_d^R)_A^{(z)},\ z=1,2\}$, the system initial condition X^o domain, the excitation phase angle difference Φ domain, and the excitation amplitude domain $D_d{}^A$ are discretized. The initial condition is assumed to be uniformly distributed over the domain, which is the phase trajectory of the current excitation cycle. Then, the first term on the right-hand-side of Eq.(4.15) can be evaluated by the following equation

$$\begin{aligned} & p(R_k^{(2)} \mid R_l^{(1)}, A_j^{(1)}, A_i^{(2)}, D_d{}^R) \\ & = p(\Phi_p, X_p^o \mid R_l^{(1)}, A_j^{(1)}, A_i^{(2)}, D_d{}^R) = \frac{1}{m_X} \int_{\Phi_p - \Delta\Phi/2}^{\Phi_p + \Delta\Phi/2} \frac{p(A_j^{(1)}, A_i^{(2)}, \Phi)}{p(A_j^{(1)}, A_i^{(2)})} d\Phi \end{aligned} \quad (4.16)$$

where, m_x is the total number of intervals of initial condition X^o, and the subscripts indicate sample points of the corresponding discretized random variables. The probability vector of the response amplitude $p(R^{(2)} \mid R_l^{(1)}, A_j^{(1)}, A_i^{(2)}, D_d{}^R)$ can be obtained by varying Φ_p and X_p^o over the entire respective domains and lumping all $p(R_k^{(2)} \mid R_l^{(1)}, A_j^{(1)}, A_i^{(2)}, D_d{}^R)$. Then, the discrete form of Eq.(4.13-15) can be used to determine the intra-domain transition probability vectors as following.

$$p(R^{(2)} \mid A_j^{(1)}, A_i^{(2)}, D_d{}^R) = \sum_{l=1}^{m_R} p(R^{(2)} \mid R_l^{(1)}, A_j^{(1)}, A_i^{(2)}, D_d{}^R) p(R_l^{(1)} \mid (D_d{}^R)_A^{(1)}) \quad (4.17)$$

$$p(R^{(2)} \mid (D_d{}^R)_A^{(2)}) = \sum_{j=1}^{m_A} p(R^{(2)} \mid A_j^{(1)}, A_i^{(2)}, D_d{}^R) p(A_j^{(1)} \mid D_d{}^A) \quad (4.18)$$

$$p(R^{(2)} \mid D_d{}^R) = \sum_{i=1}^{m_R} p(R^{(2)} \mid (D_d{}^R)_A^{(2)}) p(A_i^{(2)} \mid D_d{}^A) \tag{4.20}$$

where, m_R and m_A is the number of intervals in the discretized $(D_d^R)_A^{(1)}$ domain and excitation amplitude domain, respectively. The probability of the excitation amplitude of the next cycle being in domain D_d^R can be computed by

$$p(A_n^{(z)} \mid D_d{}^R) = \int_{A_n-\Delta A/2}^{A_n+\Delta A/2} p(A \mid D_d{}^A) dA, \qquad n = 1,2,\ldots,m_A, \quad z = 1,2 \tag{4.21}$$

Thus, the overall stationary response amplitude PDF can be approximated as

$$p(R^{(1)}) = p(R^{(2)}) = \sum_{j=1}^{m_A} p(R^{(1)} \mid D_d{}^R) p(D_d) \tag{4.22}$$

4.7 Prediction, Experimental Results, and Simulation

To validate the prediction capability of the semi-analytical method, predicted response amplitude PDFs are presented and compared to experimental and numerical simulation results. The durations of experiments were sufficiently long to achieve stationarity, however, data were recorded only for short period of time due to limited storage capacity and large number of cases considered. Since long duration of simulations are relatively easy to obtain, and may provide better "data set" for calibrating of the semi-analytical method, simulation results were performed for 25000 excitation cycles. The experimental tests were conducted with several distinct configurations for single-degree-of-freedom (SDOF) and multi-degree-of-freedom systems. In this study, experimental results from tests D16, D17 and D18 are selected for comparison with predictions. In these tests,

narrowband excitations are used as input to SDOF system with large sphere, 90° mooring lines configuration, which exhibit highly nonlinear behavior among several different configurations. "Tests" D15 and D19 are generated numerically using the Shinozuka formulation in numerical simulation of narrowband wave with target variances of Test D15 and 19 about one-half times that of Test D16 and two time that of Test D18, respectively. These two different target variances are selected to examine the influence of the variance on the accuracy in predicting response amplitude probability. The excitation and system parameter sets are shown in Table 4.1. Note that ρ is the auto-correlation of the cosine components of the excitation envelope process with time lag equal to the peak excitation period (Ochi, 1990).

Test	D15	D16	D17	D18	D19
System Parameters	Cs= 0.76 a_1=9.3 a_2=4.0 a_3=4.0				
Excitation Parameters, Eq.(5)					
ω_f	π				
σ_f^2	0.0675	0.1434	0.2178	0.2210	0.4050
ρ	0.0206	0.0344	0.0632	0.0634	0.1236
$\sqrt{\lvert\Sigma\rvert}$	0.0041	0.0194	0.0434	0.0448	0.1488

Table. 4.1 Parameters of narrowband excitation on SDOF, 90° configuration.

The probability of the system response being in one attraction domain through inter-domain transitions and corresponding transition probability matrix, K are listed in Table 4.2. Subscripts 1, 2, and 3 represent the small harmonic domain, 1/2 subharmonic domain, and large harmonic domain, respectively.

Test	σ_f^2	Transition Matrix, K	Normalized Eigenvector
D15	0.0675	$\begin{bmatrix} 0.954 & 0.911 & 0.889 \\ 0.046 & 0.089 & 0.074 \\ 1.601 & 0.000 & 0.038 \end{bmatrix}$	$\begin{Bmatrix} p_1(D_1) \\ p_2(D_2) \\ p_3(D_3) \end{Bmatrix} = \begin{Bmatrix} 0.952 \\ 0.048 \\ 0.000 \end{Bmatrix}$
D16	0.1434	$\begin{bmatrix} 0.790 & 0.768 & 0.720 \\ 0.210 & 0.232 & 0.123 \\ 0.000 & 0.000 & 0.158 \end{bmatrix}$	$\begin{Bmatrix} p_1(D_1) \\ p_2(D_2) \\ p_3(D_3) \end{Bmatrix} = \begin{Bmatrix} 0.785 \\ 0.215 \\ 0.000 \end{Bmatrix}$
D17	0.2178	$\begin{bmatrix} 0.701 & 0.689 & 0.567 \\ 0.299 & 0.311 & 0.136 \\ 0.000 & 0.000 & 0.297 \end{bmatrix}$	$\begin{Bmatrix} p_1(D_1) \\ p_2(D_2) \\ p_3(D_3) \end{Bmatrix} = \begin{Bmatrix} 0.697 \\ 0.303 \\ 0.000 \end{Bmatrix}$
D18	0.2210	$\begin{bmatrix} 0.698 & 0.688 & 0.563 \\ 0.302 & 0.312 & 0.136 \\ 0.000 & 0.000 & 0.300 \end{bmatrix}$	$\begin{Bmatrix} p_1(D_1) \\ p_2(D_2) \\ p_3(D_3) \end{Bmatrix} = \begin{Bmatrix} 0.695 \\ 0.305 \\ 0.000 \end{Bmatrix}$
D19	0.4050	$\begin{bmatrix} 0.665 & 0.664 & 0.375 \\ 0.333 & 0.334 & 0.119 \\ 0.002 & 0.002 & 0.506 \end{bmatrix}$	$\begin{Bmatrix} p_1(D_1) \\ p_2(D_2) \\ p_3(D_3) \end{Bmatrix} = \begin{Bmatrix} 0.664 \\ 0.332 \\ 0.004 \end{Bmatrix}$

Table.4.2 Inter-domain transition probability in the subharmonic resonance region.

Observe that when the excitation intensity, i.e., variance, increases, the excitation amplitudes become large and the excitation amplitude probability

distribution is shifted to right. As the excitation amplitude increases from Test D15 to D19, the probability that the system response staying in the small amplitude domain decreases. Thus, the value of $p_{11}(1|1)$ in the transition matrix K decreases while both $p_{22}(2|2)$ and $p_{33}(3|3)$ increases.

The overall response amplitude PDFs obtained by Eq. (4.22), numerical simulation results, and experimental results are presented in Fig. 4.10 for the five cases examined. It can be observed that, in each case, predictions obtained from the analytical procedure accurately match both the experimental and simulation results.

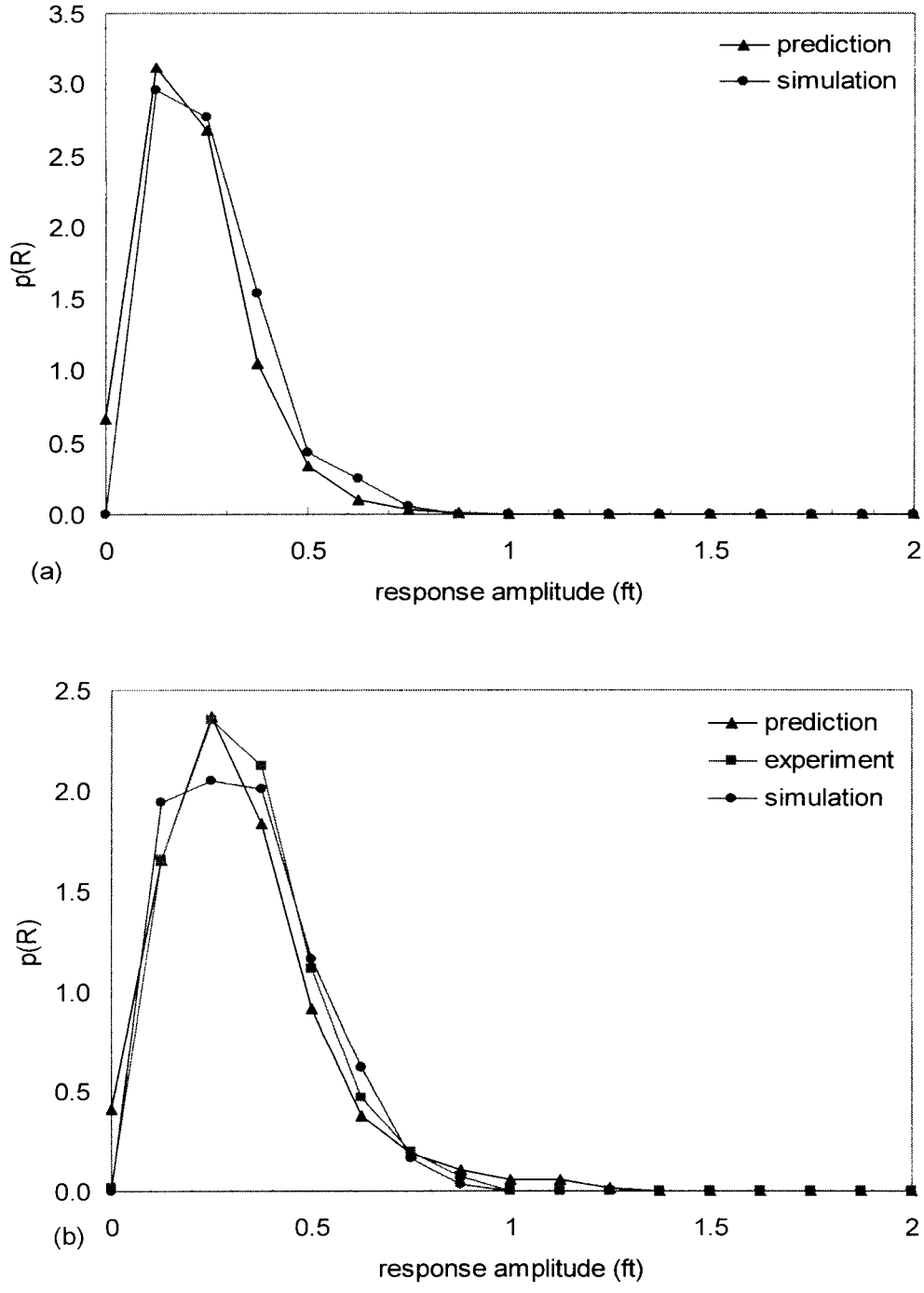

Fig. 4.14 Overall response amplitude distribution : (a) Test D15 (b) Test D16.

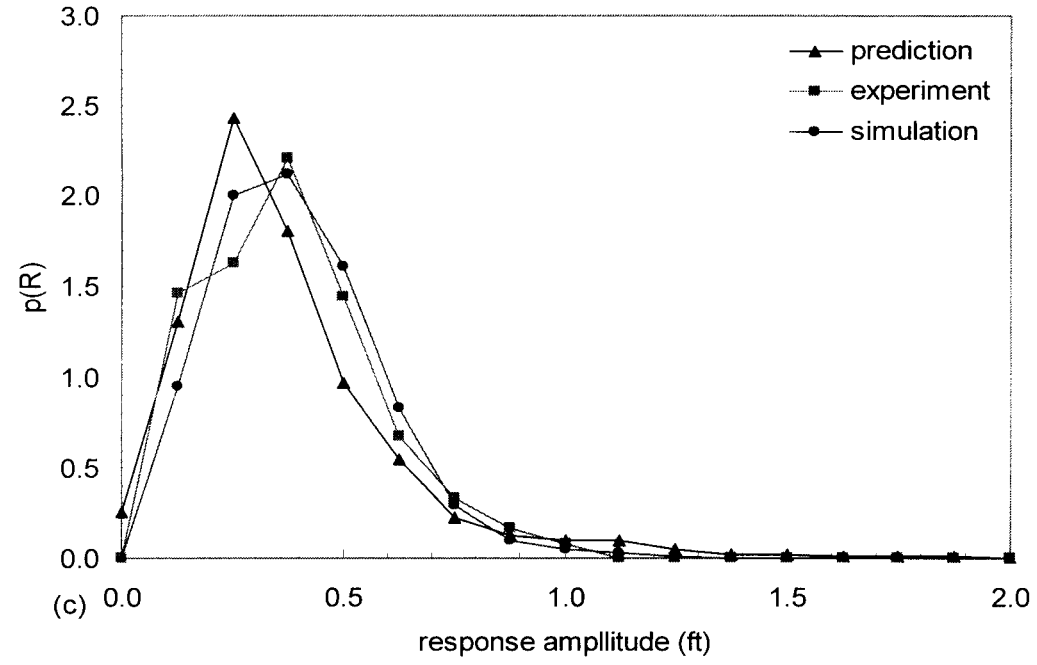

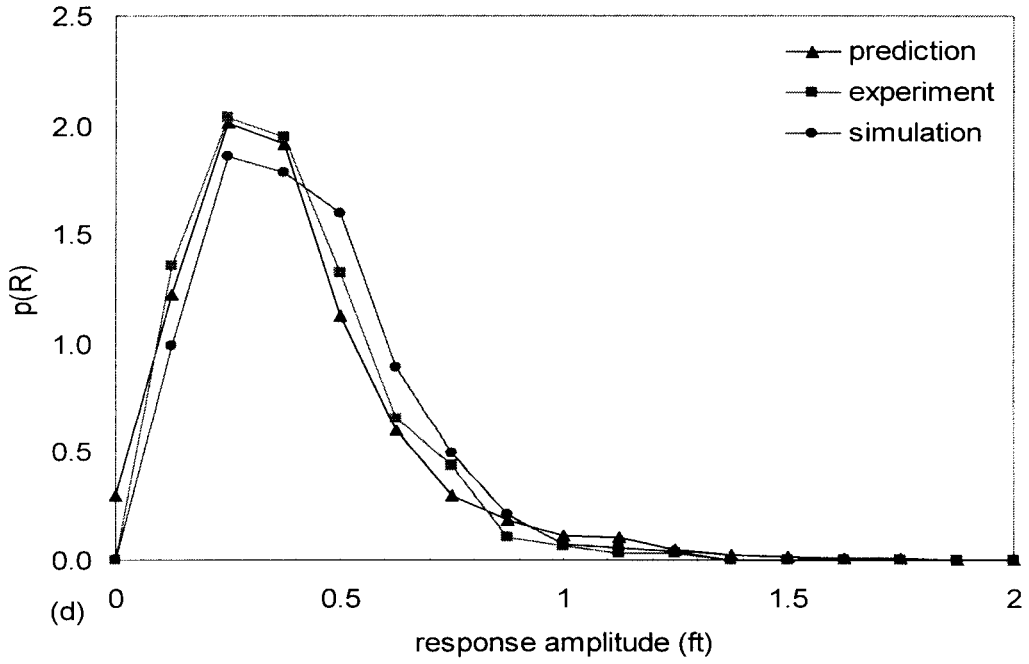

Fig. 4.14 Overall response amplitude distribution (continued) : (c) Test D17 (d) Test D18.

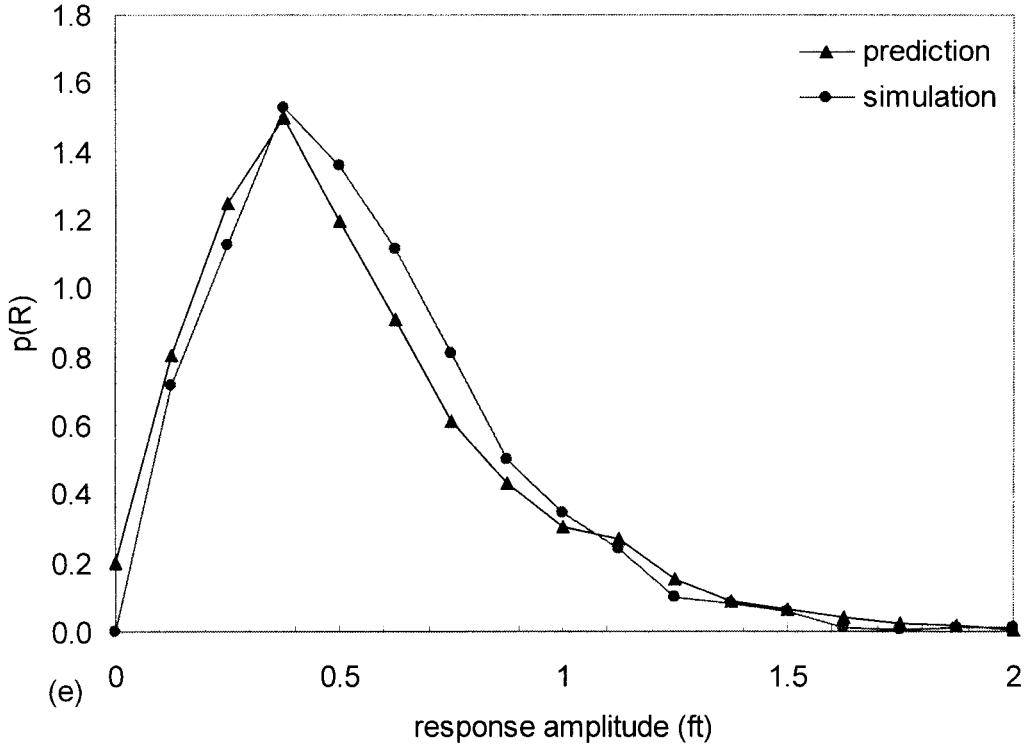

Fig. 4.14 Overall response amplitude distribution (continued): (e) Test D19.

5. SUMMARY AND CONCLUDING REMARKS

5.1 Summary

The behaviors of two nonlinear dynamical systems subjected to narrowband random excitations are investigated in this study. For convenience of development of the probabilistic analysis procedure, a simple (Duffing) system with nonlinearity limited to the restoring force only is first examined. With the knowledge gained from the analysis of the Duffing system, the resulting probabilistic analysis procedure is modified and applied to analyze the stochastic behavior of a nonlinear ocean system under random wave excitation. The analytical model of the ocean system is derived from a multi-point mooring system experiment conducted at the O.H. Hinsdale Wave Research Laboratory at Oregon State University. The system is modeled as a nonlinear structure (with a third order polynomial restoring force) with nonlinear damping (hydrodynamic drag force) (NSND). The system coefficients are obtained from a nonlinear system-identification technique developed by Narayanan (1999).

The formulation of the analysis method is described and validated by numerical simulation. The analysis method is applied to investigate the complex system response behavior among co-existing attractors in the subharmonic resonance region. The system response is considered as in a transient-state due to the successive variations in the excitation parameters, and transitions among co-existing attractor are model as inter-domain transitions. The probability of

response amplitude being in a particular attraction domain given that it belongs to some other domains in the current excitation cycle is evaluated and the transition probability matrix K is obtained. By solving the associated eigenvalue problem, the time-invariant steady-state probability is then obtained.

In addition to inter-domain transitions, variations of the response amplitude within an attraction domain take place as the excitation parameter varies. These variations are considered intra-domain transitions. The intra-domain transition probability is obtained by considering the characteristic response behavior under deterministic excitation and the functional relationship between excitation parameter and response amplitude. Because the form of this functional relationship is quite complex and an analytical expression is not available, a numerical technique is developed and employed to compute the intra-domain transition probability.

For the Duffing system, numerical simulations are performed to validate the capability and accuracy of the semi-analytical method in predicting the response amplitude probability density function. The effects of varying excitation bandwidth and variance on the response amplitude probability distribution are also investigated.

For the NSND model, the response amplitude probability distribution is predicted by the semi-analytical method with stochastic excitation parameters obtained from the corresponding measured experimental results. Predictions are

compared with the experimental and simulation results to confirm the validity of semi-analytical method.

5.2 Concluding Remarks

The assumption that the nonlinear system response characteristics under deterministic excitations are preserved under narrowband excitation environment has been confirmed via simulations and predictions for the Duffing System, and simulations, predictions as well as experimental results for the moored ocean system. Due to the random nature of the narrowband excitation process, excitation parameters vary gradually. These slow variations can be approximated by a succession of finite discrete changes in the system excitation parameters. Thus, transient-state response characteristics are employed to interpret the system response behavior under narrowband excitations.

The stationary probability vector associated with inter-domain transitions can be characterized by the excitation amplitude domain boundaries as well as the excitation bandwidth and variance. Note that the locations of the domain boundaries are determined by the excitation frequency that is assumed to be the dominant frequency of the narrowband process. Thus, the locations of the domain boundaries are time invariant. However, when the excitation bandwidth increases, variations in the excitation frequency may shift the domain boundaries hence significantly affecting the response inter-domain transition behaviors.

A significant improvement in the accuracy of predicting response amplitude probability distribution is achieved by the semi-analytical method. This is because the stochastic nonlinear response behavior under narrowband excitation is accurately characterized by the analytical procedure through inter-domain and intra-domain transitions.

For the NSND model, overlapping of the excitation amplitude domains between large amplitude domain and small amplitude domain is observed. However, excitation amplitude domains of small amplitude response and 1/2 subharmonic response do not overlap. As shown in the response amplitude curve, there is a discontinuation in the excitation amplitude domain of small amplitude response.

According to the inter-domain transition probabilities, it is observed that the steady state probability of response amplitude being in large harmonic attraction domain is relatively small compared with those in small amplitude harmonic, and 1/2 subharmonic domains for all of the five cases examined. The entries of the transition matrix K are related to the stochastic properties of the excitations, and for the excitation parameters used to analyze the experiments, the probability of system response being in the large amplitude domain is found to be practically negligible. Thus, the contribution to the overall response amplitude distribution from the intra-domain transition probability of large harmonic attraction domain is also negligible.

Overall response amplitude probability distribution is obtained by combining the inter-domain and intra-domain transition probabilities using the Bayesian

formulation. As concluded above, the inter-domain transition probability of particular domains could be practically zero, and thus their contributions to the overall PDF negligible. Hence the inter-domain transition probabilities should be first determined to eliminate the need for calculations of intra-domain transition probabilities of attraction domains with negligible transition probabilities.

The predicted response amplitude probability distributions are compared with both experimental and simulation results and found to match both results accurately. The shape of the probability distribution, and the location of its mode and maximum of the response amplitude are in good agreement with experimental results. These results validate the capability of the semi-analytical method in predicting nonlinear system response under narrowband excitation.

The response amplitude probability distribution can be obtained from the analytical procedure when the stochastic property of excitation amplitude is specified. The predicted results for the wide range of excitation parameter can be readily used in structural design, control, and other applications without simulations.

Based on the capability and accuracy of the semi-analytical method in predicting response amplitude probability distribution for both Duffing system and NSND model, it is concluded that the method can be reliably applied to analyze these types of nonlinear system responses.

5.3 Recommended Future Study

Predicting the response amplitude probability distribution by the semi-analytical method takes significant amount of computational efforts compared to direct numerical simulations, even though the analytical method takes advantage of the stochastic properties of the nonlinear system response. Most of the computational time is devoted to obtaining the probability of the response amplitude in the next cycle over the entire discretized domains. The computational time increases significantly with increasing number of discretized intervals due to the lack of an analytical functional relationship between the response amplitude in next cycle and excitation amplitude, phase angle difference in both current and next cycle and initial conditions. Development of an analytical functional relationship will significantly improve the computational efficiency.

Wave force on a structural system is determined by the Morrison equation considering the wavelength and the dimension of the sphere used in experiments. However, for large structural systems in relatively shallow water depth, a large-body (diffraction) theory may be needed to characterize the fluid-structure interaction system. Thus, extension of the semi-analytical method to a structural system under random excitations using large-body theory modeling is recommended for future study.

BIBLIOGRAPHY

Bouleau, N. and Lépingle, D. (1994). Numerical Methods for Stochastic Processes. John Wiley and Sons, Inc.

Clough, R.W. and Penzien, J. (1993). Dynamics of Structures, 2nd Edition McGraw-Hill.

Davies, H.G. and Nandlall, D. (1986). Phase Plane for Narrow-Band Random Excitation of a Dulling Oscillator. Journal of Sound and Vibration, 104, 277-283.

Davies, H.G. and Rajan, S. (1988). Random Superharmonic and Subharmonic esponse: Multiple Time Scaling of a Duffing Oscillator. Journal of Sound and Vibration, 26, 195-208.

Davies, H.G. and Liu, Q. (1990). The Response Envelope Probability Density Function of a Dulling Oscillator with Random Narrow-Band Excitation. Journal of Sound and Vibration, 139, 1-8.

Dimentberg, M.F. (1971). Oscillations of a System with Nonlinear Cubic Characteristics under Narrow Band Random Excitation. Mechanics and Solids, 6, 142-146.

Dimentberg, M.F. (1988). Statistical Dynamics of Nonlinear and Time-Varying Systems. John Wiley & Sons Inc.

Gillespie, D T (1992). Markov Processes. Academic Press, Inc., San Diego.

Gottlieb, 0. and Yim, S. (1992). Nonlinear Oscillations, Bifurcations and Chaos in a Multi-Point Mooring System with a Geometric Nonlinearity Applied Ocean Research, 24, 1-257.

Guckenheimer, J. and Holmes, P. (1986). Nonlinear Oscillations. Dynamical Systems and Bifurcation of Vector Fields. Springer-Verlag, New York.

Hagedorn, P. (1988). Nonlinear Oscillations. Oxford, New York.

Jordan, D.W. and Smith, P (1987). Nonlinear Ordinary Differential Equations Second Edition. Clarendon Press, Oxford.

Koliopulos, P.K. and Bishop, S.R. (1993). Quasi-Harmonic Analysis of the Behavior of a Hardening Dulling Oscillator Subjected to Filtered White Noise Nonlinear Dynamics, 4, 279-288.

Koliopulos, P.K., Bishop, S.R., Stefanou, G.D. (1991). Response Statistics of Nonlinear System under Variations of Excitation Bandwidth. Computational Stochastic Mechanics, London, 33, 5-348.

Koliopulos, P.K. and Langley, R.S. (1993). Improved Stability Analysis of The Response of a Dulling Oscillator under Filtered White Noise. International Journal of Non-Linear Mechanics, 28, 145-155.

Langley, R.S. (1986). On Various Definitions of the Envelope of a Random Process. Journal of Sound and Vibration, 105, 503-512.

Lin, H. and Yim, S.C.S. (1995). Noisy Nonlinear Motions of Moored Systems. Part 1: Analysis and Simulation. Journal of Waterways, Port, Coastal, and Ocean Engineering, 123 (5), 287-295.

Narayanan, S. (1999). Experimental Analysis of a Nonlinear Moored Structure. Ph.D. Dissertation. Oregon State University.

Nayfeh, A.H. and Mook, D.T. (1979). Nonlinear Oscillations. Wiley, New York.

Newland, D.E. (1993). An Introduction to Random Vibrations. Spectral & Wavelet Analysis. (3rd Ed.) Longman, New York.

Nigam, N C. (1983). Introduction to Random Vibrations. The MIT Press, London.

Ochi, M. K. (1990). Applied Probability and Stochastic Processes in Engineering and Physical Sciences. John Wiley and Sons, New York.

Rajan, S. and Davies, H.G (1988) Multiple Time Scaling of the Response of a Duffing Oscillator to Narrow-Band Random Excitation. Journal of Sound and Vibration, 123, 497-506.

Press, W.H. (1986). Numerical Recipes: the art of scientific computing. Cambridge University Press, New York.

Roberts, J. B. and Spanos, P.D. (1986). Stochastic Averaging: An Approximate Method of Solving Random Vibration Problems. International Journal of Non-Linear Mechanics, 21, 111-134

Roberts, J.B. and Spanos, P.D. (1990). Random Vibration and Statistical Linearization. John Wiley and Sons, New York.

Rice, S. O. (1954). Selected Papers on Noise and Stochastic Processes, Mathematical Analysis of Random Noise. Dover, New York.

Shih, I. (1998). Stochastic Analysis of Complex Nonlinear System Response Under Narrowband Excitations. Ph.D. Dissertation. Oregon State University.

Shinozuka, M. (1971). Simulation of Multivariate and Multidimensional Random Processes. Journal of the Acoustical Society of America, 49, 357-367.

Shinozuka, M. and Deodatis, G. (1991). Simulation of Stochastic Processes by Spectral Representation. Appl Mech Rev, Vol 44, no 4, 191-203.

Stratonovich, R.L. (1963). Topics in the Theory of Random Noise. Gordon and Breach, New York.

Thompson, J.M.T., and Stewart, H.B. (1986). Nonlinear Dynamics and Chaos. John Wiley and Sons, New York.

Yim, S., Myrum, M.A, Gottlieb, 0., Lin, H And Shih, I. (1993). Summary and Preliminary Analysis of Nonlinear Oscillations in a Submerged Mooring System Experiment. ONR Report No OE-93-03.

Yim, S. and Lin, H. (1992). Probabilistic Analysis of a Chaotic Dynamical System Applied Chaos, 219-241. John Wiley and Sons, New York.

Yim, S. and Lin, H. (2000). Noisy Nonlinear Motions of a Moored System, II: an Experimental Study, Journal of Waterway, Port, Coastal and Ocean Engineering, ASCE, Vol.6, No.3, 113-120.

APPENDICES

APPENDIX A

THE SEMI-ANALYTICAL PROCEDURE

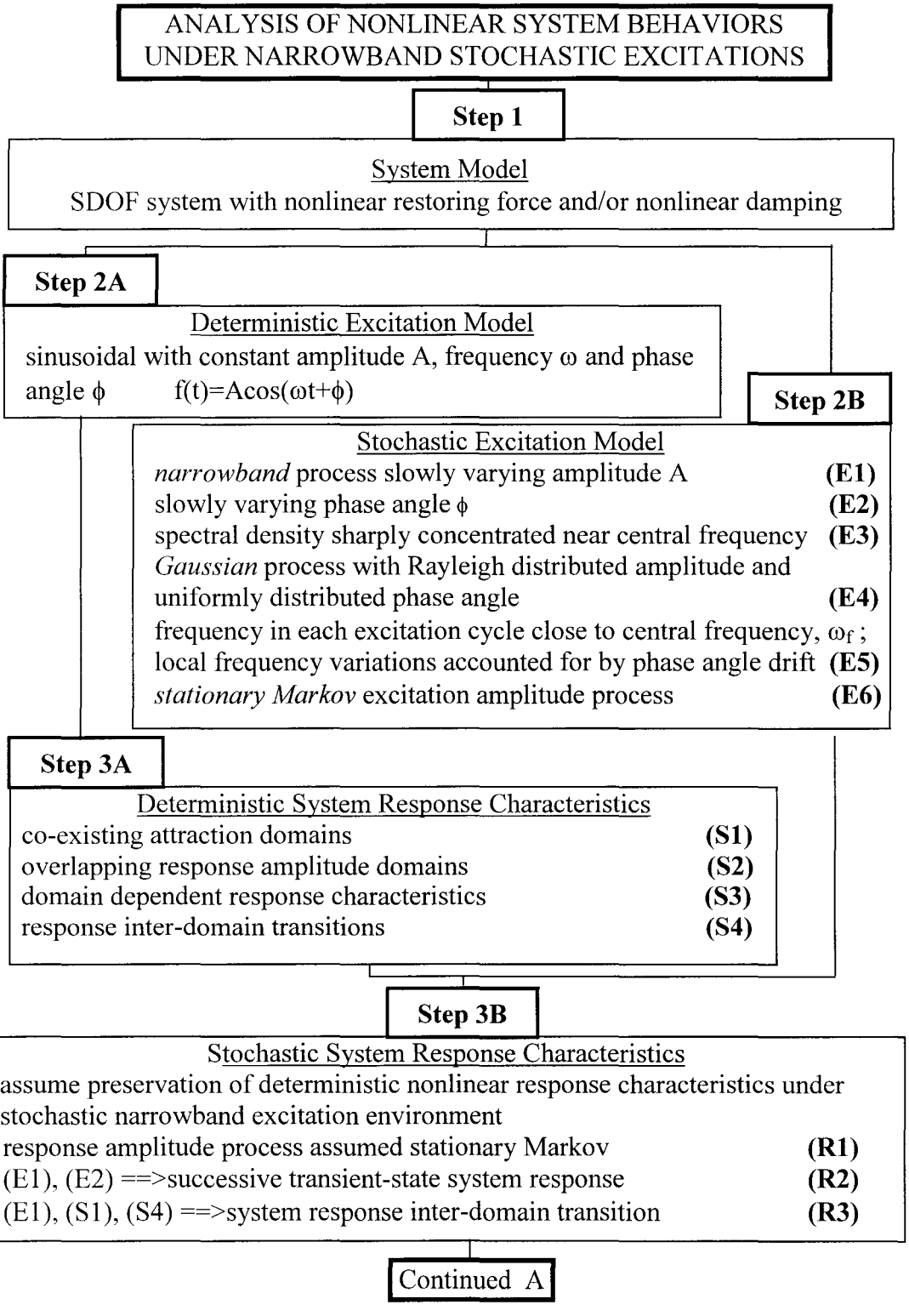

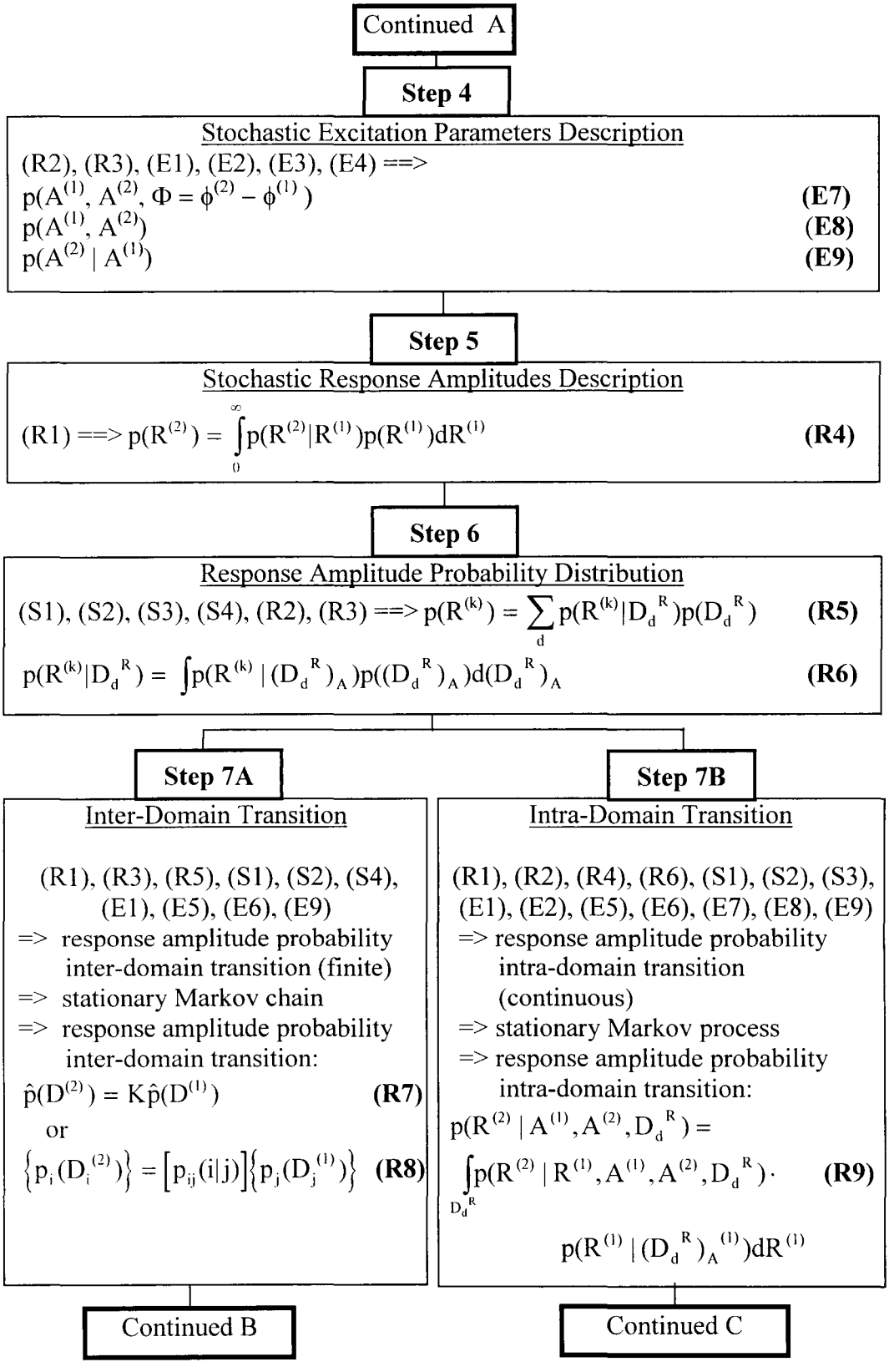
Continued A
Step 4
Stochastic Excitation Parameters Description
(R2), (R3), (E1), (E2), (E3), (E4) ==>
$p(A^{(1)}, A^{(2)}, \Phi = \phi^{(2)} - \phi^{(1)})$ (E7)
$p(A^{(1)}, A^{(2)})$ (E8)
$p(A^{(2)} \mid A^{(1)})$ (E9)
Step 5
Stochastic Response Amplitudes Description
(R1) ==> $p(R^{(2)}) = \int_0^\infty p(R^{(2)}|R^{(1)})p(R^{(1)})dR^{(1)}$ (R4)
Step 6
Response Amplitude Probability Distribution
(S1), (S2), (S3), (S4), (R2), (R3) ==> $p(R^{(k)}) = \sum_d p(R^{(k)}|D_d^R)p(D_d^R)$ (R5)
$p(R^{(k)}|D_d^R) = \int p(R^{(k)} \mid (D_d^R)_A)p((D_d^R)_A)d(D_d^R)_A$ (R6)
Step 7A
Inter-Domain Transition
(R1), (R3), (R5), (S1), (S2), (S4), (E1), (E5), (E6), (E9)
=> response amplitude probability inter-domain transition (finite)
=> stationary Markov chain
=> response amplitude probability inter-domain transition:
$\hat{p}(D^{(2)}) = K\hat{p}(D^{(1)})$ (R7)
or
$\{p_i(D_i^{(2)})\} = [p_{ij}(i|j)]\{p_j(D_j^{(1)})\}$ (R8)
Step 7B
Intra-Domain Transition
(R1), (R2), (R4), (R6), (S1), (S2), (S3), (E1), (E2), (E5), (E6), (E7), (E8), (E9)
=> response amplitude probability intra-domain transition (continuous)
=> stationary Markov process
=> response amplitude probability intra-domain transition:
$p(R^{(2)} \mid A^{(1)}, A^{(2)}, D_d^R) = \int_{D_d^R} p(R^{(2)} \mid R^{(1)}, A^{(1)}, A^{(2)}, D_d^R) \cdot p(R^{(1)} \mid (D_d^R)_A^{(1)})dR^{(1)}$ (R9)
Continued B
Continued C

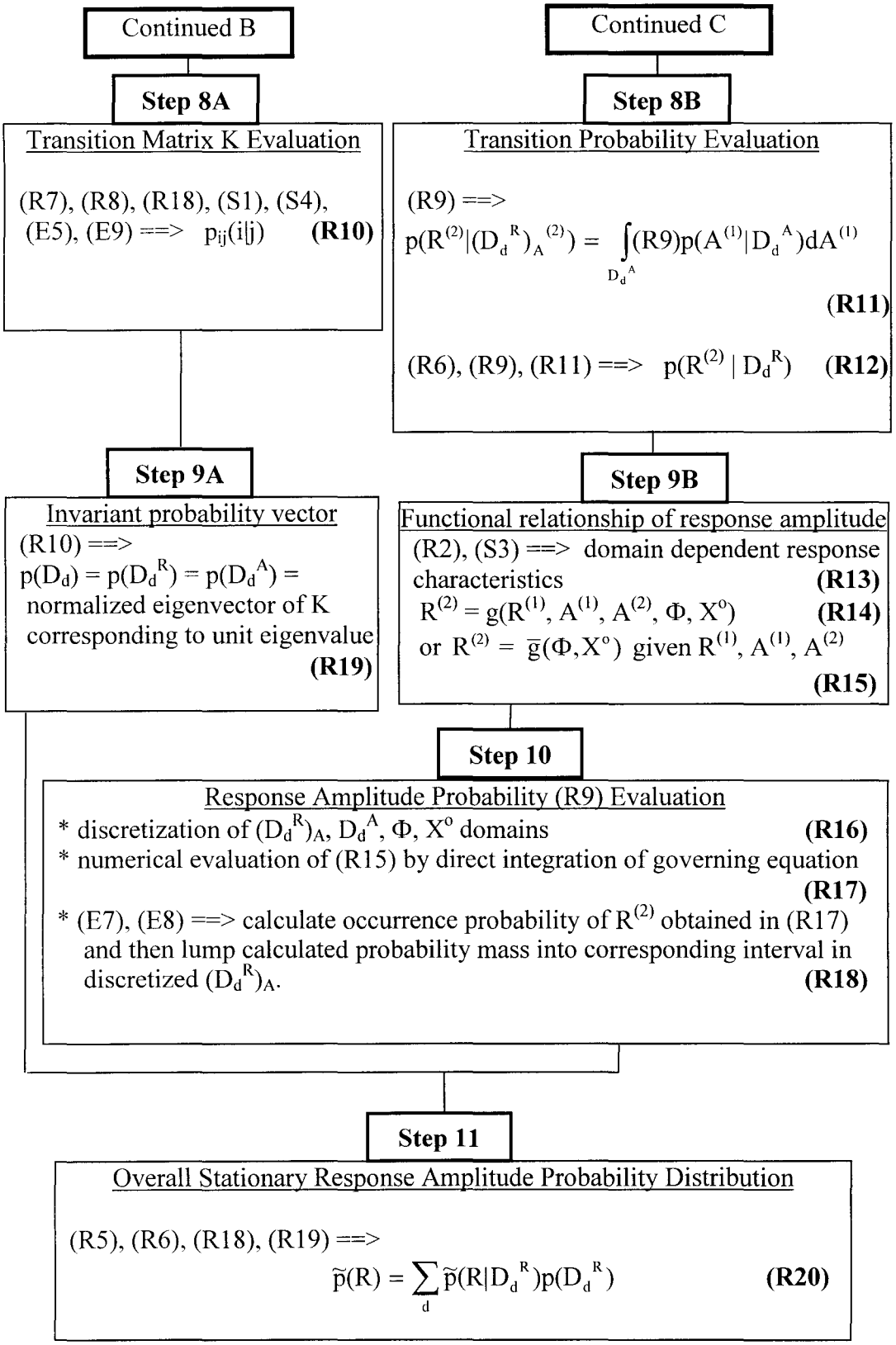
Continued B
Step 8A
Transition Matrix K Evaluation
(R7), (R8), (R18), (S1), (S4), (E5), (E9) ==> $p_{ij}(i|j)$ (R10)
Continued C
Step 8B
Transition Probability Evaluation
(R9) ==>
$p(R^{(2)}|(D_d^R)_A^{(2)}) = \int_{D_d^A} (R9)p(A^{(1)}|D_d^A)dA^{(1)}$ (R11)
(R6), (R9), (R11) ==> $p(R^{(2)} | D_d^R)$ (R12)
Step 9A
Invariant probability vector
(R10) ==>
$p(D_d) = p(D_d^R) = p(D_d^A)$ = normalized eigenvector of K corresponding to unit eigenvalue (R19)
Step 9B
Functional relationship of response amplitude
(R2), (S3) ==> domain dependent response characteristics (R13)
$R^{(2)} = g(R^{(1)}, A^{(1)}, A^{(2)}, \Phi, X^o)$ (R14)
or $R^{(2)} = \bar{g}(\Phi, X^o)$ given $R^{(1)}, A^{(1)}, A^{(2)}$ (R15)
Step 10
Response Amplitude Probability (R9) Evaluation
* discretization of $(D_d^R)_A$, D_d^A, Φ, X^o domains (R16)
* numerical evaluation of (R15) by direct integration of governing equation (R17)
* (E7), (E8) ==> calculate occurrence probability of $R^{(2)}$ obtained in (R17) and then lump calculated probability mass into corresponding interval in discretized $(D_d^R)_A$. (R18)
Step 11
Overall Stationary Response Amplitude Probability Distribution
(R5), (R6), (R18), (R19) ==>
$\tilde{p}(R) = \sum_d \tilde{p}(R|D_d^R)p(D_d^R)$ (R20)

APPENDIX B

EVALUATION OF INTER-DOMAIN PROBABILITY TRANSITION MATRIX

B.1 Diagonal elements

In the subharmonic resonance region, three attraction domains co-exist as explained in Chapter 4 for the particular NSND system coefficients and excitation parameter considered. The conditional probabilities of the response amplitude transition within attraction domain, i.e., $p_{11}(1|1)$, $p_{22}(2|2)$, and $p_{33}(3|3)$, can be determined by Eq.(4.11).

B.2 Off-diagonal elements

B.2.1 Transitions from large amplitude domain

As shown in the response amplitude curve, there is no upper boundary for the large amplitude domain. The transition from large amplitude domain to 1/2 subharmonic domain can occur when the excitation amplitude becomes less than the lower boundary A_{3L} of large amplitude domain. Therefore, $p_{23}(2|3)$ can be evaluated as

$$p_{23}(2\,|\,3) = \int_{A_{2L}}^{A_{3L}} p(A^{(2)} \mid A^{(1)} \in D_3{}^{A})dA^{(2)} \qquad \text{(B.1)}$$

Since there exist three domains, $p_{13}(1|3)$ is the complements of $p_{33}(3|3)$ and $p_{23}(2|3)$. Thus,

$$p_{13}(1|3) = 1 - p_{23}(2|3) - p_{33}(3|3) \tag{B.2}$$

B.2.2 Transitions from 1/2 subharmonic domain

When the excitation amplitude exit the 1/2 subharmonic domain through the upper boundary A_{2U}, there exist more than one possible destination domain. To determine the transition probability from 1/2 subharmonic domain to large amplitude domain, mean energy level is taken into account. Considering evolution of the total system energy and the average total energy over one excitation cycle, the mean energy level of the large amplitude response is much higher than that of small amplitude response. Therefore, as far as small amplitude domain co-exist with the large amplitude domain, transition from D_2 to D_1 cannot occur. Thus, the excitation amplitude should exit the 1/2 subharmonic domain through the upper boundary A_{1U} as well as the upper boundary A_{2U}. This can be rewritten as

$$p_{32}(3|2) = \int_{A_{1U}}^{\infty} p(A^{(2)} \mid A^{(1)} \in D_2^{\,A}) dA^{(2)} \tag{B.3}$$

Once $p_{32}(3|2)$ is determined, $p_{12}(1|2)$ can be computed from the complement of $p_{22}(2|2)$ and $p_{32}(3|2)$.

$$p_{12}(1|2) = 1 - p_{22}(2|2) - p_{32}(3|2) \tag{B.4}$$

B.2.3 Transitions from small amplitude domain

Transition from the small amplitude domain to the 1/2 subharmonic domain can occur when the excitation exit through the lower and upper boundaries of 1/2 subharmonic domains. When the excitation amplitude exits through the upper boundary A_{2U} of the 1/2 subharmonic domain from the upper part of the small amplitude domain, the input energy decreases. Thus, the total system energy also decreases. Therefore, the transition to the higher energy level, i.e., transition to large amplitude domain, cannot occur. In addition, an exit from the lower part of the small amplitude domain through the lower boundary A_{2L} of 1/2 subharmonic domain also lead the system response to the 1/2 subharmonic domain due to the large difference between the mean energy level of large amplitude and 1/2 subharmonic domain. Therefore, the probability of the system response transition to the 1/2 subharmonic after an exit from the small amplitude domain can be calculated as

$$p_{21}(2\,|\,1) = \int_{A_{2L}}^{A_{2U}} p(A^{(2)} \mid A^{(1)} \in D_1^{\,A})dA^{(2)} \tag{B.5}$$

$p_{31}(3|1)$ can also be determined by

$$p_{31}(3\,|\,1) = 1 - p_{11}(1\,|\,1) - p_{21}(2\,|\,1) \tag{B.6}$$

APPENDIX C

PROGRAM LIST

```
      program rprobdis
!*****************************************************************
!  prob-dis.for ---> For calculating response amplitude probability
!                    distribution.
!*****************************************************************
      implicit double precision (a-h,o-z)
      dimension x(4),dphi(100),pdf(100)
      common /exci/  aw,wf,pi,cs,a1,a2,a3,co1,co2,co3,co4,Atmp1,Atmp2,ro,D,
      cm,cd,pern,depth,wlength
      pi=4.0*atan(1.0)
      n=2
      ro=1.94
      open(unit=1,file='rprobdis.inp',status='unknown')
      open(unit=2,file='rprobdis.pmf',status='unknown')
      open(unit=3,file='rprobdi1.dat',status='unknown')
      open(unit=4,file='rprobdi2.dat',status='unknown')
      open(unit=5,file='rprobdi3.dat',status='unknown')
      open(unit=6,file='rprobdi4.dat',status='unknown')
      read(1,*) rm
      read(1,*) D
      read(1,*) si
      read(1,*) a1,a2,a3
      read(1,*) cm,ca,cd
      read(1,*) cdp
      read(1,*) pern
      read(1,*) depth,depsph
      read(1,*) sr
      read(1,*) steprate
      call wave(pern,depth,wlength)
      read(1,*) namp
      read(1,*) cy1
      read(1,*) ddevi1
      read(1,*) dnpts0a,dnpts0b,dnpts1a
      stpmax=1./sr
      stpmin=stpmax*steprate
      tol=1d-6
      phs=0.d0
      icount=0
```

```
      wf=2*pi/pern
      rk=2*pi/wlength
      rma=ca*(D**3)*pi/6
      cs=2*si*sqrt(a1*(rm*(1+ca)))
      co1=rm+rma
      co2=ro*cdp*(pi*D**2/4)
      Atmp1=cosh (rk*depsph)
     Atmp2=sinh (rk*depth)
     do 501 ia=1,namp
        read(2,*) aws,daw1
        read(2,*) xi1,xi2
        read(2,*) ndph,idx
        read(2,*) ncy,dcy
        read(2,*) cys,dnpts1b
      do 10 i=1,ndph
        read(2,*) dphi(i),pdf(i)
10    continue
      do 20 k1=1,ncy
      cy=cys+(k1-1)*dcy
      npts0=Idint(cy*2*pi*sr/wf)
      npts1=Idint(cy1*2*pi*sr/wf)
      npts0da=Idint(npts0*dnpts0a)
      npts0db=Idint(npts0*dnpts0b)
      npts1da=Idint(npts1*dnpts1a)
      npts1db=Idint(npts1*dnpts1b)
      do 70 k=1,ndph
      pern=2*pi/wf
      tint=1./sr
      stp=stpmin
      stpl=0.
      err=0.
      t=0
      x(1)=xi1
      x(2)=xi2
      aw1=aws
      aw2=aws
      aw=aws
      ph1=phs
      ph2=phs
      phi=phs
      daw=0.
      dph=0.
      tt=0.
      do 50 ii=1,2
```

```
 if(ii.eq.1) then
  npts=npts0
  dnptsta=npts0da
  dnptstb=npts0db
  ddevi=10.
 endif
 if(ii.eq.2) then
  npts=npts1
  dnptsta=npts1da
  dnptstb=npts1db
  daw=daw1
  dph=dphi(k)
  ddevi=ddevi1
 endif
 tsta=tt+dnptsta/sr
 tstb=tt+dnptstb/sr
 aw1=aw
 aw2=aw+daw
 ph1=phi
 ph2=phi+dph
 remax=0.
 remin=100.
 xa=x(1)
 pxa=0.
 ta=0.
 iflag=0
 islopp=0
 do 30 i=1,npts
  awww=(aw-aw1)*(aw2-aw)
  pph=(phi-ph1)*(ph2-phi)
  if((awww.gt.0.).or.(aw.eq.aw1)) then
   aw=aw+(aw2-aw1)/ddevi
  else
   aw=aw2
  endif
  if((pph.gt.0.).or.(phi.eq.ph1)) then
   phi=phi+(ph2-ph1)/ddevi
  else
   phi=ph2
  endif
  tl=t+tint
  if(x(1).gt.xa) islop=1
  if(x(1).eq.xa) islop=islopp
  if(x(1).lt.xa) islop=-1
```

```
      if(t.ge.tsta.and.t.le.tstb) then
       indslo=islopp*islop
        if(indslo.le.0) then
          if(iflag.eq.0) then
            iflag=1
            go to 35
          endif
          if(abs(xa).gt.abs(pxa)) then
            xamax=abs(xa)
            tamax=ta
          else
            xamax=abs(pxa)
            tamax=pta
          endif
        if(xamax.gt.remax) remax=xamax
        if(xamax.lt.remin) remin=xamax
35      pxa=xa
       pta=ta
        endif
       endif
      xa=x(1)
      ta=t
      islopp=islop
      call rkck(n,t,x,stp,tl,stpmax,stpmin,tol,stpl,err)
      if(err .eq. 1) go to 100
      stp=stpl
30     continue
      if(idx.eq.1) write(3,114) remax,remin,pdf(k)
      if(idx.eq.2) write(4,114) remax,remin,pdf(k)
      if(idx.eq.3) write(5,114) remax,remin,pdf(k)
      if(idx.eq.4) write(6,114) remax,remin,pdf(k)
      icount=icount+1
      tt=t
50    continue
      write(*,*) icount
70    continue
20    continue
501    continue
114    format(2x,f12.8,2x,f12.8,2x,f16.14)
100    continue
```

```
      close(1)
      close(2)
      close(3)
      close(4)
      close(5)
      close(6)
      end
      SUBROUTINE rkck(n,x,y,h,b,hmax,hmin,tol,hl,err)
      IMPLICIT DOUBLE PRECISION (A-H,O-Z)
      PARAMETER (NMAX=10)
      DIMENSION y(n),ytem(nmax),ak1(nmax),ak2(nmax),ak3(nmax)
      DIMENSION ak4(nmax),ak5(nmax),ak6(nmax),yout(nmax),yerr(nmax)
      PARAMETER (the2=0.25,the3=0.375,the4=2028./2197.,the5=1.,the6=0.5)
      PARAMETER (c21=0.25,c31=3./32.,c32=9./32.,c41=1932./2197.)
      PARAMETER (C42=-7200./2197.,C43=7296./2197.,C51=8341./4104.)
      PARAMETER (C52=-32832./4104.,C53=29440./4104.,C54=-845./4104.)
      PARAMETER (C61=-6080./20520.,C62=41040./20520.,C63=-28352./20520.)
      PARAMETER (C64=9295./20520.,C65=-5643./20520.,W1=33440./282150.)
      PARAMETER (W3=146432./282150.,W4=142805./282150.)
      PARAMETER (W5=-50787./282150.,W6=10260./282150.,E1=1045./376200.)
      PARAMETER (E3=-11264./376200.,E4=-10985./376200.)
      PARAMETER (E5=7524./376200.,E6=13680./376200.)
      downsw=0.
300   continue
      call frk(x,y,ak1)
      do 11 i=1,n
       ytem(i)=y(i)+c21*h*ak1(i)
11    continue
      call frk(x+the2*h,ytem,ak2)
      do 12 i=1,n
       ytem(i)=y(i)+h*(c31*ak1(i)+c32*ak2(i))
12    continue
      call frk(x+the3*h,ytem,ak3)
      do 13 i=1,n
       ytem(i)=y(i)+h*(c41*ak1(i)+c42*ak2(i)+c43*ak3(i))
13    continue
      call frk(x+the4*h,ytem,ak4)
      do 14 i=1,n
       ytem(i)=y(i)+h*(c51*ak1(i)+c52*ak2(i)+c53*ak3(i)+c54*ak4(i))
14    continue
      call frk(x+the5*h,ytem,ak5)
      do 15 i=1,n
       ytem(i)=y(i)+h*(c61*ak1(i)+c62*ak2(i)+c63*ak3(i)+c64*ak4(i)+c65*ak5(i))
15    continue
```

```
      call frk(x+the6*h,ytem,ak6)
      do 16 i=1,n
       yout(i)=y(i)+h*(w1*ak1(i)+w3*ak3(i)+w4*ak4(i)+w5*ak5(i)+w6*ak6(i))
16    continue
      do 17 i=1,n
       yerr(i)=h*(e1*ak1(i)+e3*ak3(i)+e4*ak4(i)+e5*ak5(i)+e6*ak6(i))
17    continue
      if(downsw .eq. 1.) go to 400
      emax=0.
      do 18 i=1,n
       if(dabs(yerr(i)) .gt. emax) emax=dabs(yerr(i))
18    continue
      if(emax .le. tol/2.) then
      x=x+h
      do 19 i1=1,n
      y(i1)=yout(i1)
19    continue
      if(emax .lt. tol/1250.) then
      del=5.
      else
      del=(tol/(2.*emax))**0.25
      endif
      h=del*h
      if((h.ge.0.) .and. (h .gt. hmax)) h=hmax
      if((h.lt.0.) .and. (abs(h).gt.hmax)) h=-hmax
      x1=x+h
      if(((h.ge.0.) .and. (x1.ge.b)) .or. ((h.lt.0.) .and. (x1.le.b))) then
      hl=h
      h=b-x
      if(dabs(h) .le. hmin*0.1) go to 500
      downsw=1.
      endif
      go to 300
      else
      del=(tol/(2*emax))**0.25
      if(del .le. 0.1) del=0.1
      h=del*h
      if(dabs(h) .lt. hmin) then
      write(*,*) ' ERROR !  SINGULAR POINT ! '
      err=1.
      go to 500
      endif
      go to 300
      endif
```

```
400   continue
      do 410 i=1,n
       y(i)=yout(i)
410   continue
      x=x+h
500   continue
      return
      END
      Subroutine frk(t,x,ak)
      implicit double precision (a-h,o-z)
      dimension x(2),ak(2)
      common /exci/  aw,wf,pi,cs,a1,a2,a3,co1,co2,co3,co4,
      Atmp1,Atmp2,ro,D,cm,cd,pern,depth,wlength
      co3=ro*D**3*cm*(pi/6)*wf**2*aw*(Atmp1/Atmp2)
      co4=ro*D**2*cd*(pi/4)*wf**2*aw**2*(Atmp1/Atmp2)*abs((Atmp1/Atmp2))
      x1=x(1)
      x2=x(2)
      theta=-wf*t+phi
      ak(1)=x2
      ak(2)=(co3*(dsin(theta))+co4*(dcos(theta))*abs(dcos(theta))-
(cs*x2+a1*x1+a2*x1**2+a3*x1**3+co2*x2*abs(x2)))/co1
      tmp=(co3*(dsin(theta))+co4*(dcos(theta))*abs(dcos(theta)))/co1
      return
      end
      Subroutine wave(pern,depth,wlength)
      implicit double precision (a-h,o-z)
      common /exci/  aw,wf,pi,cs,a1,a2,a3,co1,co2,co3,co4,
      Atmp1,Atmp2,ro,D,cm,cd
      write(*,*) 'Start computing the wave length..... '
      write(*,*) 'Number of iterations...'
       icount=0
      const=(4*(pi**2)*depth)/(32.17*(pern**2))
      L0=32.17*(pern**2)/(2*pi)
      x0=2*pi*depth/L0
202       fx1=x0*(tanh(x0))-const
          fx1p=tanh(x0)+x0*(1-(tanh(x0))**2)
          xnext=x0-fx1/fx1p
          y=xnext*(tanh(xnext))-const
          err=abs(y)
          if(err .lt. 0.0001) goto 204
          if(icount .gt. 3000) then
          write(*,*) 'Error!, Not convergent ! '
          goto 204
          endif
```

```
          x0=xnext
          icount=icount+1
          write(*,*) icount
          goto 202
204   wlength=2*pi*depth/xnext
      write(*,*) 'wave period  water depth  wave length.'
      write(*,206) pern,depth,wlength
206   format(2x,f10.3,5x,f5.3,5x,f10.3)
      write(*,*) 'error is'
      write(*,208) err
208   format(2x,f16.12)
      return
      end
```